Abstract

The intracellular proteolytic fragment of CD44
alters CD44 function in chondrocytes

by Liliana Mellor

July, 2010

Director: Dr. Warren Knudson

DEPARTMENT OF ANATOMY AND CELL BIOLOGY

CD44 is an adhesion molecule involved in several biological functions and the primary receptor for hyaluronan (HA). In cartilage, CD44 participates in the interplay between cells and the extracellular matrix to fine tune cellular responses to cytokines and growth factors. CD44 thus can act as a mediator between individual chondrocytes and the extracellular matrix. The extracellular domain of CD44 binds to the HA/proteoglycan rich extracellular matrix, while the intracellular domain interacts with receptors like Smad1 and with the actin cytoskeleton inside the cell. Recently, we have demonstrated that chondrocyte CD44 is proteolytically cleaved from the cell surface by an endogenous, sequential, two step process. First, there is an initial extracellular cleavage of CD44 by a matrix metalloproteinase, which releases a soluble CD44 in the extracellular matrix, followed by a γ-secretase transmembrane cleavage, which releases an intracellular tail domain of CD44.

The main focus of this study is to understand the effects of releasing a CD44 intracellular domain (ICD) that occurs via the action of the γ-secretase

cleavage, and how intracellular accumulation of such fragments might interfere with endogenous, intact, CD44 function. The first aim evaluates whether intracellular accumulation of ICD fragments can affect CD44 ability to bind to HA and retain a pericellular coat by acting as a negative competitor. Another aim was to explore the mechanisms responsible for any effects ICD over-expression might have on CD44 function. Our data suggests that intracellular CD44-ICD over-expression exerts dominant-negative effects on full length native CD44 by competing with binding to the cytoskeleton via ankyrin-3. This is the first study that looks at possible effects of releasing multiple ICD fragments via γ-secretase cleavage in chondrocytes and as such, will provide useful information on possible significance of CD44 fragmentation in cartilage during osteoarthritis.

The intracellular proteolytic fragment of CD44 alters CD44 function in chondrocytes

A Dissertation

Presented To

The Faculty of the Department of Anatomy and Cell Biology

East Carolina University

In Partial Fulfillment

of the Requirements for the Degree

Ph.D.

by

Liliana Mellor

July, 2010

The intracellular proteolytic fragment of CD44

alters CD44 function in chondrocytes

by

Liliana Mellor

APPROVED BY:

DIRECTOR OF
DISSERTATION:_____
Warren Knudson, PhD

COMMITTEE
MEMBER:_____
Cheryl B. Knudson, PhD

COMMITTEE
MEMBER:_____
Ann O. Sperry, PhD

COMMITTEE
MEMBER:_____
Anthony A. Capehart, PhD

CHAIR OF THE DEPARTMENT OF ANATOMY AND CELL BIOLOGY:

_____
Cheryl B. Knudson, PhD

DEAN OF THE GRADUATE SCHOOL:

_____
Paul Gemperline, PhD

TABLE OF CONTENTS

LIST OF TABLES

LIST OF FIGURES

LIST OF ABBREVIATIONS

° C	degrees celcius
A	adenine
aa	amino acids
Ab	antibody
ADAM	a disintigrin and a metalloprotease domain
Ala	alanine
ANK	ankyrin
ARD	ankyrin-repeat domain
Arg	arginine
Asn	asparagine
BAC	bovine articular chondrocyte
BB16 cells	v-src-transformed rat fibroblasts
BCA	bicinchoninic acid
BMP	bone morphogenetic protein
bp	base pair
BSA	bovine serum albumin
BU52	antibody specific to CD44 extracellular domain
C-ERMAD	carboxyl-terminal ERM associated domain
C-terminal	carboxyl-terminal
C28/I2	Immortalized human chondrosarcoma cell line
Ca^{2+}	calcium
CD44	clusters of differentiation forty-four

CD44-EXT	CD44 extracellular truncation
CD44-FL	CD44 full length
CD44-ICD	CD44 Intracellular domain
CD44H	hematopoietic isoform of CD44
CD44s	standard isoform of CD44
CD44v10	variant exon 20 isoform of CD44
CFM	chondrocyte feeding medium
CO_2	carbon dioxide
COS-7	african green monkey kidney cell line
CS	cleavage site
Cys	cysteine
DAPI	4',6-diamidino-2-phenylindole, dihydrochloride
DAPT	γ-secretase inhibitor
dBAC	de-differentiated bovine articular chondrocyte
DMEM	Dulbeccos' modified Eagle's medium
DNA	deoxyribonucleic acid
ECL	enhanced chemi-luminescence
ECM	extracellular matrix
EDTA	ethylenediaminetetraacetic acid
EGFP	enhanced green fluorescent protein
ERM	ezrin/radixin/moesin
FBS	fetal bovine serum
FERM	4.1 protein/ezrin/radixin/moesin

FITC	Fluorescein isothiocyanate
FRT	flip recombination target
g	gravity
G1	globular domain one
GFP	green fluorescent protein
GM6001	general MMP inhibitor
GM7373A	aortic endothelial cell line
HA	hyaluronan
HA oligos	Hyaluronan oligosaccharides
HA'ase	hyaluronidase
HABP	hyaluronan binding protein
HAS	hyaluronan synthase
HCl	hydrochloric acid
HEK-293	human embryonic kidney cell line
Hr	hour
HRP	horse radish peroxidase
Hyal2	hyaluronidase-2
ICAM	intercellular adhesion molecule-1
IL-1	interlukin-1
Ile	isoleucine
IP3R	inositol triphosphate receptor three
K	lysine
kb	kilobase

kD	kilodalton
Lys	lysine
M	molar
mAb	monoclonal antibody
MCS	multiple cloning site
$MgCl_2$	magnesium chloride
ml	milliliter
mM	millimolar
mm	millimeter
MMPs	matrix metalloproteases
MT1-MMP	membrane type I matrix metalloprotease
N	asparagine
N-ERMAD	amino-terminal ERM associated domain
NaCl	sodium chloride
ng	nanogram
nm	nanometer
NP-40	nonidet P-40
OA	osteoarthritis
pAb	polyclonal antibody
PBS	phosphate buffered saline
PCR	polymerase chain reaction
pERM	phospho-ERM
PFA	paraformaldehyde

PIP	phosphatidylinositol
PIP2	phosphatidylinositol-4, 5 bisphosphate
PKC	protein kinase C
PKC	protein kinase C
PMA	phorbol myristate acetate
pSmad	phospho-Smad
Q	glutamine
R-Smad	receptor-Smad
RCS	rat chondrosarcoma cell line
RFP	red fusion protein
RNA	ribonucleic acid
rpm	rotations per minute
Ser	serine
SKOV-3	ovarian carcinoma cell line
Smad 1	mothers against decapentaplegic homolog one
SOC	super optimal culture
solCD44	soluble CD44
T	thymidine
TBE	tris borate EDTA
TBS	tris buffered saline
TGF-β	transforming growth factor beta
TIMP	tissue inhibitor of metalloproteinases
TNF	tumor necorsis factor

TPA	12-*O*-tetradecanoylphorbol-13-acetate
Tris	tris (hydroxymethyl) aminomethane
UV	ultra violet
V	volts
α1C	α helix one of subdomain C
β5C	β strand five of subdomain C
μg	microgram
μl	microliter
μM	micromolar

CHAPTER 1: BACKGROUND AND SIGNIFICANCE

Articular cartilage homeostasis is the result of an equilibrium between catabolic and anabolic factors. CD44 participates in the interplay between cells and the extracellular matrix to fine tune cellular responses to cytokines and growth factors. In articular cartilage, CD44 binds to hyaluronan (HA), the major unbranched glycosaminoglycan of the extracellular matrix, while inside the cell the conserved cytoplasmic tail of CD44 binds to the actin cytoskeleton. These interactions are vital for CD44 to act as a mediator between individual chondrocytes and the extracellular environment to maintain tissue homeostasis.

It has been previously reported that CD44 undergoes a sequential proteolytic cleavage in many tissues and pathologies. First, a membrane type I matrix metalloprotease (MT1-MMP) and/or an ADAM-like protease such as ADAM17 or ADAM10 cleaves the extracellular domain of CD44, releasing a soluble fragment (solCD44) outside the cell. Sequentially, the transmembrane domain is cleaved by γ-secretase, releasing an intracellular fragment (CD44-ICD) inside the cell. Previous studies suggest that the released CD44-ICD goes directly to the nucleus and actives transcription of different genes (Okamoto et al. 2001), however, it is still unknown whether a fraction can remain in the cytoplasm, and if so, what is the biological significance.

Our laboratory recently demonstrated that CD44 proteolytic cleavage observed in our model system *in vitro* is similar to CD44 fragmentation present in osteoarthritic (OA) chondrocytes (Takahashi et al., 2010). This study presented here addresses the biological consequences of having a cytoplasmic CD44-ICD, and further investigates the mechanisms of how CD44-ICD can interfere with the endogenous full-length CD44 function.

1. Osteoarthritis

Osteoarthritis (OA) is the most common disease of the joints that limits mobility due to the degradation of articular cartilage in the affected joint. Symptoms can vary from minimal pain to acute pain and stiffness, depending on the degree of cartilage degeneration and functional limitation. It is the most common form of arthritis, and affects nearly 21 million Americans, most over the age of 45. With the increasing rate of obesity in the U.S., estimates suggest a doubling in prevalence from the year 2000 to 2020 (Felson, 1998). There are multiple risk factors that can lead to OA including genetic factors, constitutional factors such as gender (females are more prone to develop OA), race (higher percentage of African-Americans develop OA when compared to Caucasians), age, obesity, high bone density, and biomechanical risk factors such as joint injury, reduced muscle strength, joint laxity and joint malalignment (National Collaborating Centre for Chronic Conditions, 2008).

Osteoarthritis is the result of both mechanical and biological effects that destabilize the normal coupling of degradation and synthesis of articular cartilage

chondrocytes and extracellular matrix (ECM) and subchondral bone (Kuettner, 1998). Gene expression and metabolism in osteoarthritic cartilage is characterized by increased cell proliferation, synthesis of fibrocartilage matrix and secretion of matrix metalloproteases (MMPs), and inflammatory cytokines such as IL1α and TNFα (Goldring, 2000; Holloway et al., 2004). Due to the lack of understanding of the underlying mechanism that produces an increased catabolic rate and a decreased anabolic rate that leads to cartilage degeneration, the most available treatments for OA are targeted towards reducing pain. As a result, OA remains one of the few chronic diseases of aging without an effective treatment (Felson, 2009).

This study attempts to understand the underlying mechanism for articular cartilage degeneration by studying the interactions of hyaluronan (HA), one of the major components of articular cartilage extracellular matrix, and its cell surface receptor CD44. Constant communication between extracellular matrix and chondrocytes through CD44/HA interactions is essential to maintain cartilage homeostasis, and disruption of this interaction leads to cartilage degradation. One mechanism that may be detrimentally affecting CD44/HA interactions is the proteolytic cleavage of CD44.

2. Articular cartilage

Articular cartilage is the major load-bearing tissue of the synovial joint with very limited regenerative capacity. It is composed of chondrocytes, which account for less than 5% of the total tissue volume (Kuettner, 1994), but are the entities responsible for

maintenance and secretion of the extracellular matrix. As shown in Figure 1, cartilage can be sub-classified into several layers. From superficial to deep: the superficial layer contains resting chondrocytes; the zone of proliferation contains chondrocytes undergoing mitosis; the zone of hypertrophy contains swollen hypertrophic chondrocytes stacked on top of each other; and the zone of calcification contains dead calcified cartilage matrix. Articular cartilage is characterized by lack of blood supply, innervation, lymphatics and cell-cell contact. Each chondrocyte is surrounded by an extensive extracellular matrix and together, cells and matrix play an important role in communication to withstand the highly repetitive stresses that occur in the synovial joint (Blain, 2009). Interactions between the cell and the extracellular matrix are vital to maintain cartilage homeostasis (Knudson and Knudson, 1993). These interactions are mediated via cell surface receptors, which direct assembly and retention of the matrix and provide a linkage to the cytoskeleton and cytosolic components of signaling pathways (Knudson, 2003).

2.1. The extracellular matrix of articular cartilage:

Extracellular matrix in articular cartilage can be divided into a pericellular compartment, referring to ECM components directly associated with cell surface receptors along the cell membrane of each individual cell; the territorial compartment comprising the complex aura of ECM that forms around each cell; and the interterritorial compartment, which includes the less-dense ECM between territorial compartments of adjacent cells. The extracellular matrix is composed of a complex collagen network, proteoglycans and non-collagenous glycoproteins; however, the major component is

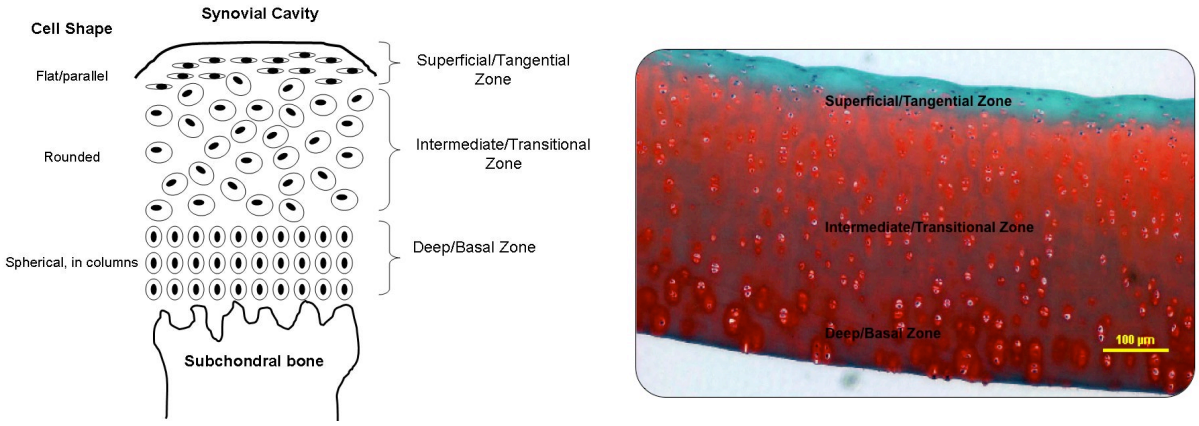

Figure 1: Characteristic zones in articular cartilage. A. The illustration shows the different morphology of chondrocytes among individual zones. **B.** Histological sample of bovine articular cartilage stained with safranin O and fast green counter-stain showing the three morphological zones. The red dye from the safranin O reflects the rich proteoglycan content of the articular cartilage.

water, which accounts for roughly 70% of the total tissue volume (Kuettner, 1994). Large water volume provides cushioning for the mechanical pressures produced in the joints, protecting the articular cartilage of adjacent bones.

The interwoven collagen fibers represent about 50% of the organic dry weight in articular cartilage, and provide a network that gives tensile strength and support to the tissue, and the capacity to contain the swelling pressure of the embedded aggrecan proteoglycan (Knudson and Knudson, 1993). In adult cartilage, about 90% of the total collagens are type II collagen, a type found only in a few other tissues. Chondrocytes are responsible for collagen synthesis in articular cartilage, and changes in collagen expression have been associated with OA cartilage (Kuettner, 1994).

Proteoglycans play an important role in regulating osmotic pressure in the synovial joint. The negative charge of proteoglycans interacts with water molecules allowing the tissue to undergo reversible deformation during mechanical pressure. Aggrecan is the most abundant proteoglycan in articular cartilage, accounting for about 90% of the mass of proteoglycans in the tissue (Kuettner, 1994). The globular G1 core protein domain of aggrecan binds to hyaluronan directly—a binding that is further stabilized by a link protein to form a proteoglycan aggregate (Figure 2). Hyaluronan is a high molecular weight glycosaminoglycan composed of repeating disaccharides of glucuronic acid and *N*-acetylglucosamine. The nonbranching linear hyaluronan macromolecule and acts as the core filament for aggrecan aggregates (Knudson, 1993).

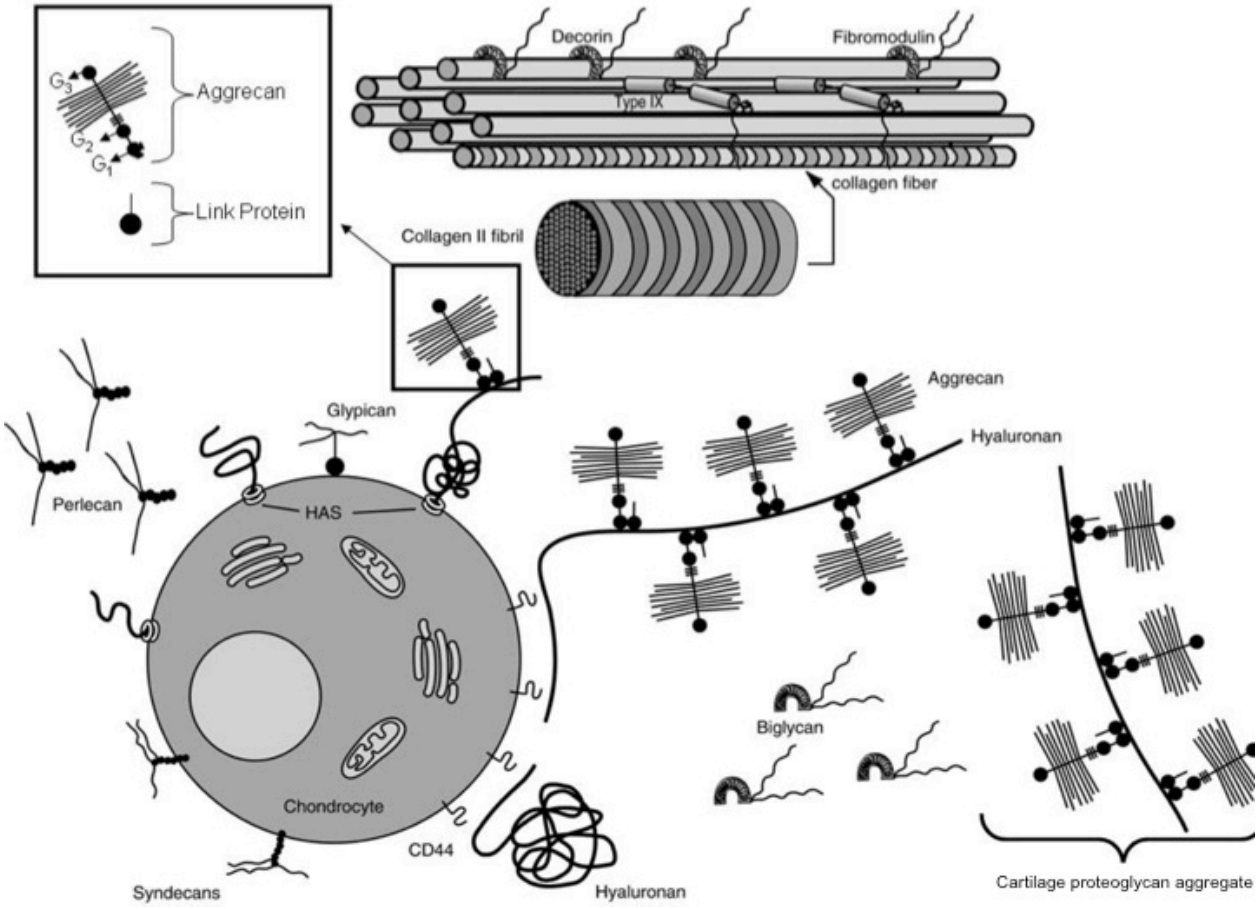

Figure 2: The extracellular matrix of chondrocytes. Figure depicts the interaction between a normal articular chondrocyte with its adjacent extracellular matrix. Several components of the cartilage / chondrocyte extracellular matrix are highlighted including the cartilage-specific collagens, various proteoglycans present in cartilage and HA. Of particular interest to this study, the model depicts how HA is synthesized at the plasma membrane via HA synthases (HAS), as well as the retention of HA by the cell surface receptor CD44. Also highlighted is the binding of the globular G1 domain of aggrecan to HA, that together with bound link proteins, forms the cartilage proteoglycan aggregate (modified from Knudson and Knudson 2005).

Hyaluronan is synthesized directly at the cell membrane of chondrocytes by a membrane hyaluronan synthase complex termed HAS (Figure 2). In chondrocytes, HAS-2 is the primary enzyme (Nishida et al., 1999) and newly-synthesized hyaluronan is released directly into the extracellular matrix after termination of chain elongation. Once released hyaluronan interacts with the cells via cell membrane receptors such as CD44 (Knudson, 1993; Knudson, 1996). It has been shown that hyaluronan is critical to maintain the structure of the extracellular matrix, and it also affects adhesion, migration and differentiation of embryonic chondrocytes in early limb formation (Knudson and Toole, 1985; Knudson and Toole, 1987; Maleski and Knudson, 1996). CD44 interacts with the extracellular environment by binding to hyaluronan, while inside the cell the intracellular domain binds to different elements of the cytoskeleton and cytosolic proteins via the intracellular domain to activate different signaling pathways.

2.2. Cytoskeletal components in articular chondrocytes:

The chondrocyte cytoskeleton plays a major role in maintaining the chondrocyte phenotype (Benya et al., 1988; Benya and Shaffer, 1982; Nofal and Knudson, 2002) and activating signaling pathways in response to mechanical stimuli or changes in the composition of the extracellular matrix—events mediated by matrix receptors. The cytoskeleton is composed of actin microfilaments, tubulin microtubules and intermediate filaments. The actin microfilaments contribute to changes in cell shape, movement of organelles, cell adhesion and migration, endocytosis, secretion, and extracellular matrix formation. Microtubules contribute to organelle trafficking, cell motility and division, and

cell morphogenesis and organization. The less studied vimentin intermediate filaments are believed to be involved in signal transduction (Blain, 2009).

In normal articular cartilage (non-OA), the three dimensional cytoskeleton of chondrocytes is cortical in the middle and deep zone cells, as well as in the more flattened disc-shaped cells that are present in the superficial zone (Figure 1). However, morphological changes are often observed in osteoarthritic cartilage, in which the chondrocytes develop a complex fibrous structure extending from the cytoplasm in all directions (Holloway et al., 2004).These elongated processes are more prominent in the superficial and middle zone of OA cartilage, but it is still unknown whether these cells contribute directly to the breakdown of cartilage tissue through the release of catabolic agents from the cell processes, or whether the processes are a result of matrix degradation (Holloway et al., 2004).

3. Structure and function of CD44

CD44 is a type I transmembrane protein found in the cell surface of many tissues, including articular cartilage and plays a critical role in a diversity of cell behaviors including cell adhesion, migration, invasion and survival (Cichy and Pure, 2003) as well as pericellular matrix assembly (Knudson, 1993). In humans, it is encoded by a single gene located in chromosome 11p13 and comprises at least 20 exons (Martin et al., 2003). CD44 is synthesized as a small 37 kD protein, but due to alternative splicing of the variable exon region and post-translational modifications such as variable N- and O-linked glycosylation, the molecular size varies between 80-200 kD

(Marhaba and Zoller, 2004). The standard isoform (CD44s) also known as the hematopoietic isoform of CD44 (CD44H) comprise exons 1-5, 16-18 and 20, and is composed of 341 amino acids (Martin et al., 2003). Once localized in the plasma membrane, the N-terminal of CD44 is oriented as the extracellular domain, followed by a transmembrane domain and C-terminal cytoplasmic domain (Figure 3).

The extracellular domain of CD44H is composed of 248 amino acids, and can be subdivided into two regions; membrane proximal and membrane distal. The membrane distal N-terminal region is encoded by exons 1-5 and is highly conserved (85%) in mammalian species. The membrane distal region contains the so-called "link-homology domain" due to its homology to HA binding regions present on link proteins and aggrecan. The link-homology domain is stabilized by three pairs of disulfide bonds and is responsible for binding ligands present within the extracellular matrix (Martin et al., 2003). The principal ligand for CD44 is HA, but other extracellular macromolecules have also been reported to bind including type I collagen, fibronectin, fibrin, laminin and chondroitin sulfate (Naor et al., 1997). Binding of CD44 to hyaluronan has multiple effects on cell proliferation, motility and survival of both malignant and nonmalignant cells (Anderegg et al., 2009).

The less conserved (35-50%) membrane proximal region is encoded by exons 16-17 and in part by exon 5 (Martin et al., 2003). This domain is responsible for different CD44 isoforms by expressing post-translational glycosylation and alternative

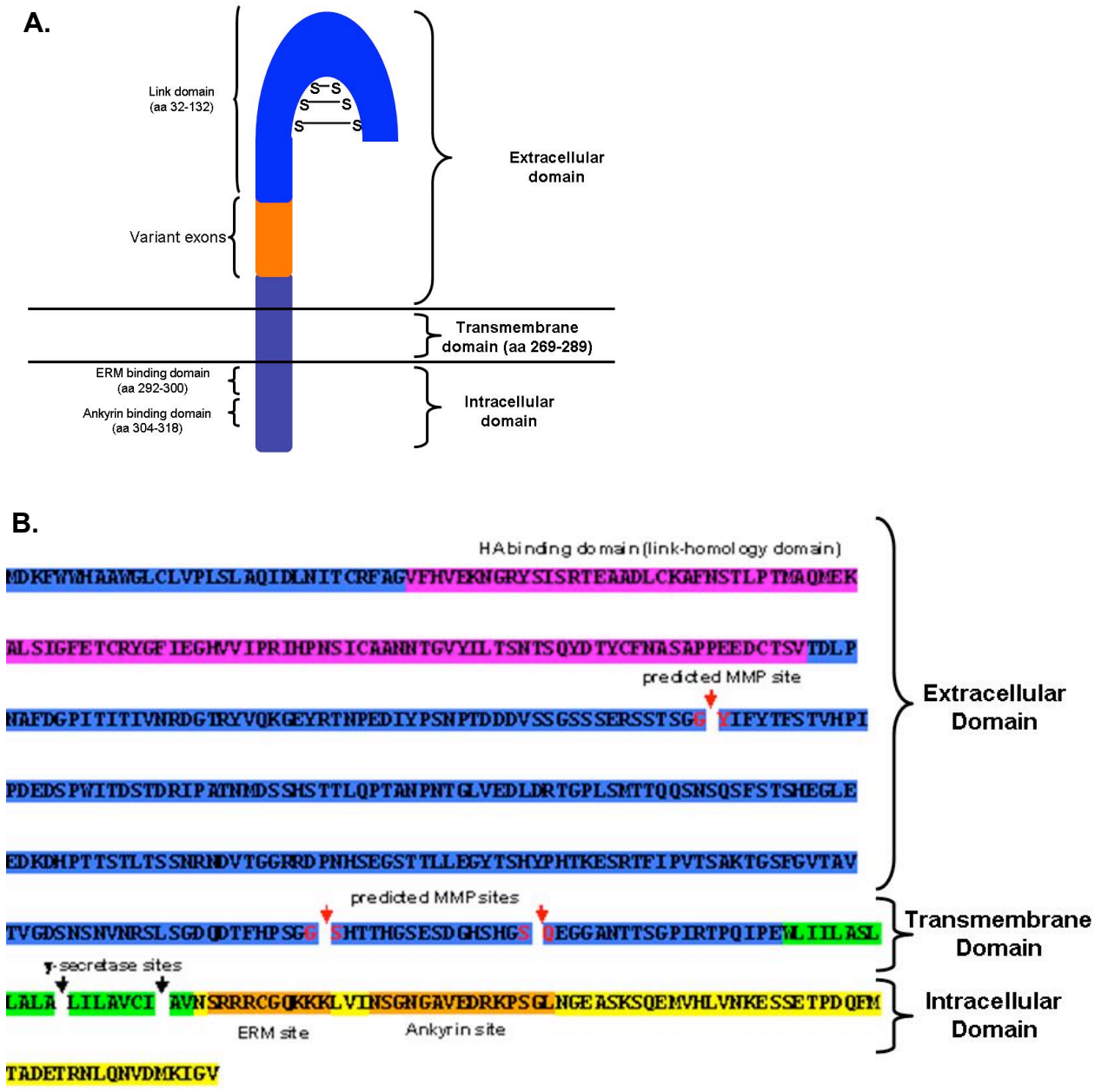

Figure 3: CD44 structure. **A.** CD44 is composed of an extracellular, transmembrane and intracellular domain. The extracellular domain contains the binding motif to HA, as well as a variable region in which different CD44 isoforms can be generated via alternative splicing of variant exons. The cytoplasmic tail contains putative ERM and ankyrin binding domains that interact with the actin cytoskeleton. **B.** CD44 sequence showing the extracellular domain (blue) containing the HA binding site (pink) and three predicted MMP cleavage sites, the transmembrane domain (green) with two γ-secretase sites, and the intracellular domain with an ERM and ankyrin binding domains (orange).

splicing (of exons 6-15). This short stalk region at the end of the link domain connects the extracellular domain with the transmembrane domain.

The short transmembrane domain is composed of 23 hydrophobic amino acids and a cysteine residue (cys^{286}) encoded by exon 18. It has been suggested that the transmembrane domain may be involved in CD44 oligomerization and transport of the protein into lipid rafts (Marhaba and Zoller, 2004; Thankamony and Knudson, 2006). Thankamony and Knudson found that mutation of cys^{286} to ala^{286} or ser^{286} had no effect on HA binding but prevented the movement of CD44 into lipid rafts and prevented CD44-mediated endocytosis of HA.

The highly conserved (80-90%) intracellular domain is encoded in part by exon 18 and all of exon 20 (Martin et al., 2003). It is composed of 72 amino acids and is thought to be important in regulating the functions of CD44 including HA binding, HA endocytosis, signal transduction and cell migration. The CD44 intracellular domain has no intrinsic kinase activity, thus signal transduction is likely mediated through interactions with the cytoskeleton via an ERM (ezrin/radixin/moesin) and ankyrin binding domains (Knudson and Peterson, 2004). The ERM binding domain of CD44 includes amino acids 292-300, which is located between the transmembrane domain and the intracellular membrane-proximal domain. Distal to the ERM binding domain is the ankyrin binding motif including amino acids 304-318 (Marhaba and Zoller, 2004).

Studies have shown that disruption of the actin cytoskeleton using cytochalasin D disrupts CD44/HA interactions and decreased matrix retention (Lesley et al., 1992; Liu et al., 1996; Nofal and Knudson, 2002). In addition, over-expressing a negative competitor to the CD44/ankyrin binding motif blocked HA-mediated Ca^{2+} signaling in endothelial cells (Singleton and Bourguignon, 2004). Therefore, binding of CD44 cytoplasmic tail to the cytoskeleton is essential for CD44 ability to retain a pericellular coat and mediate outside-in signaling.

It is still unclear whether CD44 can interact with both ERM and ankyrin simultaneously forming a single complex, or whether CD44/ERM and CD44/ankyrin are two separate mutually exclusive complexes that are utilized in a tissue dependent manner. To date, there is only indirect evidence to suggest that CD44 interacts with cytoskeletal proteins in articular chondrocytes (Nofal and Knudson, 2002). A direct interaction between the cytoplasmic tail of CD44 and cytoskeleton adaptor proteins has not been shown.

3.1. CD44/ERM interactions:

A crystal structure analysis of the FERM/CD44 complex revealed that the CD44 ERM binding region contains a cluster of basic amino acids, Lys-Lys-Lys, followed by a nonpolar region (Figure 3B) which binds to the groove formed between helix α1C and the β-strand 5 of subdomain C (β5C) of the FERM domain (Mori et al., 2008). A functional analysis of the ezrin binding site in CD44 found that deletion of residues 289-295 or 296-300 completely abolished association with ezrin, and that phosphorylation of

CD44 at Ser325 does not regulate ezrin binding. Interestingly, the CD44 ERM binding domain mutants did not affect HA binding, suggesting that HA binding to CD44 is not dependent upon intracellular binding of CD44 to these cytoskeleton adaptor proteins (Legg and Isacke, 1998). Based on these results, the proposed mechanism for CD44/ERM interactions suggest that ERM proteins do not have an inside-out effect on transmembrane receptor signaling, but rather regulate outside-in signaling events. Contrary to previous reports that CD44 and ERM play an important role in localization of the other (Hirao et al., 1996), ezrin mutants did not affect CD44 localization to the plasma membrane (Legg and Isacke, 1998).

ERM proteins exist in two states; an active state involved in protein-protein interactions, and a dormant state present in the cytoplasm. During the dormant state, the amino-terminal N-ERMAD (N-ERM Associated Domain) interacts with the carboxyl-terminal C-ERMAD (C-ERM Associated Domain), changing the conformation of the protein and masking the binding sites for both the cytoskeletal and binding partners (Louvet-Vallee, 2000). ERM proteins can be activated by phosphorylation of serine/threonine residues by protein kinase C (moesin) and Rho kinase (ezrin/radixin). This phosphorylation disrupts the interaction between N-ERMAD and C-ERMAD, unmasking the binding sites for actin and ERM binding proteins (Matsui et al., 1998). Another suggested mechanism for ERM activation is by binding to phosphotidylinositides. *In vitro* studies have shown that addition of phosphatidylinositol phosphate (PIP) and phosphatidylinositol-4, 5 bisphosphate (PIP2) to the media is

necessary to detect CD44/ERM interactions (Hirao et al., 1996a) an observation that was later confirmed by *in vivo* studies (Matsui et al., 1999).

ERM proteins can also be switched to the dormant state. One proposed mechanism for inactivation of ERM proteins is dephosphorylation of activated ERM, which changes the conformation of the protein and disrupts its interaction with the cell membrane and the cytoskeleton. In myeloid cells, treatment with actin or kinase inhibitors disrupted CD44/ERM interactions and reduced HA binding (Brown et al., 2005). Another study looking at the effects of hyaluronidase-2 (Hyal2) over-expression in *v-src*-transformed rat fibroblasts (BB16 cells), found that parental cells had higher levels of pERM and cell motility when compared to their Hyal2 transfectants. Hyal2 interacts with CD44 disrupting binding to HA, which in turn disrupts CD44/ERM binding and ERM phosphorylation (Duterme et al., 2009).

In summary, it has been shown that ERM proteins act as cross-linkers or adapters between transmembrane proteins (CD44, ICAM-1,-2 and CD43) and the actin cytoskeleton in different tissues. However, although it has been suggested that CD44 interacts with the actin cytoskeleton in articular chondrocytes, there are no reports on the mechanism for this interaction such as interactions between CD44 and ERM proteins. This lack of detectable ERM/CD44 binding may be due to predicted dissociation of CD44/ERM complexes under low ionic strength conditions (Tsukita and Yonemura, 1997). It has been reported that, in fact, CD44/ERM interactions cannot be

detected *in vitro* or *in vivo* under physiological conditions, and activation of Rho or protein kinase C seems to be a requirement to activate binding.

3.2. CD44/Ankyrin interactions:

Ankyrin is another family of adaptor proteins known to act as cross-linkers between cell surface receptors and cytoskeletal components. In mammals, ankyrins are encoded by three different genes (ANK1, ANK2, ANK3) and each gene produces many different isoforms through alternative splicing. At first, ankyrin was believed to act as a cross-linker between band 3 membrane protein to the cytoskeleton in erythrocytes, but now it is known to be highly expressed in different tissues and to interact with diverse membrane proteins (Bourguignon et al., 1998). ANK1 (ankyrin R), also known as erythrocyte ankyrin, is located on chromosome 8 in both humans and mice. It is highly expressed in erythrocytes, purkinje cells, and motor neurons in the spinal column and in the hippocampus. ANK2 (ankyrin B), also known as the brain ankyrin, is the predominant ankyrin in the nervous system. It is encoded by a gene in human chromosome 4q and mouse chromosome 3 (Peters et al., 1995). ANK3 (Ankyrin G) was the last member of the ankyrin family to be described, but interestingly, ANK3 is the most abundant and diverse of the ankyrin family. ANK3 can be found in kidney, most epithelial tissues, macrophages as well as cardiac, smooth and skeletal muscle tissues (Peters et al., 1995).

All ankyrins have three conserved domains: the N-terminal ankyrin-repeat domain (ARD) which consists of 33 amino acids, a spectrin binding domain and a C-

terminal regulatory domain (Singleton and Bourguignon, 2004). CD44 as well as other ankyrin binding partners, bind to the ARD through a conserved ankyrin binding domain within the cytoplasmic tail of CD44 (figure 3B). Biochemical studies and *in vitro* mutagenesis of the ankyrin binding domain indicate that CD44/ankyrin interactions are required for both "outside-in" and "inside-out" cell activation events. In addition, ankyrin binding domain of CD44 shares a large degree of sequence homology with the ankyrin binding domains of two Ca^{2+} channel proteins (the inositol triphosphate receptor, IP3R and ryanodine receptor). This homology suggests an important role for ankyrin in CD44/ankyrin interactions necessary for HA binding, but also interactions necessary to regulate Ca^{2+} influx and subcellular localization of IP3Rs (Bourguignon et al., 1998).

Cytoskeletal proteins such as filamin, anexin II, ezrin, myosin and RhoA are known to localize within specialized plasma microdomains that contain lipid components such as cholesterol and sphingolipids, also known as lipid rafts. This localization implies that cholesterol rich microdomains are involved in a variety of cellular functions related to cytoskeleton-receptor interactions. As discussed above, a fraction of the total cell surface CD44 also localizes within lipid rafts, namely the fraction of CD44 that becomes palmitoylated at Cys^{286} and possibly Cys^{295} (Thankamony and Knudson, 2006). A study in aortic endothelial cells (GM7372A) showed that the CD44 isoform expressed in these cells (CD44v10), interacts with two other proteins when present within lipid rafts; CD44v10 interacts with ankyrin and IP3R via the ARD domain of ankyrin. This raft-dependent sorting and interaction plays an important role in

regulating Ca^{2+} signaling mediated by CD44/HA binding. In the absence of HA, the CD44v10-ankyrin- IP3R complex failed to form and associate into the lipid rafts.

In addition, disruption of the lipid rafts using methyl-β-cyclodextrin or interference of CD44/ankyrin binding by over-expressing ankyrin's ARD fragments (these fragments act as competitive inhibitors), not only prevented ankyrin- IP3R receptor accumulation in lipid rafts, but also blocks HA-mediated Ca^{2+} signaling in endothelial cell functions (Singleton and Bourguignon, 2004).

Taken all together, CD44 has been demonstrated to bind to the cytoskeleton via ERM or ankyrin adaptor binding proteins, both of which act as cross-linkers between cell receptors and actin. However, *in vitro* binding assays demonstrated that the binding affinity for CD44 and ankyrin interactions is much higher than that of CD44 and ERM (Lokeshwar et al., 1994; Tsukita and Yonemura, 1997). To date, there are no reports of which adaptor protein functions as the intermediate in the linkage between CD44 and the actin cytoskeleton in articular chondrocytes. In the study by Singleton and Bourguignon, they used ARD fragments of ankyrin to determine the mechanism of CD44 / ankyrin / IP3R interactions (Singleton and Bourguignon, 2004). In our study, over-expression of a CD44-ICD fragment will be used in a similar way to probe for CD44-FL and cytoskeleton adaptor protein interactions. Additionally, intracellular competitive binding between the CD44-ICD and the cytoskeleton complexes may also affect CD44 functions that are dependent on cytoskeleton interactions.

3.3. Proteolytic cleavage of CD44:

Proteolytic cleavage of cell surface receptors is a key mechanism in cell migration and tumor metastasis. During cell migration, cells rely on a highly polarized cell morphology. When cell surface receptors bind to the ECM, actin polymerization creates protrusions of the leading edge. Degradation of adhesion structures and of ECM by metalloproteinases allow the cell to advance forward by releasing matrix steric resistance at the leading edge, and detachment of the trailing edge by processes such as disassembly of adhesion structures and proteolytic cleavage of cell surface receptors (Marrero-Diaz et al., 2009).

There is substantial evidence that CD44 undergoes a sequential proteolytic cleavage in a variety of cell types and tissues (Cichy and Pure, 2003; Lammich et al., 2002; Murakami et al., 2003; Okamoto et al., 2001; Okamoto et al., 1999; Pelletier et al., 2006). Similar to Notch and Amyloid Precursor Protein, CD44 is cleaved in the extracellular domain releasing a soluble peptide (solCD44) followed by a cleavage in the transmembrane domain, which releases an intracellular fragment (CD44-ICD) (Figure 4).

In the case of Notch, ligand binding to its receptors Delta and Jagged induces an extracellular proteolytic cleavage by ADAM metalloproteases, which is followed by a transmembrane domain cleavage by γ-secretase enzyme, releasing a Notch intracellular domain (ICD) inside the cell that translocates to the nucleus and promotes transcription. This signaling pathway occurs during several developmental and

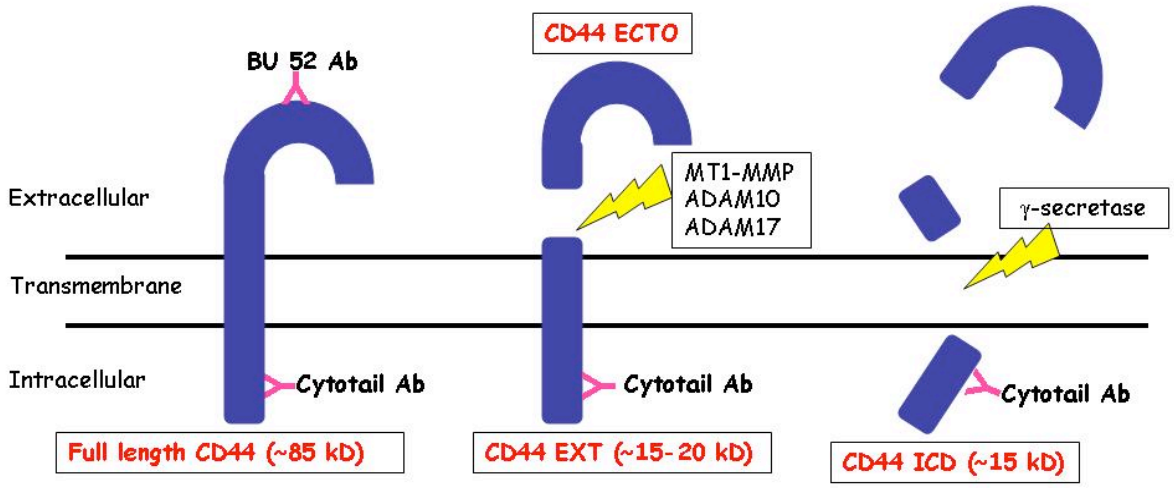

Figure 4: Sequential proteolytic cleavage of CD44 by a metalloproteinase and γ-secretase. Full length CD44 (CD44-FL) can be detected on a western blot with an antibody specific to the extracellular domain (BU52) or with CD44-cytotail antibody as an ~85 kD. After CD44 undergoes the first proteolytic cleavage by a metalloproteinase such as MT1-MMP or ADAM 10/17, the CD44-EXT fragment produced can be detected on a western blot with the CD44-cytotail antibody as a ~15-20 kD. Lastly, after γ-secretase cleavage, the CD44-ICD can be detected with the CD44-cytotail antibody as a ~15 kD by western blotting.

physiological processes, and Notch mutations have been associated with several pathologies such as T-cell acute lymphoblastic leukemia (Bray, 2006).

This sequential proteolytic cleavage of CD44 may play a role in several pathological conditions. High levels of solCD44 have been detected in the serum of patients with different types of malignant cancer and metastasis (Guo et al., 1994; Masson et al., 1999; Yamane et al., 1999), arthritic synovial fluid (Haynes et al., 1991a), and cell culture media (Nakamura et al., 2004; Okamoto et al., 1999b), and has been associated with unfavorable outcomes in non-Hodgkin's lymphoma (Nagano and Saya, 2004) and resistance to chemotherapy in breast cancer patients (Kopp et al., 2001). In addition, solCD44 is used as a marker for breast cancer (Lackner et al., 1998), gastric and colon cancer (Guo et al., 1994), colorectal cancer (Masson et al., 1999), cervical cancer (Kainz et al., 1995), and non-Hodgkin lymphoma (Lockhart et al., 1999). Recently, our laboratory found that CD44 expression in OA chondrocytes resembles the pattern shown of CD44 proteolytic cleavage in different tissues (Takeda et al., 2010).

Due to the important cell-cell and cell-matrix interaction properties of CD44, cancer biologists have shown an increased interest in CD44 shedding and over-expression as an important mechanism for cancer metastasis and migration (Kajita et al., 2001). As a result, proteolytic cleavage of CD44 is a major area of research interest in cancer biology and other fields, but the processes that regulate this cleavage as well as the consequences, remain elusive.

3.3.1 The release of soluble CD44

The first step of the sequential proteolytic processing of CD44 is an extracellular cleavage, which releases a soluble fragment (solCD44). This cleavage is regulated by multiple signaling pathways including activation of PKC, the influx of extracellular Ca^{2+}, members of the Rho family of small GTPases, and the Ras oncoprotein (Okamoto et al., 1999). There are three different sites on the extracellular domain of CD44 that can get cleaved, possibly by different enzymes and mechanism (Figure 3B).

Matrix metalloproteinase (MMPs) are a family of enzymes known to degrade the ECM. A sub-group of this family known as membrane-type metalloproteinases (MT-MMPs) are bound to the plasma membrane either through a transmembrane domain (Cao et al., 1995; Sato et al., 1994) or a glycosylphosphatidylinositol anchor (Kojima et al., 2000). MT1-MMP is the major membrane-type MMP expressed in tumor cells, and it appears to have an important role in cell migration and metastasis (Nakamura et al., 1999; Ueno et al., 1997). Interestingly, CD44 over-expression is also common in different types of cancer, and believed to be involved in cancer migration. Both MT1-MMP and CD44 were found to co-localize in the lamellipodia of migrating cells, and expression of MT1-MMP leads to an increase in CD44 shedding both *in vitro* (Kajita et al., 2001) and *in vivo* (Marrero-Diaz et al., 2009). A mutant form of CD44 that cannot be processed by MT1-MMP did not stimulate migration, suggesting that co-expression of MT1-MMP and CD44 is a possible mechanism involved in cell migration in which MT1-MMP cleaves the extracellular domain of CD44, allowing the cells to move forward (Kajita et al., 2001).

Another study further identified the cleavage sites of the CD44 extracellular domain (Nakamura et al., 2004). Nakamura and colleagues recognized three different sites (CS1, CS2, CS3, figure 3B) that generate three different solCD44 fragments (37-40 kD, 50-60 kD, 65-70 kD respectively). Furthermore, cleavage sites CS1 and CS2 were inhibited using an MMP specific inhibitor (TIMP-2) but not by TIMP-1, which inhibits soluble MMPs but not MT-MMPs or ADAMs; therefore, these two sites were recognized as MT1-MMP targeted sites. Cleavage site CS3 was inhibited by TIMP3, a general inhibitor of all MMPs and ADAMs, but not by TIMP-1 and TIMP-2, suggesting that the enzyme responsible for that cleavage site belong to the ADAM family (Nakamura et al., 2004).

ADAMs (A Disintegrin and A Metalloprotease domain) is a family of multidomain and multifunctional cell surface proteases that are related to MMPs. From N to C terminus, all ADAMs contain a pro, metalloprotease, disintegrin, cystine-rich, spacer, transmembrane and cytoplasmic tail domains (White, 2005). They play a key role in initiating activation of key signaling pathways and regulating interactions between tumor cells and their microenvironment (Stamenkovic and Yu, 2009). It has been suggested that ADAM-10 and ADAM-17 are also involved in cleavage of the extracellular domain of CD44 (Murai et al., 2006; Nagano and Saya, 2004; Nakamura et al., 2004; Stamenkovic and Yu, 2009).

Although the mechanism by which the CD44 extracellular domain is cleaved is still unclear, this step is a requirement for the second cleavage that occurs in the

transmembrane domain. In a study, metalloprotease inhibitors successfully blocked all CD44 shedding, including the intracellular fragments, which are a result of presenilin-dependent γ-secretase enzyme. Inhibitors specific to γ-secretase still cleaved the extracellular domain of CD44, but blocked the shedding of the intracellular domain (Okamoto et al., 2001).

3.3.2 The release of CD44 intracellular domain

The second step in the sequential proteolytic shedding of CD44 includes a transmembrane cleavage by the presenilin-dependent γ-secretase enzyme. γ-secretase is a protease that cleaves bitopic membrane proteins within the lipid bilayer. This enzyme also requires multiple components for enzymatic activity both *in vivo* and *in vitro* (Beel and Sanders, 2008). Presenilins are polytopic membrane proteins that are major constituents of the γ-secretase mediated transmembrane cleavage (Esler and Wolfe, 2001; Strooper and Annaert, 2001). In the case of CD44 transmembrane proteolysis, presenilin-1 was directly associated with the γ-secretase activity that releases the CD44 intracellular fragment (Murakami et al., 2003). Other substrates of γ-secretase activity include Notch and Amyloid Precursor Protein.

The target cleavage site within the transmembrane domain of CD44 occurs C-terminal to Ala280 or Ile287, releasing a short peptide outside the cell, and the CD44 intracellular domain (CD44-ICD) (Figure 4). Some studies suggest that the released CD44-ICD translocates to the nucleus and promotes transcription through the TPA-responsive element and activates gene expression, including CD44 itself (Okamoto et

al., 2001). In addition, CD44-ICD has been proposed to be involved in early events of tumorigenesis and cancer metastasis by directly activating signaling pathways (Pelletier et al., 2006).

Although nuclear translocation of the released CD44-ICD may occur, many questions still remain unanswered in regards to other possible roles of the released cytoplasmic CD44-ICD, including possible effects on endogenous CD44 and its cytoskeletal interactions. We propose that the CD44-ICD, like the ectodomain, would act as an intracellular competitor to the interaction between endogenous full-length CD44 and cytoskeletal binding proteins.

CHAPTER 2: MATERIALS AND METHODS

1. Engineering expression plasmid constructs and fusion proteins.

To study the effects of CD44-ICD over-expression on endogenous full-length CD44 function, several expression plasmids containing full-length CD44H (CD44-FL), CD44-ICD and Smad1 were prepared and characterized. Some of these expression plasmids provided for the establishment of epitope-tag fusion proteins. As seen in figure 5, different tags were used including C-terminal Myc, C-terminal EGFP (Enhanced Green Fluorescent Protein) or, N-terminal GFP (Green Fluorescent Protein). For the CD44-ICD, the Ala^{288} was chosen as the upstream start site because the Ile^{287} - Ala^{288} site within the transmembrane domain represents a major site for γ-secretase cleavage of CD44 (Okamoto et al., 1997). All of the CD44-ICD constructs were generated by PCR-mediated amplification of CD44-FL, already cloned into a pCDM8 vector and characterized for expression and function (Jiang et al., 2002).

1.1. Cloning strategies:

1.1.1 Generation of CD44-ICD-myc and untaggedCD44-ICD

A two-step cloning approach was used to generate an expression plasmid containing a CD44-ICD-myc or an untagged CD44-ICD insert (Figure 6). Primer design required careful engineering to incorporate restriction sites that can be used for directional cloning into the pCMV/myc/cyto vector (*Invitrogen*, Carlsbad, CA). The

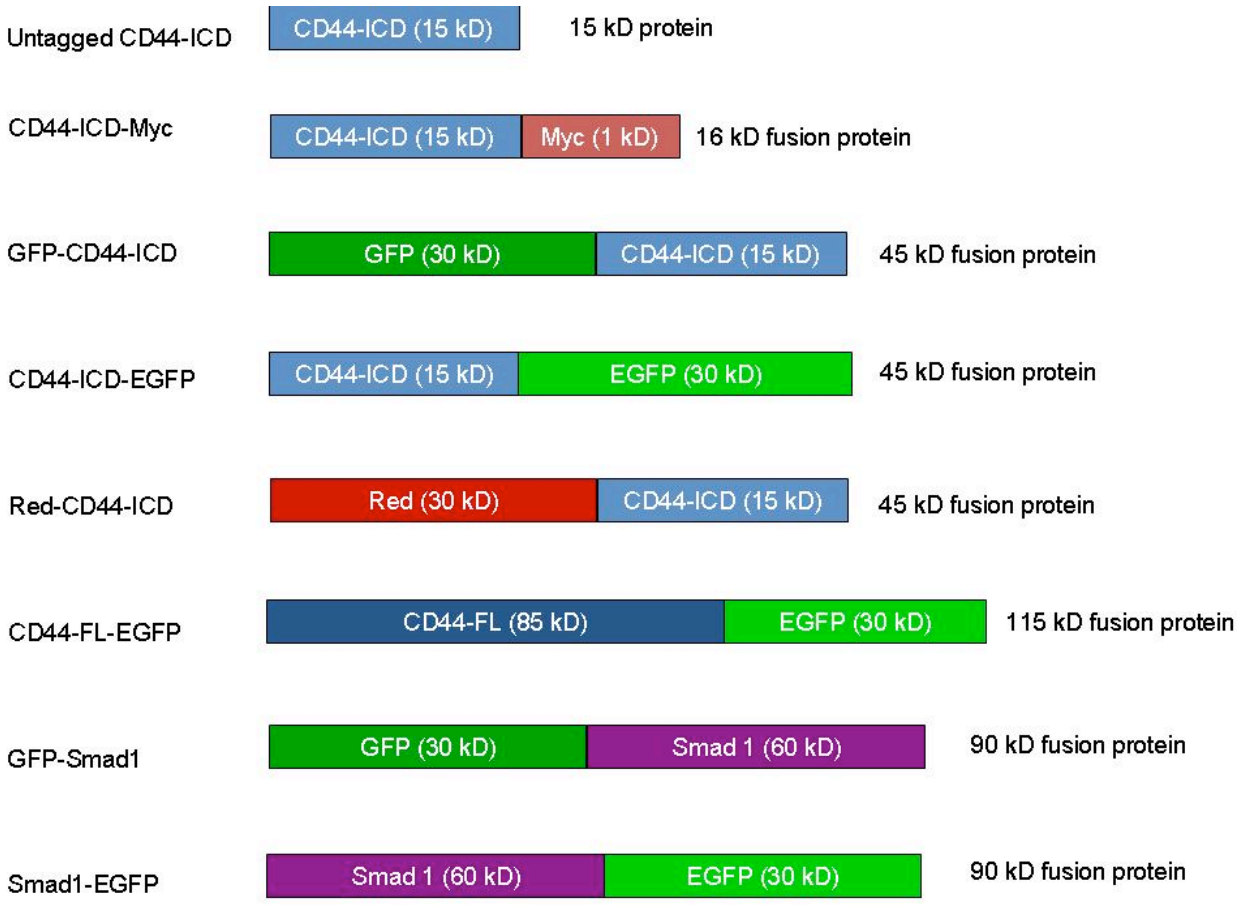

Figure 5: Summary of all fusion proteins. All constructs engineered during this study are shown, including location of the epitope tag (N- terminal vs. C-terminal) and size of the insert, the epitope tag and the estimated size of the fusion protein.

A.

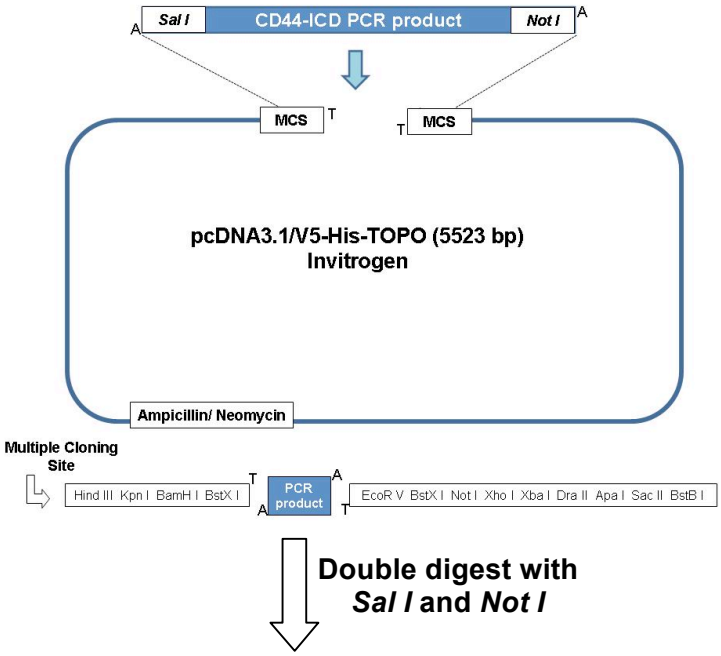

B.

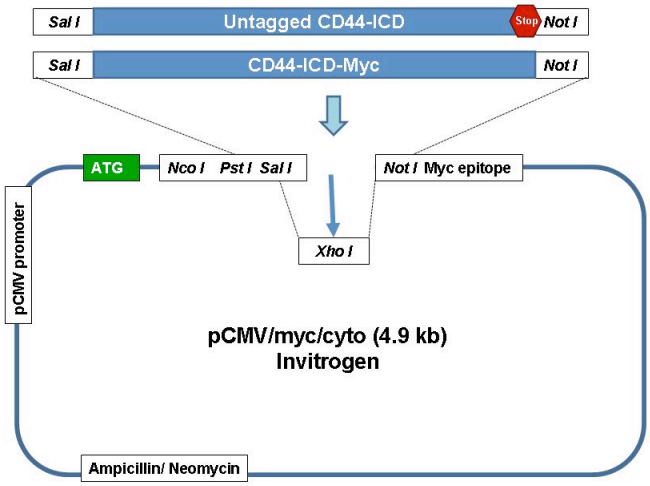

Figure 6: Cloning strategy to generate an untagged CD44-ICD and a CD44-ICD-myc. **A.** PCR product amplified using primers with engineered *Sal I* and *Not I* sites was subcloned into a TOPO vector. **B.** A sequential double restriction digest using *Sal I* and *Not I* restriction enzymes removed the CD44-ICD from the TOPO vector, and the insert was then subcloned into the final pCMV/myc/cyto vector to create an untagged CD44-ICD (primers included a stop codon) and a CD44-ICD-myc (primers omitted the stop codon).

pCMV/myc/cyto vector was chosen because it provides a start (ATG) site in the multiple cloning site (MCS) and a Kozak consensus sequence to facilitate expression of the protein. In order to use this start site, primers were carefully designed to be in-frame with the ATG site.

Both myc-tagged and untagged constructs were generated using the same upstream primer with an engineered *Sal I* site on the 5′ end: 5′GTCGACGCAGTCAAV AGTCGAAGAAGGTGTGG3′. Primers were designed and generated using Integrated DNA Technologies (Coralville, IA) website. The downstream primer for both constructs included an engineered *Not I* site at the 3'. However, the untagged CD44-ICD included a stop codon (UAA) at the end of the sequence designed to generate the more native 15 kD CD44-ICD protein. The CD44-ICD-myc construct omitted the stop codon but was carefully designed to be in-frame so as to integrate the C-terminal myc sequence. The addition of the myc tag added 1.5 kD to the 15 kD size of the CD44-ICD. The downstream primers used were: untagged CD44-ICD: 5′TTACACCCCAATCT TCATGTCCACATTC3′; and CD44-ICD-myc: 5′CGCCGGCGCACCCCAATCTTCATG TCCACATTC3′.

The first step of the two-step cloning strategy used was to PCR-amplify the CD44-ICD sequence using pCDM8-CD44H as a template, introducing the new *Sal I* and *Not I* sites in the process. The PCR product was first sub-cloned into a pcDNA3.1/V5-His-TOPO vector (*Invitrogen*) (Figure 6A). This intermediate cloning step allowed for the generation of a large amount of CD44-ICD insert and, for more efficient restriction

digestion. A sequential double restriction digest using *Sal I* and *Not I* restriction enzymes (*Invitrogen*) was performed to remove the CD44-ICD insert from the TOPO vector and achieve directional cloning into pCMV/myc/cyto vector (Figure 6B).

1.1.2. Generation of GFP-CD44-ICD

In order to generate a CD44-ICD containing a GFP at the N-terminal (5′ end), the PCR-amplified CD44-ICD sequence including the stop site (shown above) was cloned into a pcDNA3.1/NT-GFP-TOPO vector (*Invitrogen)* to generate a GFP (Green Fluorescent Protein) epitope-tagged fusion protein with CD44-ICD. Since the GFP tag in this plasmid is upstream to the multiple cloning site, this plasmid will also provide an efficient start site to express the CD44-ICD peptide. As such, it was again important to engineer the CD44-ICD insert to be properly subcloned in-frame. When the GFP is expressed as a protein, it adds ~30 kD of molecular size to the fusion protein. Therefore, the GFP-CD44-ICD fusion protein was expected to be ~45 kD.

1.1.3. Generation of CD44-ICD-EGFP

In order to generate a CD44-ICD containing an EGFP (Enhanced Green Fluorescent Protein) at the C-terminal (3′ end), the CD44-ICD was subcloned into a pEGFP-N2 vector (*Clontech,* Mountain View, CA). Because the EGFP tag is C-terminal to the insert, a start site must be provided and the insert has to be in-frame with the EGFP. To achieve successful protein expression of the CD44-ICD in this plasmid, the untagged CD44-ICD previously cloned was PCR amplified including the start site and

Kozak sequence from the pCMV/myc/cyto vector and subcloned into a pcDNA3.1/V5-His-TOPO vector (Figure 7A).

Primers were carefully designed to amplify sequence upstream the vector ATG start site and include appropriate restriction sites that could be used for directional cloning into the pEGFP-N2 vector. The upstream primer was engineered to include a *Hind III* 5'CAAGCTTTAACTAGAGAACCCGTGGCC3', and the downstream primer included an *Apa I* site: 5′TTCGGGCCCCACCCCAATCTTCATGTCCACATTCTGCAGGTTG3′. The PCR product was subcloned into pcDNA3.1/V5-His-TOPO vector and digested with *Hind III* and *Apa I* restriction enzymes and subcloned into pEGFP-N2 vector. The expected size of the CD44-ICD-EGFP fusion protein was 45 kD (Figure 7B).

1.1.4. Generation of RFP-CD44-ICD

In order to introduce a red fluorescence tag that was N-terminal to CD44-ICD, a pDsRed2-C1 vector (*Clontech*) was used to subclone the CD44-ICD. Taking the previously cloned GFP-CD44-ICD, a double digest using *Hind III* and *Apa I* restriction enzymes was used to cut the CD44-ICD insert from the plasmid, and ligated into an open pDsRed2-C1 vector. After ligation, the plasmid was transformed into chemically competent TOP 10 cells and grown in agar plates containing 100 µg kanamycin.

A.

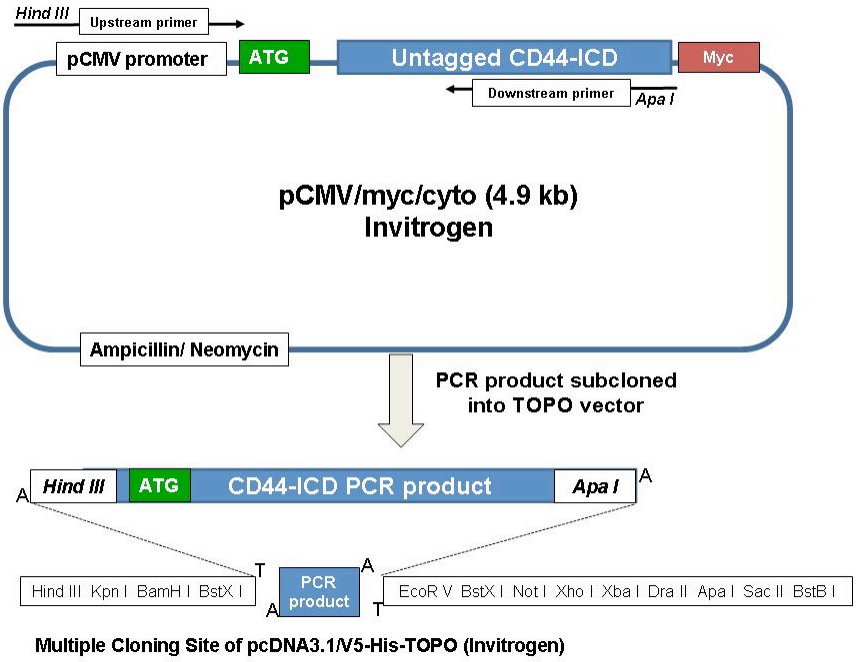

B.

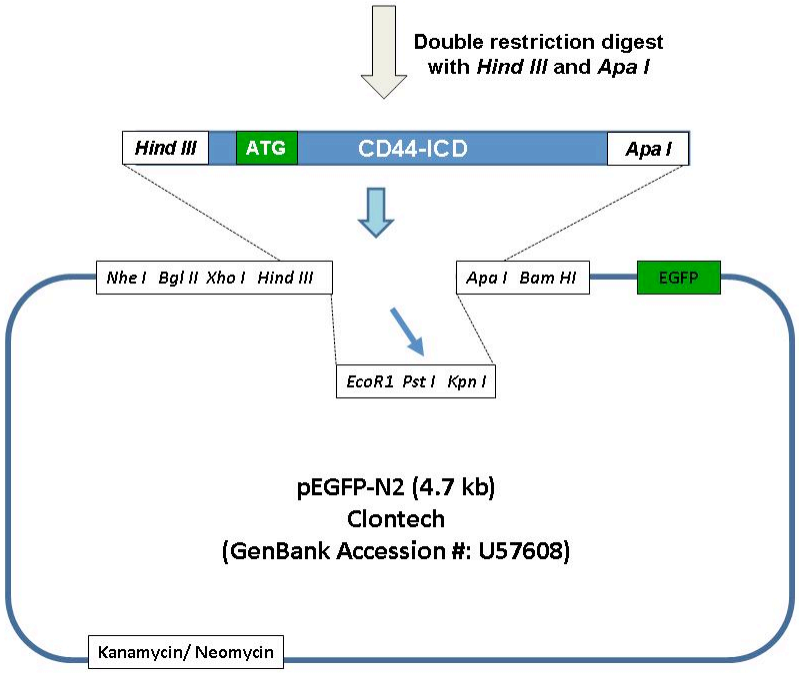

Figure 7: Cloning strategy to generate CD44-ICD-EGFP. **A.** Primers were designed with *Hind III* and *Apa I* sites to amplify the previously cloned CD44-ICD-myc, including the start site from the pCMV/myc/cyto vector. The PCR product was then subcloned into a pcDNA3.1/V5-His-TOPO vector. **B.** A double restriction digest using *Hind III* and *Apa I* removed the CD44-ICD from the TOPO vector. The insert was subcloned into an open pEGFP-N2 vector to generate a CD44-ICD with an EGFP (Enhanced Green Fluorescent Protein) tag at the C-terminus, the CD44-ICD-EGFP.

1.1.5. Generation of CD44-FL-EGFP

In order to visualize the endogenous fragmentation of a full-length CD44 (CD44-FL) and the generation of a CD44-ICD in situ, a CD44-FL-EGFP expression plasmid was prepared in our laboratory, similar to one described above for CD44-ICD-EGFP. To perform this task, CD44-FL within the pCDM8 plasmid was PCR amplified and subcloned in-frame by directional cloning into the pEGFP-N2 plasmid. An upstream primer was designed that included a start/Kozak sequence of the CD44-FL as found in the pCDM8 plasmid with the addition of a *Hind III* restriction site in the 5′ end: 5′CAAGCTTTCGCTCCGGACACC**ATG**GACAAG 3′. The downstream primer was the same as the one used to subclone the CD44-ICD into the pEGFP-N2 plasmid; namely, one that provided in-frame sequence with the C-terminal EGFP and an *Apa I* restriction site: 5′TTCGGGCCCCACCCCAATCTTCATGTCCACATTCTGCAGGTTG3′.

The CD44-FL was PCR amplified using a pCDM8-CD44H as a template and then subcloned into an intermediate pcDNA3.1/V5-His-TOPO plasmid (*Invitrogen*). The CD44-FL insert was then digested using *Hind III* and *Apa I* restriction enzymes (*Invitrogen*) and the gel-purified product ligated into a digested pEGFP-N2 vector. The approximate expected size of the CD44-FL-EGFP fusion protein containing the EGFP epitope tag at the C-terminus is ~120 kD fusion protein.

1.1.6. Generation of GFP-Smad1

Primers were designed to PCR-amplify and subclone human Smad1 from a Smad1 template previously cloned into a pcDNA 3.1/myc-His A (*Invitrogen*). The upstream primer included the ATG start site for Smad1: 5′GCAGATATCGGT ACC**ATG**AATGTGA3′ and the downstream primer included the stop site since the GFP tag is N-terminal to the insert: 5′GCATATTCAGATCCTCTTC**TTA**GATGAG3′. Because the PCR product is larger than 1,000 bp (1471 bp), a high fidelity Pfx Platinum Taq polymerase (*Invitrogen*) was used for amplification, and dATP-tails were added after the amplification step. This last step provided the necessary 3′dA residues necessary for TOPO TA cloning the Smad1 PCR product into a pcDNA3.1/NT-GFP-TOPO vector.

Each reaction included 5 µl of Pfx amplification buffer, 1.5 µl of dNATPs, 1 µl of $MgSO_4$, 0.5 µl of each upstream and downstream primer, 1 µl of DNA template, 0.5 µl of high fidelity Pfx Platinum Taq polymerase and 40 µl of sterile water. The cycling conditions were: initial denaturation of at 94ºC for 2 minutes, followed by 30 cycles of 15 second denaturation at 94 ºC, 30 seconds annealing at 55 ºC and 1 minute extension at 68 ºC. After amplification, the vial was briefly placed on ice and 0.5 µl of ampli Taq DNA polymerase (*Invitrogen*) was added and then incubated at 72ºC for 10 minutes and proceeded to cloning immediately.

1.1.7. Generation of Smad1-EGFP

To generate a Smad1 containing an EGFP (Enhanced Green Fluorescent Protein) tag at the C-terminus, a previously cloned human Smad1 in a pcDNA 3.1/myc-His A plasmid was digested directly with *Hind III* and *Apa I* restriction enzymes for directional cloning into pEGFP-N2 plasmid. The product was gel purified and ligated to a *Hind III* and *Apa I* digested pEGFP-N2 vector. The EGFP tag adds ~30 kD to the 60 kD Smad1 protein to create a ~90 kD fusion protein Smad1-EGFP.

1.2. Conventional Polymerase Chain Reaction (PCR)

A typical PCR reaction included 2 µl of template DNA, 1 µl of each upstream and downstream primers (0.3 µM each), 25 µl of AmpliTaq Gold PCR Master Mix (*Applied Biosystems*), and 21 µl of sterile water. The cycling conditions had an initial denaturation for 2 minutes at 95ºC and a 2 minute annealing cycle at 72 ºC, followed by thirty amplification cycles, each of 1 minute denaturation at 95 ºC, 1 minute annealing at 60 ºC and 1 minute extension at 72ºC. Amplifications were performed using a PTC-100TM Programmable Thermal Controller thermocycler (*MJ Research, Inc.,* Watertown, MA) or using a Mastercycler Pro S thermocycler (*Eppendorf*, Fisher Scientific.). An aliquot of the amplification products were analyzed by electrophoresis on 1.2% agarose gels with products detected by staining with ethidium bromide.

1.3. Agarose gel electrophoresis

Plasmid DNA, PCR products and restriction digests were analyzed by electrophoresis on 1% (for bands larger than 500 bp) or 1.5% (for bands smaller than 500 bp) agarose gels (*IBI scientific*, Peosta, IA) prepared in Tris-Borate EDTA (TBE) buffer containing 5 µl of ethidium bromide. Electrophoresis conditions for most agarose gels were typically 1 hour at 80 V. The stained products were scanned and quantified using a fluorimaging system (Chemi-Doc, *Bio-Rad*, Hercules, CA) and compared to a 100 bp DNA ladder standard (*ID Labs,* Carlsbad, CA). Band intensities of digitized images were quantified using Quantity-One software (Bio-Rad).

1.4. Cloning and transformation

Following PCR amplification, CD44-ICD was sublconed into a pcDNA3.1/V5-His-TOPO vector using the TOPO® cloning reaction kit provided with the vector. Each reaction consisted of 2 µl of fresh PCR product, 1 µl of salt solution, 1 µl of sterile water and 1 µl of TOPO® vector. The reaction was incubated for five minutes at room temperature, and then placed on ice and proceeded to One shot® chemical transformation (*Invitrogen*).

Two µl of the TOPO® cloning reaction were mixed into a vial of One shot® TOP10 Chemically Competent *E. coli* (*Invitrogen*), and incubated on ice for 5 minutes. Cells were heat-shocked for 30 seconds in a 42ºC water bath, and immediately transferred to ice for one minute. A 250 µl aliquot of room temperature super optimal culture (SOC)

media was added to the cells and incubated at 37ºC while shaking horizontally at 200 rpm for one hour. Different volumes (25 µl, 50 µl, 75 µl and 100 µl) were spread onto pre-warmed agar plates containing ampicillin (100µg/ml) and incubated at 37ºC overnight. Five colonies were randomly selected for DNA purification and analysis.

1.5. Plasmid preparations

1.5.1. Miniprep:

Selected colonies were stabbed with an applicator stick, mixed with 4 ml of Luria Broth (LB) media containing ampicillin (100µg/ml) and grown overnight at 37ºC with shaking. Plasmid DNA was isolated and purified using a miniprep kit (*Qiagen*, Hilden, Germany). Two milliliters of the cultured bacteria were centrifuged at 6,800 x g for 3 minutes in a conventional table-top microcentrifuge at room temperature. The bacterial pellet was re-suspended in 250 µl of re-suspension buffer (buffer P1) by pipetting up and down several times. A 250 µl aliquot of lysis buffer (buffer P2) was added to the mix and inverted 4-6 times vigorously. Next, 350 µl of neutralization solution (buffer N3) was added and mixed thoroughly by vigorously inverting the tube 4-6 times, and centrifuged at 13,600 x g for 10 minutes.

The supernatant was added to a spin column provided in the kit and centrifuged for 1 minute. The flow-through was discarded and the spin column was washed by adding 500 µl of buffer PB and centrifuged for an additional minute. The spin column was washed with 750 µl of wash buffer (buffer PE) and centrifuged for another minute. The column was placed in a new 1.5 ml microcentrifuge tube, and 50 µl of elution buffer

(buffer EB) was added to the spin column and incubated for 1 minute at room temperature to elute the DNA. The tube was centrifuged for an additional minute at full speed (~13,000 x g) and the 50 µl of eluted DNA was collected in the centrifuge tube.

To estimate the yield, 10 µl of plasmid DNA were diluted into 490 µl of water and the absorbance at 260 and 280 nm was read on a spectrophotometer. To determine the purity of the sample, the 260/280 ratio was expected to be between 1.7-1.9. Ratios below 1.7 suggest that the sample is contaminated with protein, and ratios above 1.9 suggest that the sample may contain substantial amounts of RNA. The amount of plasmid DNA was calculated by multiplying the dilution factor, absorbance reading at 260 nm and extinction coefficient of DNA (50 µg/ml). Typical DNA concentration varies between 0.1-0.3 µg/ml.

1.5.2. Maxiprep:

To purify higher plasmid DNA from higher volumes of bacteria, a maxiprep DNA purification kit was used (*Qiagen*). A 200 µl aliquot of inoculated bacteria grown for a miniprep was added to 100 ml of LB media containing ampicillin (100 µg/ml) and incubated overnight at 37ºC while shaking vigorously. The bacteria were harvested by centrifugation at 3,000 x g for 15 minutes at 4˚C. The pellet was re-suspended in 10 ml of re-suspension solution (buffer P1) and mixed by pipetting up and down. A 10 ml aliquot of lysis buffer (buffer P2) was added and mixed by vigorously inverting the sealed tube 4-6 times, and incubated at room temperature for 5 minutes.

Briefly, 10 ml of pre-chilled neutralization solution (buffer P3) was added to the lysate and mixed immediately by vigorously inverting 4-6 times. The lysate was immediately poured into the barrel of a filter cartridge with a cap screwed to the outlet nozzle provided in the kit, and incubated at room temperature for 10 minutes. The cap was removed from the cartridge and the plunger was gently inserted to filter the cell lysate, which was collected in a sterile 50 ml tube. Approximately 25 ml of cell lysate was recovered after filtration. Then 2.3 ml of buffer ER was added to the filtered lysate, mixed by inverting the tube 10 times and incubated on ice for 30 minutes.

During the 30 minutes incubation time, a QIAGEN-tip 500 provided in the kit was equilibrated by adding 10 ml of equilibration buffer (buffer QBT) and allowed to empty by gravity flow. After the 30 minutes incubation was over, the filtered cell lysate was added to the QIAGEN-tip 500 and allowed to enter the resin by gravity flow. The QIAGEN-tip 500 was washed twice with 30 ml of wash buffer (buffer QC), and then 15 ml of elution buffer (buffer QN) was added to elute the DNA, which was collected in a 50 ml endotoxin-free tube. To precipitate the DNA, 10.5 ml of room-temperature isopropanol were added to the eluted DNA, mixed and centrifuged at 13,000 x g for 30 minutes at 4ºC. The DNA pellet was washed with 5 ml of endotoxin-free room temperature 70% ethanol, and centrifuged at 11,000 x g for 10 minutes. The pellet was air-dried for about 10 minutes and re-dissolved in 400 µl of endotoxin-free buffer TE.

To estimate the yield, 10 µl of plasmid DNA were diluted into 490 µl of water and the absorbance at 260 and 280 nm was read on a spectrophotometer. To determine the

purity of the sample, the 260/280 ratio was expected to be between 1.7-1.9. Ratios below 1.7 suggest that the sample is contaminated with protein, and ratios above 1.9 suggest that the sample may contain substantial amounts of RNA. The amount of plasmid DNA was calculated by multiplying the dilution factor, absorbance reading at 260 nm and extinction coefficient of DNA (50 µg/ml). The DNA concentration of plasmids isolated by this maxiprep method varied between 0.5-2.0 µg/ml.

1.6. Restriction digests

Restriction endonuclease digestions were performed to cut inserts from plasmids, to detect the presence of an insert in a plasmid, or to verify the orientation of the insert in the plasmid. All restriction enzymes were from *Invitrogen* and buffers used were those provided with the enzymes (numbered 1-10). The restriction digest products were visualized on 1-1.5% agarose gels stained with ethidium bromide.

1.6.1. Sal I and *Not I*

Because these two enzymes work under different buffer conditions, a sequential double digest was performed for buffer adjustment. This double sequential digest was used to remove the CD44-ICD insert from the pcDNA3.1/V5-His-TOPO vector and subclone into the pCMV/Myc/cyto vector. To set up the digest, 2 µl of plasmid (~1-4 µg) was mixed with 2 µl of *Not I* restriction enzyme, *2* µl of buffer 3 (50 mM Tris-HCl, 10 mM $MgCl_2$, 100 mM of NaCl, at 8.0 pH), 11.3 µl of water, and incubated at 37ºC for 1 hour. After this incubation, 2µl of *Sal I* restriction enzyme and 0.7 µl of buffer 10 (100 mM

Tris-HCl, 10 mM $MgCl_2$, 150 mM of NaCl, at 7.6 pH) was added to the mixture and the mixture incubated at 37ºC for an additional 2 hours or overnight.

1.6.2. Pvu II

This digest was used to verify whether the CD44-ICD was properly cloned into the TOPO vectors in the 5'→3' direction. *Pvu II* cuts within the CD44-ICD once, between bases 175 and 176 (G-C) of the 233 bp cytotail insert, and three times within the pcDNA3.1/V5-His-TOPO vector. If the CD44-ICD was successfully cloned in the 5'→3' direction, a 472 bp and a 3119 bp bands would be produced, whereas a 536 bp and 3005 bp bands would appear if the ICD was cloned in the 3'→5' direction.

Each reaction included 1 µl of plasmid DNA, 2 µl of *Pvu II* restriction enzyme, 2 µl of buffer 6 and 15 µl of sterile water. The digest was incubated for 2 hours or overnight at 37ºC.

1.6.3. Hind III and *Apa I*

This double restriction digest was used for directional cloning of both CD44-ICD and CD44-FL into the pEGFP-N2 vector and pDsRed2-C1. Because both restriction enzymes were compatible, so there was no need to perform a sequential digest. Each reaction included 2 µl of DNA, 2 µl of *Hind III* restriction enzyme, 1 µl of *Apa I* restriction enzyme, 2 µl of buffer 4 and 13 µl of sterile water. The sample was incubated at 37 ºC for 2 hours or overnight.

1.7. Gel extraction and purification

The 233 bp fragment CD44-ICD was visualized on 1.5 % agarose gels stained with ethidium bromide and excised (under UV light and behind a light shield) using a sterile scalpel and purified using QIAEX II Agarose Gel Extraction kit (*Qiagen*). The gel slice was placed in a sterile microcentrifuge tube and weighed. Three volumes of buffer QX1 were added to 1 volume of gel (i.e. 300 µl of buffer QX1 were added for each 0.1 g of gel), followed by 30 µl of QIAEX II solution. The mix was incubated at 50ºC for 10 minutes, vortexing every 2 minutes to keep QIAEX II in suspension to melt the agarose. The sample was then centrifuged for 1 minute at 12,000 x g, and the supernatant was carefully removed with a pipette to separate the DNA (pellet). The pellet was washed once with 500 µl of buffer QX1 and twice with 500 µl of buffer PE, with a centrifuge step of 1 minute at 12,000 x g in between washes.

The pellet was allowed to air-dry for 10-15 minutes until it became white. Then, 20 µl of sterile water was added, the tube vortexed to re-suspend the pellet, and incubated for 5 minutes at room temperature. The tube was centrifuged for an additional minute under same conditions. The supernatant containing the purified DNA was then transferred to a new sterile tube and used for ligation.

1.8. DNA ligation of inserts into plasmids

In order to ligate the purified CD44-ICD insert into the pCMV/myc/cyto vector, the same double sequential restriction digest was performed on the empty vector to open

up the multiple cloning site between the *Sal I* and *Not I* restriction sites. Once the empty vector was digested and the CD44-ICD insert was purified, 2.4 µl of the open vector was combined with 12 µl of the purified insert (5 fold insert: vector), 1 µl of *T4 DNA ligase* enzyme (*Invitrogen*), 4 µl of *T4 DNA ligase* buffer and 0.6 µl of sterile water and incubated overnight at room temperature. After ligation, the plasmid was transformed into chemically competent One Shot® TOP10 *E. coli* bacteria.

1.9. Characterization of plasmid constructs

Once colonies were detected following transformation, typically 5 random, well spaced colonies would be expanded as minipreps. The plasmids purified from these minipreps would then be characterized by a variety of methods to insure the presence and orientation of the insert. Most often, a restriction digest was performed using the restriction sites engineered into the PCR primers that were used to PCR amplify the insert. This method was used to verify whether the insert was successfully cloned in the target vector.

Alternatively, the plasmid would be used as a template for PCR amplification using these same PCR primers and the presence of insert detected as a PCR product on agarose gels. In addition, a single digest with *Pvu II*, which cuts once within the CD44-ICD insert, was used to verify the cloning direction of CD44-ICD as, discussed in 1.6.2. Plasmids were also characterized by DNA sequencing (Department of Biology Core, ECU) using either universal primers (T3, T7 and SP6 sequences within expression plasmids) or the PCR amplifying primers that we supplied. Lastly, plasmids were

transfected into different cell lines and protein expression of the insert detected by immunohistochemistry or western blotting.

2. Site directed mutagenesis

In order to introduce site directed mutations into a sequence, the GeneTailor™ Site Directed Mutagenesis System from *Invitrogen* was used. This system allows introduction of specific CD44-ICD mutations by using pCMV/myc/cyto-CD44-ICD vector as a template and incorporating the desired mutation site within the upstream primer. Three point mutations where targeted in the CD44-ICD sequence to produce a non-relevant peptide, a CD44-ICD with a mutated ERM binding domain and a CD44-ICD with a mutated ankyrin binding domain.

*2.1. **Mutation strategies***

2.1.1. Point mutation used to generate a non-relevant control peptide

As a negative control, a ~15 kD non-relevant peptide was generated to ensure that any biological changes resulting from CD44-ICD over-expression were specific to the CD44-ICD sequence and not due to over-expression of a 15 kD fragment. Using pCMV/myc/cyto-CD44-ICD vector as a template, a single base pair was added at the beginning of the coding sequence of the CD44-ICD, creating a frame-shift that was predicted to translate a new, unique irrelevant protein but one with identical translation initiation properties of the CD44-ICD construct.

Computer-based translation predictions suggested that the frame shift would generate an open reading frame that would encounter a stop codon close to the natural stop codon of CD44-ICD. Thus, the control peptide would differ in size from the CD44-ICD by only a few amino acids. The mutation primer (extra dG shown in bold) was: 5′CCCGTGGCCACCATGGCCCA**G**GGTGCAGCTGCAG3′ and the partially-overlapping opposite strand primer was: 5′TGGGCCATGGTGGCCACGGGTTCTCG3′.

2.1.2. Point mutation used to destroy CD44 ERM binding domain mutations

Yonemura and colleagues believed that positively charged juxta-membrane amino acids in the cytoplasmic sequence of proteins known to bind to ERM proteins, are necessary for proper ERM binding. In the CD44 sequence, the three lysine (K) residues located just distal to the transmembrane domain are believed to be crucial for CD44 binding to ERM, as mutating the $K^{298}K^{299}K^{300}$ to $Q^{298}I^{299}N^{300}$ resulted in no CD44-ERM binding (Yonemura et al., 1998). For this reason, our mutating strategy was targeted to the positively charged residues KKK to QIN, as suggested by the previous study.

Using pCMV/myc/cyto-CD44-ICD vector as a template, an upstream primer containing the ERM binding domain mutation (bold) was designed: 5′AGTCGAAGAAGGTGTGGGCAG**CAGACAAAC**CTAGTGATCAA3′ and the partially-overlapping downstream primer was: 5′CTGCCCACACCTTCTTCGACTGTTGACTGC3′.

2.1.3. Point mutation used to destroy CD44 Ankyrin binding domain mutations

Studies addressing the crucial amino acids in the ankyrin binding domain of CD44 included truncated versions of the CD44 sequence rather than point mutations, and therefore to our knowledge, the critical amino acids that serve as binding sites are still unknown. We sought to target plausible residues within the putative ankyrin binding domain of CD44. Given that a cluster of three positively charged amino acids were determined to be crucial in CD44 binding to ERM adaptor proteins, we targeted twin basic residues in the ankyrin binding domain sequence of CD44 as a reasonable first approach: Arg^{313}-Lys^{314}. Following a similar strategy to the point mutations of the ERM binding domain, we mutated these two residues to Ile^{313}-Asn^{314} by using pCMV/myc/cyto-CD44-ICD vector as a template, an upstream primer containing the ankyrin binding domain mutation (bold): 5′AATGGAGCTGTGGAGGAC**ACAAAC**CCAAGTGGACTC3′ and the partially-overlapping downstream primer was: 5′GTCCTCCACAGCTCCATTGCCACTGTTG3′.

*2.2. **Methylation reaction***

An initial step in the site-directed mutagenesis procedure is methylation of the parental, target plasmid DNA. In this way, the daughter strands that are generated and contain the mutation can be separated from the original template DNA by selective degradation of methylated DNA. The DNA methylase enzyme, methylates cytosine residues throughout the double-stranded plasmid DNA sequence. The plasmid DNA was methylated by mixing 1 µl (100 ng) of plasmid DNA, 1.6 µl of methylation buffer, 1.6

µl of 10x SAM, 1 µl of DNA methylase and 10.8 µl of sterile water, and incubated at 37ºC for one hour.

2.3. ***Mutagenesis reaction and PCR parameters***

The next step in site directed mutagenesis included a PCR reaction using the methylated plasmid DNA as a template and the partially-overlapping primers containing the mutation site. A high fidelity Platinum *Taq* DNA polymerase was recommended for plasmids up to 8 kb, which would include our pCMV/myc/cyto at 4.9 kD. Each PCR reaction included 5 µl of 10X high fidelity PCR buffer, 1.5 µl of 10 mM dNTP, 1 µl of 50 mM $MgSO_4$, 1.5 µl of each upstream and downstream primer, 2 µl of methylated plasmid DNA, 0.5 µl of high fidelity Platinum *Taq* DNA polymerase and 37 µl of sterile water. The PCR parameters included an initial denaturation for 2 minutes at 94ºC, followed by 20 amplification cycles, each of 30 seconds denaturation at 94 ºC, 30 seconds annealing at 55ºC and a 5 minute (1 minute/ 1 kb DNA) extension at 68ºC, followed by an additional 10 minute extension at 68ºC. Amplifications were performed using a PTC-100TM Programmable Thermal Controller thermocycler (*MJ Research, Inc.,* Watertown, MA).

2.4. ***Transformation of mutated plasmids and destruction of template DNA***

One Shot® MAX Efficiency® DH5á™-T1^R competent cells were used for transformation of the amplified mutated plasmid. These bacteria were used because

they selectively degrade methylated plasmid DNA. Thus, any positive colonies will be derived from bacteria containing non-methylated plasmid. Each vial of cells (1 per transformation) was thawed on ice for 5-7minutes, and 2 µl of the mutagenesis PCR product was added to a vial of cells and mixed by tapping gently.

The vial was incubated on ice for 10 minutes and then heat shocked for 30 seconds at 42ºC. The vial was then placed on ice for an additional minute, and 200 µl of pre-warmed SOC media was added to the cells. Cells were incubated at 37ºC while shaking horizontally at 200 rpm for one hour. Different volumes (25 µl, 50 µl, 75 µl and 100 µl) were spread in pre-warmed agar plates containing ampicillin (100µg/ml) and incubated at 37ºC overnight. Five colonies were randomly selected for plasmid purification and analysis.

3. Cell Culture and Design of Cell-Based Experiments

*3.1. **Bovine articular chondrocytes***

3.1.1. Tissue digestion and cell isolation

Bovine articular chondrocytes (BAC) were isolated from the metacarpophalangeal joints of 18-24 month old bovine steers that were obtained from a local slaughterhouse and stored for 1-3 days until dissection. Hooves were washed, skinned and sanitized with 70% ethanol. After being placed in a hoof holder under a dissection hood, an incision was made to cut the exposed anterior and lateral ligaments and the synovial capsule. Using a sterile scalpel, 10 mm deep slices were removed

from both upper and lower condyles and placed into sterile cups containing 0.9% $NaCl_2$ solution. After removing most of the articular cartilage, the dry weight was obtained and the tissue was then digested for one hour in 0.4% pronase (*EMD scientific*, San Diego, CA) solution prepared in serum free Dulbeco's Modified Eagle's Medium/Ham's F12 medium (*Mediatech*, Manassas, VA) at 37 ºC in a 5% CO_2 environment while stirring, in order to isolate the cells from the complex extracellular matrix. Tissue was washed twice with serum free media and then incubated overnight in 0.025% collagenase P (*Roche*, Indianapolis, IN) solution under the same conditions.

The tissue/collagenase mixture was next pushed through a 100 µm strainer to remove large debris and the liberated cells collected in a sterile 50 ml tube. Cells were centrifuged for 5 minutes at 1,300 x g and washed twice in serum free DMEM/Ham's F12 medium. After the second wash, cells were pushed through a 40 µm cell strainer and cells were centrifuged for another 5 minutes. The cell pellet was re-suspended in chondrocyte feeding media (CFM), which is prepared in DMEM/Ham's F12 medium containing 10% Fetal Bovine Serum (*Hyclone*, South Logan, UT), 1 ug/ml ascorbic acid and primocin. Cells were counted using a hemocytometer and either plated as a high density monolayer (2.0×10^6 cells/cm^2) or cultured in alginate beads.

3.1.2. Alginate beads culture

After the last centrifugation step in the chondrocytes isolation, $4x10^6$ cells were re-suspended in 1 ml of an 1.2% alginate solution (*Kelco*, Chicago, IL) prepared in 150 mM NaCl. The alginate/cell mix was passed through a 22 gauge syringe and collected in 30 ml of 102 mM calcium chloride prepared in 0.9% $NaCl_2$ to form small alginate beads, each containing approximately 40,000 chondrocytes per bead. Beads were transferred to a culture dish containing CFM and incubated for at least 48 hours.

In order to release cells from the beads to use for experiments, beads were removed from CFM and washed twice in serum free culture media. The beads were then re-suspended in a dissociation buffer (0.055 M sodium citrate, 0.15 M NaCl, pH 6.8) and mixed gently until beads were no longer visible. Released cells were collected by centrifugation for 5 minutes at 1,300 x g and washed twice with sterile PBS. Cells were plated in CFM as needed for experiments.

3.1.3. Passaging of BACs to obtain dBACs

Cells that were not grown in alginate bead cultures, were plated at either high density (2.0×10^6 cells/cm^2) or low density (0.5×10^6 cells/cm^2) in 10% FBS-CFM. High density cultures were able to preserve the typical round chondrocyte morphology for several days, and therefore were used for primary chondrocyte experiments. When

cells were plated at low density, they slowly began to lose the cortical cytoskeleton and began to de-differentiate into more fibroblast-like cells (dBACs).

In some studies the dBACs were passaged using trypsin and grown at low density. Passage number was recorded and labeled P0 for primary BAC cultures (no passages) or P1, P2, P3 for consecutive passages of dBACs.

3.2. **Other cell lines used**

Several other cell lines were used in conjunction with BACs. COS-7 cells (African green monkey kidney epithelial cells, obtained from *American Type Culture Collection*), a *SV40*-immortalized cell line, allow for a high level of transfection efficiency and high protein expression of plasmid constructs with an SV40 promoter, which allows substantial replication of the vector by the large T-antigen. Another useful property of COS-7 cells is the lack endogenous CD44 expression (Jiang et al., 2002) eliminating background expression of endogenous CD44 isoforms or domains.

Two chondrocyte-like cell lines were used in this study. The rat chondrosarcoma cell line (RCS) was a continuous long term culture line derived from the Swarm rat chondrosarcoma tumor (Choi et al., 1971). The RCS cell line in the Knudson laboratories was a gift of Dr. James H Kimura (formerly of Rush University Medical Center) and represented an early clone of these cells that eventually became known as

long-term culture RCS (Kucharska et al., 1990). Another chondrocyte line used was the human immortalized chondrocyte line (C28/I2). The C28/I2 cells were derived from *SV40*-immortalization of primary cultures of human juvenile costal chondrocytes and subsequent selection by suspension over agarose (Goldring et al., 1994). The C28/I2 cells maintain some but not all phenotypic properties of adult chondrocytes while at the same time allowing continuous growth in culture and high transfection efficiency. The C28/I2 cells were a generous gift from Dr. Mary Goldring, Hospital for Special Surgery, N.Y.

All these cell lines were cultured in Dulbecco's Modified Eagle's Medium (DMEM) (*Mediatech*) containing 10% FBS (*Hyclone*) and 1% L-glutamine and penicillin-streptomycin, and incubated at 37ºC in a 5% CO_2 environment and passaged at confluence using 0.25% trypsin/ EDTA.

4. Treatment of cells to induce/inhibit CD44 cleavage

Cells grown in monolayer cultures in complete medium were switched to serum-free culture media and then treated overnight with 10 ng/ml of Interleukin-1β (IL-1 β) (*R&D systems*), 250 µg/ml of HA oligosaccharides from rooster comb HA (*Sigma*) or 10 nM of phorbol myristate acetate (PMA) to induce proteolysis of either endogenous or exogenous CD44.

In order to inhibit CD44 proteolytic cleavage *in vitro,* cells were detached from the monolayer using collagenase/pronase treatment for 3 hours and then plated overnight in culture media containing 1 μM of a general MMP inhibitor GM6001 (*EMD chemicals*) and/or 10μM of a γ-secretase inhibitor DAPT (*EMD chemicals*). After treatment, cells were lysed and proteolytic cleavage was detected by western blotting.

5. Hyaluronidase treatment

Cells were plated in a monolayer for at least 24 hours. A solution of 200 U/ml of bovine testicular hyaluronidase (HA'ase) or 5 U/ml of *Streptomyces* HA'ase (*Sigma*) prepared in serum free media was added to the monolayer for 90 minutes. Cells were either lysed or fixed after treatment and compared to a non-treated control.

6. Transient transfection

Cell transfection was obtained by using nucleofection technology (Lonza, Germany), which allows delivery of plasmid DNA directly into the nucleus. Cells were cultured to reach ~90% confluency and then detached from the plate surface by trypsin-EDTA treatment for 5 minutes, or in the case of BAC by pronase/collagenase (10 mg each) treatment for 1 hr in at 37^{o}C in a humidified cell incubator. Cells were then centrifuged for 5 minutes at 1,300 x g and the pellet was re-suspended in 10 ml of DMEM to perform a cell count.

Each transfection included 4 µg of plasmid DNA and $1x10^6$ cells ($2x10^6$ cells for BACs) re-suspended in 100 µl of room temperature Amaxa Cell Line Nucleofector® Kit V reagent (for transfection of cell lines) or Amaxa Human Chondrocyte Nucleofector® Kit reagent (for BAC). In some experiments, 1 µg of empty vector pEGFP-N2 plasmid was mixed with 3 µg of the desired plasmid DNA (total of 4 µg). These conditions were used to estimate transfection efficiency when the desired plasmid carried no fluorescent label. The mixture was transferred to an Amaxa cuvette and immediately placed in the cuvette holder of the Amaxa Nucleofector® Device.

The appropriate program was selected (COS-7, RCS, C28/I2 used A-024; BAC used U-028) and nucleofection initiated. Immediately after nucleofection, 500 µl of pre-warmed 10% FBS RPMI media (*Mediatech*) was added to the cuvette. Using the provided plastic pipette, the transfected cells were transferred to a 6 well plate containing pre-warmed 10% FBS culture media, or CFM for BACs. Twenty-four hours after transfection, the cells were observed using a Nikon TE2000 inverted phase-contrast fluorescence microscope to estimate transfection efficiency. Typically, cells were lysed 48 hours after transfections and lysates used for protein detection by western blotting.

7. Stable transfection

The Flp-In™ system from *Invitrogen* was used to create stable CD44-ICD transfectants in HEK-293 cells and RCS cells. This system involves introduction of a Flip Recombination Target (FRT) site into the desired mammalian cell line, followed by

expression of a vector containing the gene of interest, which is then incorporated into the genome by using Flp recombinase-mediated DNA recombination at the FRT site. The HEK-293 cells were purchased from Invitrogen with an FRT site already cloned into their genome and available for use. The RCS required stable transfection of a FRT site; generating a RCS FRT host cell line.

7.1. ***FRT-ICD cloning strategy***

Our laboratory subcloned the CD44-ICD from the pCMV/myc/cyto-CD44-ICD vector that I generated, into a pcDNA5 shuttle vector (pcDNA5/FRT-CD44-ICD) for recombination with HEK-293-FRT and RCS-FRT host cell lines.

7.2. ***FRT host cell lines***

The p*FRT/lacZeo* plasmid was stably transfected (following Amaxa transfection protocol) into the RCS host cell line. Following transfection, the cells were cultured in 10% FBS DMEM containing 100 ug/m of the selection reagent, zeocin. Once the FRT site is integrated into the genome, the cells become zeocin resistant. Even after selection, the HEK-293-FRT and RCS-FRT routinely cultured in 10% FBS DMEM still containing zeocin in 37ºC and 5% CO_2 environment.

7.3. ***Transfection and expression of FRT-ICD in host cell lines***

Once the FRT host cell lines were selected by growing in 10% FBS DMEM containing zeocin, the cells were used to generate stable transfectants using the Flp-In™ method designed by Invitrogen. Briefly, 1 x10^6 HEK-293-FRT or RCS-FRT host cells were re-suspended in 100 µl of Amaxa Cell Line Nucleofector® Kit V reagent together with 4 µg of pcDNA5/FRT-CD44-ICD plasmid and 36 µg of pOG44. The mixture was transferred to an Amaxa cuvette and transfected by Amaxa nucleofection using program A-024 (for both HEK-293-FRT and RCS-FRT cell lines). Following nucleofection, the cells were mixed immediately with 500 µl of pre-warmed 10% FBS RPMI media and transferred to a 6 well plate containing pre-warmed 10% FBS DMEM media. After 24 hours, fresh media was added.

7.4. ***Selection of stable transfectants***

Forty-eight hours after transfection, the cells were trypsinized and split into a 6-well plates at less than 25% confluence. Cells were cultured in hygromycin (200 µg/µl) containing media for several weeks, changing the media every 3-4 days. The co-transfected pOG44 provided expression of a FRT recombinase, an enzyme that catalyzed the homologous recombination of the FRT site (localized within the host cell genome) and the pcDNA5/FRT-CD44-ICD plasmid. Once incorporated, the pcDNA5/FRT-CD44-ICD plasmid contains a hygromycin resistance, and therefore only successfully transfected cells containing this plasmid continue to grow.

8. Immunofluorescence staining

Cells were fixed in 2% paraformaldehyde (PFA) for 30 minutes at 4ºC, quenched with 0.2 M glycine in PBS and then blocked in 1% bovine serum albumin (BSA, *Sigma*) in PBS for 30 minutes at room temperature or overnight at 4ºC. Cells were permeabilized with 0.2% triton X-100 in TBS for 10 minutes at room temperature and then washed twice with PBS. For antibody detection, cells were incubated with primary antibody for 1 hour at room temperature, washed twice with PBS and then incubated with a secondary antibody. For staining of the actin cytoskeleton using rhodamine-phalloidin (*Invitrogen*), cells were permeabilized and then incubated with rhodamine-phalloidin (1:150 dilution in PBS) for 1 hr at room temperature, and then washed twice with PBS.

After the last wash, cells were mounted in mounting media containing the blue fluorescence nuclear stain; 4′, 6-diamidino-2-phenylindole, dihydrochloride (DAPI, *Molecular probes*) and visualized using a Nikon Eclipse E600 microscope equipped with Y-Fl Epi-fluorescence (Melville, NY). Images were taken digitally in real time using a Spot-RT camera (Diagnostic Instruments, Sterling Heights, MI) and processed using NIS Elements BR imaging software (Nikon, Lewisville, TX).

9. Assays to study pericellular coat retention

9.1. ***Particle exclusion assay***

The particle exclusion assay was used to evaluate the ability of stable and transient CD44-ICD chondrocyte (BACs and RCS) transfectants to retain their pericellular matrix. Cells were plated at 50% confluence in a 6-well plate under normal cell culture conditions. The medium was then removed, and a 750 µl suspension of fixed horse red blood cells were added to each well. The plate was placed under the inverted phase contrast microscope and allowed to settle for 15 minutes. The small red blood cell particles settle onto the tissue culture substratum, but are restricted from a region surrounding the cell plasma membrane. The otherwise translucent space between the plasma membrane and the red blood cells consists of cell-associated extracellular matrix, sometimes referred to as the "pericellular matrix". The live cells and their pericellular matrices were observed and imaged using a Nikon TE2000 inverted phase contrast microscope.

9.2. ***Hyaluronan Binding Protein (HABP) assay***

Since HA is a glycosaminoglycan with no core protein, it cannot be detected using a typical antibody approach. Methods are available to visualize HA through the use of proteins that contain HA-binding sites known as link domains. One popular, commercial product is biotinylated-HABP, a fragmented derivative of bovine aggrecan/link protein complex. In this study, biotinylated-HABP was added to cultured cells to visualize HA within the pericellular matrix. For this assay, transient or stable

CD44-ICD transfectants were plated on a 4-well chamber slide at 50% confluence and cultured for 24 hours. The cells were fixed in 2% paraformaldehyde (PFA) for 30 minutes at 4ºC, quenched with 0.2 M glycine in PBS and then blocked in 1% bovine serum albumin (BSA, Sigma) in PBS for 30 minutes at room temperature. Biotinylated-HABP (Seikagaku USA, Ijamsville, MD) at a 2 µg/ml concentration was added to the cells, and incubated for one hour at 4ºC.

Cells were washed with PBS and then incubated with neutravidin-FITC (1:1,000) (Molecular Probes) in 1% BSA in PBS for 30 minutes at 4ºC. The cells were then washed with PBS and mounted in mounting media containing DAPI, and visualized using a Nikon Eclipse E600 microscope equipped with Y-FI Epi-fluorescence. Images were captured digitally in real time using a Spot-RT camera and processed using NIS Elements BR imaging software (*Nikon*, Lewisville, TX).

10. Protein analysis

10.1. ***Preparation of total protein cell lysates from cell cultures***

Cultured cells were lysed using a commercial 1X lysis buffer (*Cell Signaling*) containing 1X protease and phosphatase inhibitors (*Pierce*). For differential extractions or immunoprecipitation assays, other detergent buffers were used (below). After removing the media, cells were scraped from the surface using sterile cell scrapers and 200 µl (for each well of a 6 well plate) of lysis buffer with inhibitors were added to the

plate. Cells were re-suspended in lysis buffer, transferred to a microcentrifuge tube and incubated on ice for 10 minutes. Cells were then centrifuged at 13,600 x g for 10 minutes at 4ºC and supernatant was collected as the cell lysate, and protein concentration was determined by protein concentration assay.

10.2. ***Protein concentration assay***

Following cell lysis, a 25 µl aliquot per sample was used to determine the protein concentration using a BCA kit protein concentration assay (*Pierce*). On a 96-well plate, 9 aliquots of sequential 1:10 dilutions of Bovine Serum albumin (BSA) in lysis buffer were set up as a standard. A working reagent was prepared by mixing 50 parts of BCA (bicinchoninic acid) reagent A with 1 part of reagent B, and then 200 µl of working reagent was added to each well. The plate was incubated for 30 minutes at 37ºC and then the absorbance was read at 562 nm on a plate reader as the strong purple BCA reaction exhibits a strong linear absorbance at 562 nm with increasing protein concentrations.

10.3. ***Gel electrophoresis and western blotting***

Depending on the experiment, equal protein (10-30 µg) or equal volumes of protein lysate were mixed with 10 µl of NuPAGE® LDS sample buffer, 4 µl of NuPAGE (10X) reducing agent (for running gels under reducing conditions) and enough deionized water to add to a total of 40 µl per sample. Samples were heated for 10 minutes at

70ºC and then loaded into a 4-12% NuPAGE® Novex® Tris-acetate gradient mini gel (*Invitrogen*). Electrophoresis times were typically ~45 minutes at 200V at room temperature. Running buffer was prepared by adding 50 ml of 20X NuPAGE® MES running buffer to 950 ml of deionized water. When running under reducing conditions, 500 µl of NuPAGE® antioxidant was added to 200 ml of 1X NuPAGE® MES running buffer.

Following electrophoresis, proteins within the acrylamide gel were transferred to a nitrocellulose membrane using a Criterion blotter apparatus (BioRad). The gel was placed in a cassette between blotting paper and nitrocellulose membrane, and current applied at 100 V in 4ºC for 1 hour and 20 minutes. The nitrocellulose membrane was blocked in 5% non-fat dry milk in Tris buffered saline containing 0.1% Tween 20 (TBS-T) for 1 hour while shaking at room temperature. The membrane was washed once in TBS-T for 10 minutes and then twice for 5 minutes at room temperature while shaking. The blot was incubated with primary antibody (table 1) prepared in 5% BSA-TBS-T overnight at 4ºC while shaking.

The following day, the blot was again washed once in TBS-T for 10 minutes and then twice for 5 minutes at room temperature while shaking and then incubated with corresponding secondary antibody prepared in TBS-T for 30 minutes at room-temperature while shaking. The blot was washed once again, and detection was performed using enhanced chemi-luminescence (ECL) reagents (*Invitrogen*). Often

reacted / detected blots would be re-probed using a different primary antibody. To re-use the same blot for another antibody reaction, the original antibodies and reagents on the blot were removed with stripping buffer containing glycine and aliphatic carboxylic acid (*Invitrogen*) for 15 minutes while shaking at room temperature. The blot was then washed and blocked in 5% low fat dry milk and incubated overnight with a different primary antibody.

10.4. ***Differential extractions***

Cells were lysed first in 200 µl of a light-detergent buffer containing 50 mM Tris-HCl, 150 mM NaCl, 5 mM EDTA, 0.1% Igepal (previously known as NP-40) and 1X protease inhibitor cocktail (*Pierce*), and incubated on ice for 10 minutes. Cells were then centrifuged for 10 minutes at 1,300 x g, and supernatant was collected as the “light extraction”. The pellet was re-suspended in 200 µl of a harsher-detergent buffer containing 50 mM Tris-HCl, 150 mM NaCl, 5 mM EDTA, 0.5% Igepal (previously known as NP-40), 1% Empigen and 1X protease inhibitor cocktail (*Pierce*) and incubated on ice for an additional 10 minutes. Cells were then centrifuged for 10 minutes at 13,600 x g, and supernatant was collected as the “harsh extraction”. Lysates were run side by side on a western blot, loading equal volume rather than equal protein.

10.5. ***Co-immunoprecipitations***

In most experiments, cells were lysed in 10 mM Tris, pH 7.5 with 2 mM EDTA, 1% triton X-100 and 1 x protease and phosphatase inhibitors (Duterme et al., 2009). In other select experiments, alternative lysis buffer detergent conditions were used as described in the Results section. The cells were incubated on ice for 10 minutes and the centrifuged at 13,600 x g for 10 minutes at 4ºC, and the supernantant was collected as the cell lysate. In order to immunoprecipitate the desired protein, magnetic protein G Dynabeads® (*Invitrogen*) were used. The Dynabeads® stock solution was gently re-suspended, and 50 µl transferred to a 0.5 ml microcentrifuge tube. The tube was placed on a specially designed magnetic microfuge tube holder (*Invitrogen*) and the supernantant was removed. The magnetic beads were conjugated with the primary antibody by removal from the magnetic stand and adding / re-suspending 10 µg of a primary antibody diluted in 200 µl of PBS-tween 20 (PBS-T) with the magnetic beads. The antibody / bead mixture was allowed to incubate at room temperature while shaking for 10 minutes. The antibody / bead mixture was placed on the magnetic stand and the supernatant was removed. The conjugated beads were washed by gently pipetting in 200 µl of PBS-T three times.

In order to immunoprecipitate the target antigen, the tube was placed into the magnetic field and the wash supernatant was removed. The beads-antibody were removed from the magnetic stand and re-suspended in 100 µl of cell lysate (~100-500 µg) by gently pipetting and incubated while shaking at room temperature for 10 minutes.

The tube was placed back into the magnetic stand and supernatant was collected for further analysis (this portion is described as the “not bound” fraction). The beads-antibody-antigen complex was washed 3 times with 200 µl of PBS, separating the beads from the washing buffer in between by placement within or out of the magnetic field. After the third wash, the beads-antibody-antigen complex were re-suspended in 100 µl of PBS and transferred to a new tube.

To elute the target antigen from the beads-antibody-antigen complex, the tube was placed into the magnetic stand and supernatant was removed. Twenty µl of elution buffer (50 mM Glycine, pH 2.8) was added to the beads-antibody-antigen complex along with 10 µl of NuPAGE® LDS sample buffer, 4 µl of reducing agent and 6 µl of deionized water, and incubated 10 minutes at 70ºC. The tube was placed into the magnetic stand once again, and the supernatant was collected and loaded into a 4-12% NuPAGE® Novex® Tris-acetate gradient mini gel and analyzed by western blot analysis (this portion is described as the “bound” or “eluted” fraction).

10.6. ***HRP conjugation of primary antibodies***

Several antibodies were conjugated with horseradish peroxidase (HRP) to avoid cross-reactivity with immunoglobins of other species in co-immunoprecipitation assays by avoiding the need of using secondary reagents. Table 1 has a summary of all HRP-conjugated antibodies used in this study. Primary antibodies were conjugated using a

Lightning-Link HRP Conjugation Kit from *Innova Biosciences,* which allows rapid labeling of primary antibodies in two simple steps. First, 100 µg of antibody was mixed with 1 µl of LL-Modifier reagent for every 10 µl of antibody used. Then, the antibody mixed with the LL-Modifier was added to 1 vial of Lightning-Link mix and gently pipette twice. The mix was incubated 3 hours or overnight at room temperature, and after incubation, 1 µl of LL-quencher was added for every 1 µl of antibody used. The HRP-conjugated antibody was ready to use after 30 minutes following addition of the LL-quencher solution.

Antibody	Source	Concentration	2° Antibody	Concentration	Proteins detected	Size (kD)
Anti-CD44 (BU52)	Mouse mAb	1:500	Goat anti-Mouse	1:5,000	CD44-FL	85
					CD44-FL-EGFP	115
Anti-CD44-cytotail	Rabbit pAb	1:10,000	Donkey anti-Rabbit	1:2,500	CD44-FL	85
					CD44-FL-EGFP	115
					CD44-ICD untagged	15
					CD44-ICD-Myc	16
					CD44-ICD-EGFP	45
					GFP-CD44-ICD	45
Anti-GFP	Rabbit pAb	1:5,000	Donkey anti-Rabbit	1:2,500	CD44-FL-EGFP	115
					CD44-ICD-EGFP	45
					GFP-CD44-ICD	45
					GFP-Smad1	90
					Smad1-EGFP	90
					GFP, EGFP	30
Anti-Smad1	Rabbit pAb	1:1,000	Donkey anti-Rabbit	1:2,500	GFP-Smad1	90
					Smad1-EGFP	90
					Smad1	60
Anti-pSmad	Rabbit pAb	1:1,000	Donkey anti-Rabbit	1:2,500	pSmad1	60
Anti-ERM	Rabbit mAb	1:1,000	Donkey anti-Rabbit	1:2,500	Moesin	75
					Ezrin, Radixin	80
Anti-pERM	Rabbit pAb	1:1,000	Donkey anti-Rabbit	1:2,500	pERM	80
Anti-Ankyrin1	Rabbit pAb	1:1,000	Donkey anti-Goat	1:5,000	Ankyrin-1 isoforms	171-206
Anti-Ankyrin3	Goat pAb	1:1,000	Donkey anti-Goat	1:5,000	Ankyrin-3 isoforms	50-190
Anti-pSerine	Mouse mAb	1:500	Goat anti-Mouse	1:5,000	All pSerines	NA
Anti-β-actin	Mouse mAb	1:10,000	Goat anti-Mouse	1:2,500	β-actin	42

HRP-Conjugated	Source	Concentration
Anti-CD44-cytotail-HRP	Rabbit pAb	1:10,000
Anti-Smad1-HRP	Rabbit pAb	1:1,000
Anti-ERM-HRP	Rabbit pAb	1:1,000
Anti-pERM-HRP	Rabbit pAb	1:1,000
Anti-Ankyrin1-HRP	Rabbit pAb	1:1,000
Anti-Ankyrin3-HRP	Goat pAb	1:1,000

Table 1: Summary of all antibodies used in this study. Important features and details of antibodies used in this study are included in a tabular format. Included are: antibody name, species in which the antibody was generated (source), typical dilution of primary antibody stock used (concentration), name and dilution of the associated secondary antibody and, the name and molecular size (by western blot analysis) of proteins detected. The stock solutions of primary and secondary antibodies were diluted in PBS with 5% BSA.

CHAPTER 3: RESULTS

In articular cartilage, as in many other tissues, cell-matrix interactions are vital to maintain cartilage homeostasis. CD44 is a cell surface receptor that supports communication between the cell and the extracellular matrix. As a transmembrane receptor, CD44 binds to the extracellular macromolecule HA, and to the actin cytoskeleton inside the cell. Healthy interactions between CD44 and HA are crucial to maintain a balance between synthesis and degradation of extracellular matrix components. In certain pathological conditions such as cancer and metastasis (Cichy and Pure, 2003; Guo et al., 1994; Lammich et al., 2002; Masson et al., 1999; Murakami et al., 2003; Okamoto et al., 1999a; Okamoto et al., 2001; Pelletier et al., 2006; Yamane et al., 1999) and rheumatoid arthritis (Haynes et al., 1991b), CD44 has been shown to undergo a sequential proteolytic cleavage in which an extracellular fragment is released to the serum or synovial fluid in the form of a soluble CD44. Some studies have shown that the released soluble CD44 competes with binding of endogenous full length CD44 to HA and thus, accentuates the loss of cell-matrix interactions further altering tissue homeostasis. In addition, as a result of the sequential cleavage, an intracellular fragment is released (CD44-ICD), but the specific effects of this peptide remain unclear.

Recently, our laboratory has demonstrated that human osteoarthritic chondrocytes in culture exhibit significant cleavage of CD44 (Takeda et al., 2010). This cleavage results in the generation of an 18-20 kD C-terminal fragment of CD44 (CD44-EXT) as well as a 15 kD CD44-ICD. The general MMP inhibitor, GM6001, blocked

generation of the CD44-EXT and, generation of the CD44-ICD was blocked by the γ-secretase inhibitor, DAPT. Normal bovine chondrocytes exhibited little CD44 degradation but the cleavage can be induced by experimental conditions that mimic OA. Although we demonstrated that CD44 proteolysis in chondrocytes occurs, the biological consequences of this proteolytic process remains unknown, especially in articular chondrocytes. This study attempts to understand the significance of CD44 proteolytic cleavage in articular cartilage/chondrocytes and the potential implications of these changes during the development of OA.

We hypothesize that a CD44-ICD released into the cytoplasm of chondrocytes will function as a dominant negative competitor of CD44-FL; interfering with interactions between CD44-FL and its intracellular binding partners. If correct, the over-expression of CD44-ICD would also serve as an experimental probe to validate interactions between CD44-FL and putative intracellular binding partners.

1. Determine the biological consequences of intracellular CD44-ICD accumulation within chondrocytes.

1.1. Development of molecular probes and model systems.

The main focus of this study is to address the effects of CD44-ICD over-expression in chondrocytes, and determine any biological interactions it may have with the endogenous CD44-FL. In order to achieve this goal, many CD44-ICD, CD44-FL and Smad1 constructs were designed, including some with epitope tags at the C-

terminus (CD44-ICD-myc, CD44-ICD-EGFP, CD44-FL-EGFP, Smad1-EGFP), others with tags at the N-terminus (GFP-CD44-ICD, GFP-Smad1, RFP-CD44-ICD), and also an untagged CD44-ICD to ensure that the epitope tag did not have an effect on CD44-ICD behavior (Figure 4).

1.1.1. Development of different recombinant CD44-ICD expressing plasmids.

To generate the untagged CD44-ICD and CD44-ICD-myc, primers were designed to amplify the CD44-ICD sequence from a full-length pCDM8-CD44H. The PCR amplified product was immediately subcloned into a TOPO TA vector, which allows easy ligation using a topoisomerase, I enzyme covalently bound directly to the plasmid. The topoisomerase I enzyme adds an additional adenine (A) to the end of each DNA strand, allowing easy ligation into a vector containing complimentary overhanging thymidine (T). The only problem with this fast TOPO TA ligation system, is that the insert can be cloned in either the 5'→3' or 3'→5' direction. A restriction digest with *Pvu II* restriction enzyme, which cuts 3 times within the vector and once within the ICD insert allowed us to determine cloning directionality by comparing band sizes. Products inserted in the forward direct were expected to exhibit 472, 1071, 1097 and 3119 bp restriction bands whereas products inserted in the reverse direction expected 586, 1071, 1097 and 3005 bands (Figure 8). Three forward and one reverse inserts were detected; the strongest forward clone was used for further subcloning. Samples were also sent to the Genomics Core Facility of East Carolina University for DNA sequencing to verify results from the restriction digest.

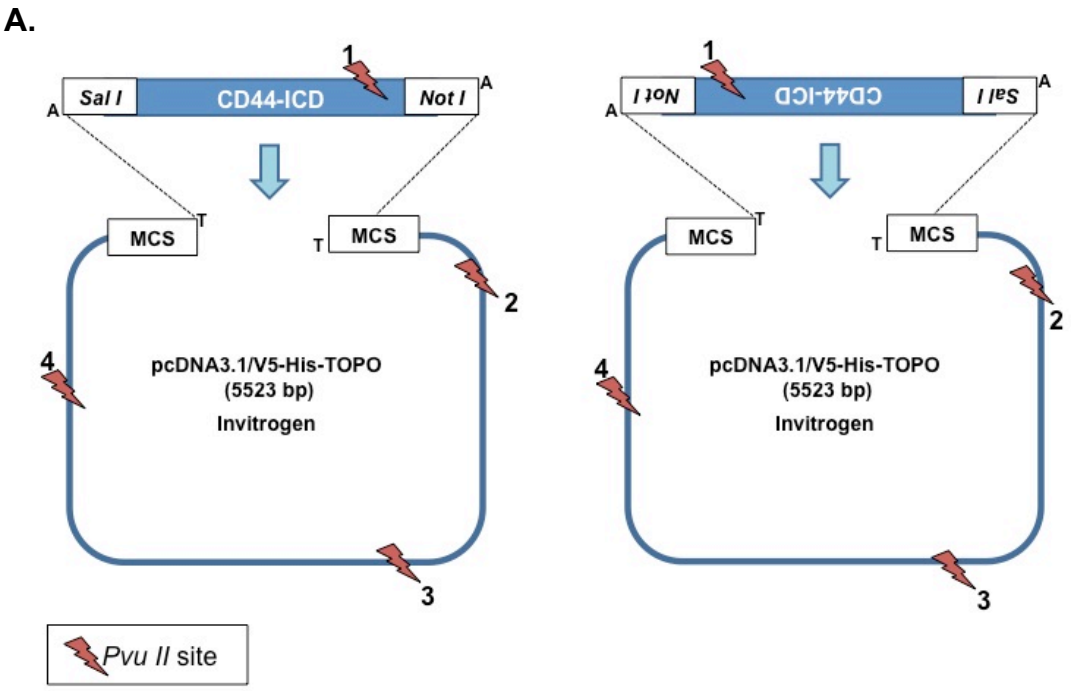

B.

Between sites	Band size (bp) 5'→3'	3'→5'
1 and 2	472	586
2 and 3	1097	1097
3 and 4	1071	1071
2 and 3	3119	3005

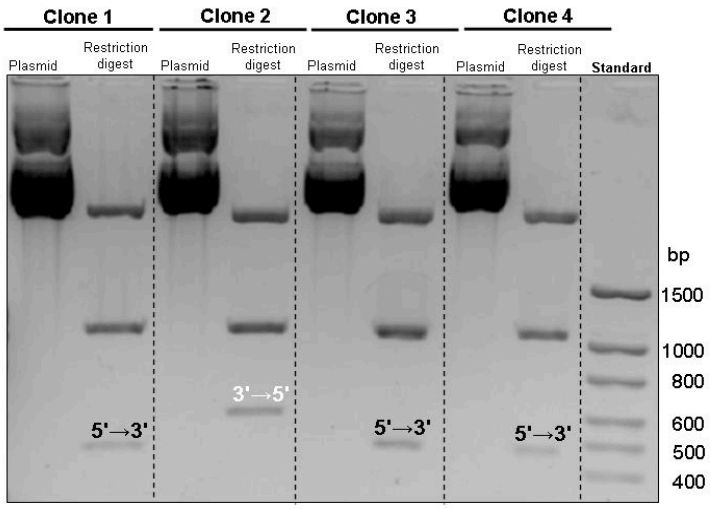

Figure 8: Restriction digest of CD44-ICD with *Pvu II* to determine cloning directionality in TOPO TA vectors. A. Predicted restriction map of Pvu II sites of pcDNA3.1/V5-His-TOPO-CD44-ICD if cloned in the 5'→3' direction (left) or in the 3'→5' direction (right). **B.** Table estimating the band sizes (bp) between *Pvu II* sites for cloning in both directions, and 1% agarose gel showing the restriction digest with *Pvu II* for 4 different clones. Only the second panel has a larger size band of 586 bp, meaning that the CD44-ICD was cloned in the 3'→5' direction, while the other 3 clones were correctly cloned in the 5'→3' direction. Sequencing results confirmed these data (not shown).

directionally inserted into an open pCMV/myc/cyto vector. Once the plasmid DNA was purified, cloning was verified by a double sequential restriction digest with the same enzymes, *Sal I* and *Not I*, which yielded a ~233 bp band (Figure 9). CD44-ICD protein expression was verified by western blotting of lysates of transiently transfected COS-7 cells with CD44 bands detected using the anti-CD44-cytotail antibody. As shown in Figure 10, a ~15 kD band was detected in cells transfected with untagged CD44-ICD plasmid, and an ~16 kD band in pCMV/myc/cyto plasmids containing the CD44-ICD-myc (not shown). As a control, cells were transfected with an empty pCMV/myc/cyto vector or non-transfected, and no bands were detected in this range. Correct insertion of CD44-ICD into pCMV/myc/cyto plasmids was also verified by DNA sequencing of the plasmids by the Genomics Core Facility of East Carolina University.

Successful cloning of the untagged CD44-ICD and CD44-ICD-myc into the pCMV/myc/cyto vector provided the necessary start codons and Kozak sequence necessary for expression of this domain in eukaryotic cells. From this point, the CD44-ICD, together with the pCMV/myc/cyto translational start sequence could be subcloned into additional plasmid vectors (pEGFP-N2 and pcDNA5.1FRT). New primers were designed to amplify the untagged CD44-ICD including the start site from the pCMV/myc/cyto vector and the natural stop of the CD44-ICD sequence. These primers also included a *Hind III* and *Apa I* restriction sites to cut the CD44-ICD product after subcloning into a TOPO TA vector. The PCR amplified product was subcloned into a TOPO TA vector, and cloning directionality was tested once again with a single restriction digest using the *Pvu II* restriction enzyme. After verifying cloning

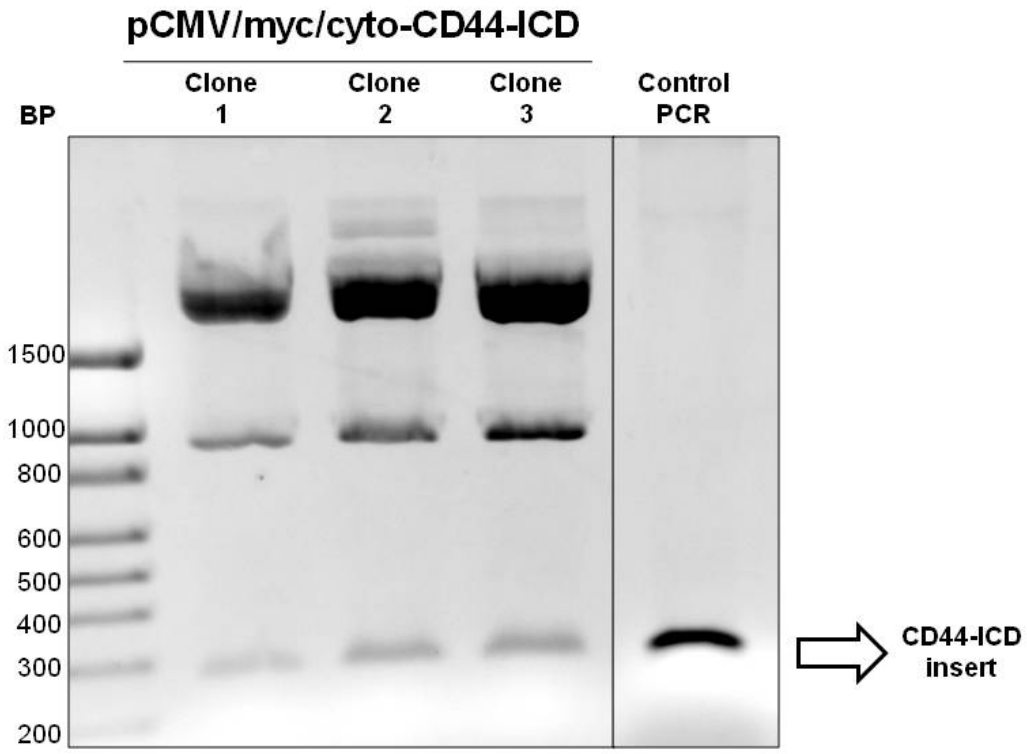

Figure 9: Agarose gel of a sequential double restriction digest with Sal I and Not I to verify successful cloning of CD44-ICD insert into pCMV/myc/cyto vector. Three clones were selected and purified, and a double restriction digest with Sal I and Not I restriction enzymes was performed to determine insertion of the CD44-ICD into the empty pCMV/myc/cyto vector. All three clones had an insert of ~233 bp. As a control, an aliquot of the PCR reaction used to amplify the CD44-ICD from the pCDM8-CD44H plasmid was run next to the restriction digests to verify that the size of the digested insert was equivalent to that of the PCR product.

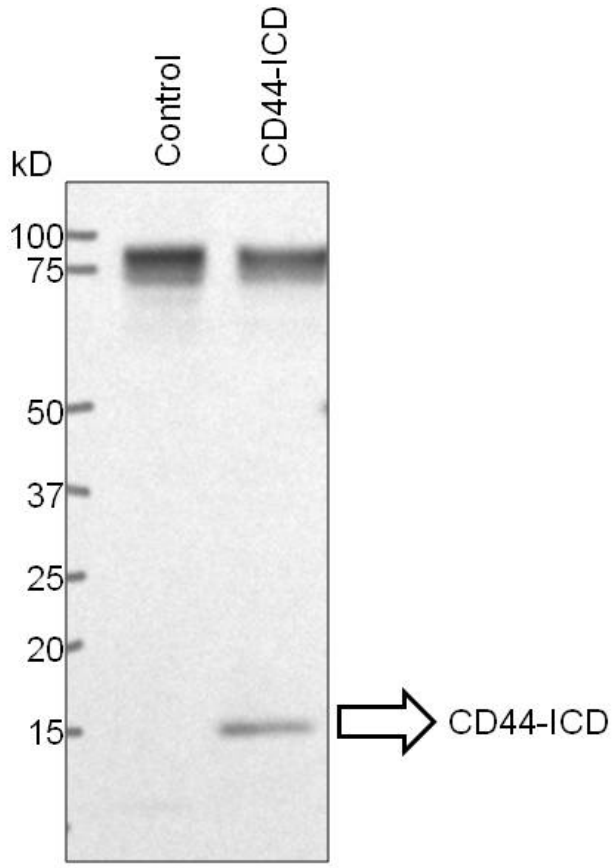

Figure 10: Western blot of COS-7 cells transiently transfected with pCMV/myc/cyto-CD44-ICD plasmid. COS-7 cells were either non-transfected (control) or transfected with untagged CD44-ICD. Cell lysates were analyzed by western blotting using anti-CD44-cytotail antibody. Protein detection with CD44-cytotail antibody shows a band at 15 kD consistent with the size of the untagged CD44-ICD

directionality, a double digest using *Hind III* and *Apa I* restriction enzymes was performed to cut the CD44-ICD insert from the TOPO vector followed by insertion into an open pEGFP-N2 plasmid. Cloning into the pEGFP-N2 was verified by a double digest with *Hind III* and *Apa I* restriction enzymes. CD44-ICD-EGFP fusion protein expression was also verified by western blotting of lysates of transiently transfected COS-7 cells, with CD44-ICD-EGFP bands detected using the anti-GFP antibody and anti-CD44-cytotail antibody. As shown in Figure 11, a ~45 kD band was detected in cells transfected with CD44-ICD-EGFP plasmid. Correct insertion of CD44-ICD into pEGFP-N2 plasmid was also verified by DNA sequencing of the plasmids by the Genomics Core Facility of East Carolina University.

To ensure that the position of such a large epitope tag on the C-terminal of CD44-ICD (the size of EGFP is ~30 kD) did not have an effect on CD44-ICD function, another CD44-ICD construct was designed with an N-terminal GFP tag. The same primers used for subcloning the untagged-CD44-ICD into the pCMV/myc/cyto plasmid were used to PCR amplify the CD44-ICD sequence from the original full-length pCDM8-CD44H plasmid. The PCR product was directly cloned into a GFP-TOPO TA vector such that the GFP and CD44-ICD were in-frame at the 5′ end of the insert. Cloning directionality was verified by *Pvu II* restriction digest and sequencing of the plasmid by the Genomics Core Facility of East Carolina University.

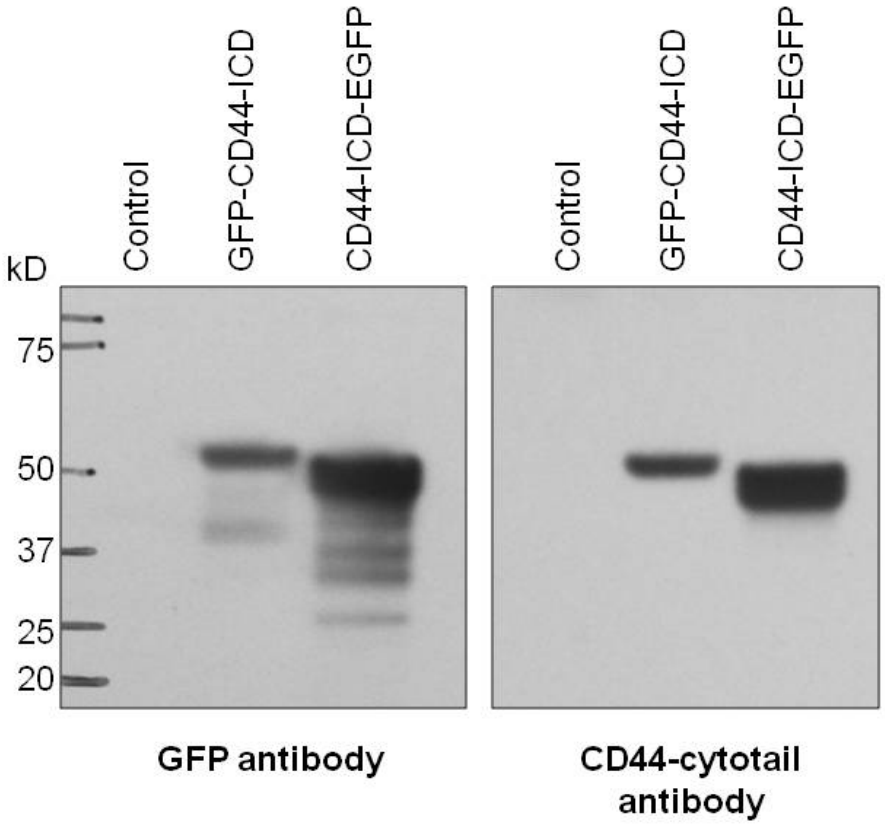

Figure 11: Western blot of COS-7 cells transiently transfected with GFP-CD44-ICD or CD44-ICD-EGFP plasmids. COS-7 cells were either non-transfected (control) or transfected with GFP-CD44-ICD or CD44-ICD-EGFP. Protein detection with an anti-GFP antibody and anti-CD44-cytotail antibody shows a band at ~45kD correspondent to the size of the CD44-ICD fusion proteins with GFP or EGFP tags.

The GFP-TOPO TA plasmid contains a promoter and start sequence to drive expression of the GFP protein and its fusion protein partner, the CD44-ICD. Protein expression was verified by western blotting of lysates from transiently transfected COS-7 cells with GFP-containing protein bands detected using the anti-GFP antibody and the anti-CD44-cytotail antibody . As shown in Figure 11, a ~45 kD band was detected in cells transfected with pGFP-CD44-ICD plasmid, similar in size to CD44-ICD-EGFP lysates.

Lastly, a CD44-ICD with an N-terminal Red Fusion Protein (RFP) tag was subcloned in order to use a different fluorescent color in co-transfection with other GFP constructs. The GFP-CD44-ICD construct was digested using *Hind III* and *Apa I* restriction enzymes and directly subcloned into an open pDsRed2-C1 vector. Protein expression was not detected with the CD44-cytotail antibody, and sequencing results confirmed that CD44-ICD was not in-frame with RFP. Cloning was repeated with a different set of primers and we were still unable to perform in-frame cloning.

1.1.2. Development of a recombinant control non-relevant peptide expressing plasmids.

To demonstrate specificity of CD44-ICD throughout this study, a “non-relevant” control expression peptide was developed using the Gene-Taylor Site-Directed Mutagenesis™ kit from *Invitrogen.* Primers were designed to add a single base pair at the beginning of the sequence, shifting the entire reading frame and thus translating a ~15 kD peptide with a different sequence than that of CD44-ICD. No premature stops

were introduced as a result of this frame shift, with the exception of one that was located only few bases before the natural stop codon.

We had no available antibody to detect the non-relevant peptide as the CD44-cytotail antibody would not recognize the new sequence. A restriction digest with Sal I and Not I restriction enzymes verified the presence of a ~233 bp insert (Figure 12), however the only way to truly identify if the point mutation was incorporated was by sequencing the DNA. This peptide was used as a control in several transfection experiments to determine whether the effects of CD44-ICD were specific.

1.1.3. Development of Smad1 expressing plasmids.

Smad1 has been shown to interact with the intracellular domain of CD44 by a yeast-two hybrid screen and co-immunoprecipitation studies (Peterson et al., 2004). Smad1 is a member of the bone morphogenetic protein (BMP) signaling pathway. Upon activation via a BMP such as BMP 7, Smad1becomes phosphorylated and dissociates from the BMP receptor and presumably, the cell surface receptor CD44. Phospho-Smad1 then translocates to the nucleus. The purpose of creating green fluorescent Smad1 fusion proteins was to visualize Smad1 translocation to the nucleus following BMP 7 activation, and to explore whether CD44-ICD could bind to Smad1 and/or affect endogenous CD44-Smad1 interactions.

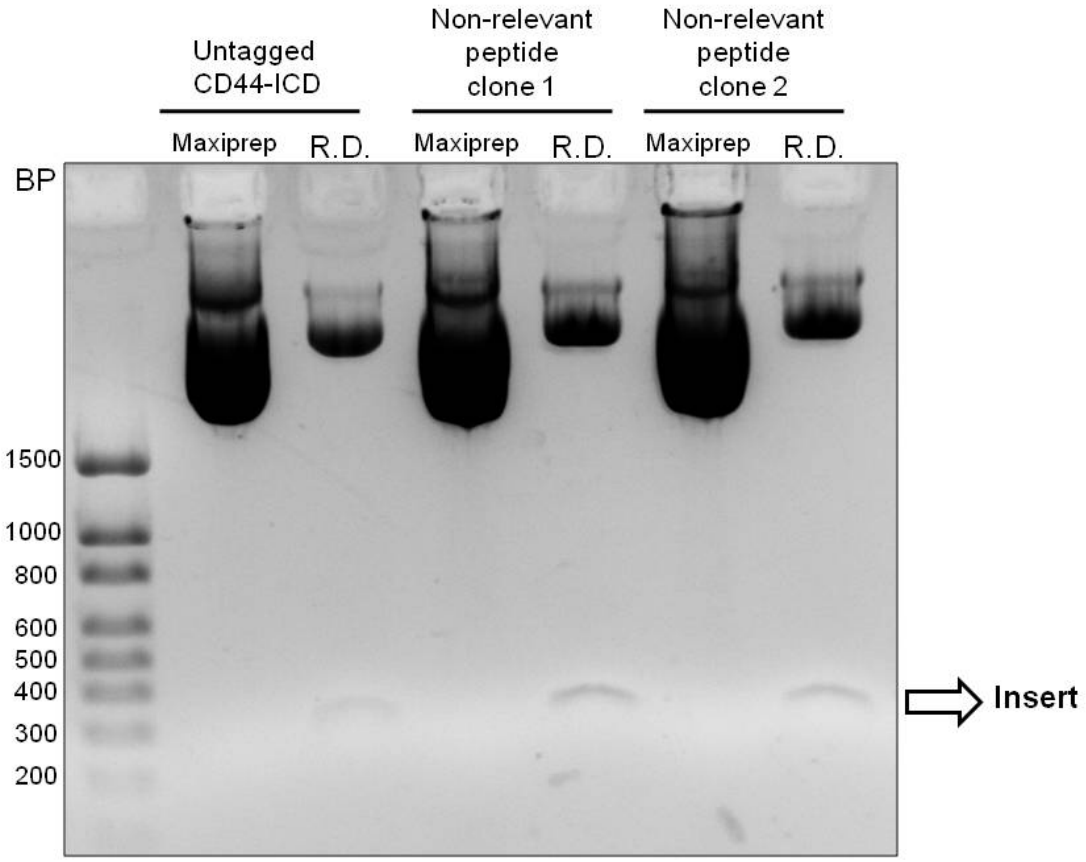

Figure 12: Agarose gel of a double sequential restriction digest with Sal I and Not I restriction enzymes to verify cloning of non-relevant peptide into pCMV/myc/cyto vector. A single point mutation was introduced into the pCMV/myc/cyto/CD44-ICD (untagged ICD) sequence to create a non-relevant peptide similar in size to CD44-ICD. A double restriction digest (lane R.D.) with Sal I and Not I restriction enzymes was performed to verify that the ~233 bp insert was cloned into the pCMV/myc/cyto vector. pCMV/myc/cyto/CD44-ICD (Untagged CD44-ICD) was used as a control.

Two Smad1 constructs were generated, one with an N-terminal GFP tag and one with a C-terminal EGFP tag to ensure that the location of the epitope tag did not influence Smad1 behavior.

First, a previously cloned Smad1 into a pcDNA 3.1/myc-His A construct was digested using *Hind III* and *Apa I* restriction enzymes to remove the ~1,400 bp Smad1 insert that was then subcloned into an open pEGFP-N2 vector to create the Smad1-EGFP fusion plasmid. Cloning was verified by a double restriction digest of Smad1-EGFP using the *Hind III* and *Apa I* restriction enzymes to ensure the 1,400 bp Smad1 insert was properly cloned (Figure 13), by protein expression of a 90 kD fusion protein (i.e. Smad = 60 kD and EGFP = 30 kD) by western blotting using Smad1 and GFP antibodies (Figure 14), and DNA sequencing.

Next, to generate a Smad1 fusion protein with a GFP tag on the N-terminus, primers were designed to PCR-amplify Smad1 from a previously cloned Smad1 present in a pcDNA 3.1/myc-His A plasmid. The PCR amplified product was sublconed into a pcDNA3.1/NT-GFP-TOPO vector to produce a GFP-Smad1 construct. Cloning was verified by double restriction digest with *Hind III* and *Apa I* which yields a ~1,400 bp (Figure 13), protein detection by western blotting using a GFP or Smad1 antibodies, and DNA sequencing.

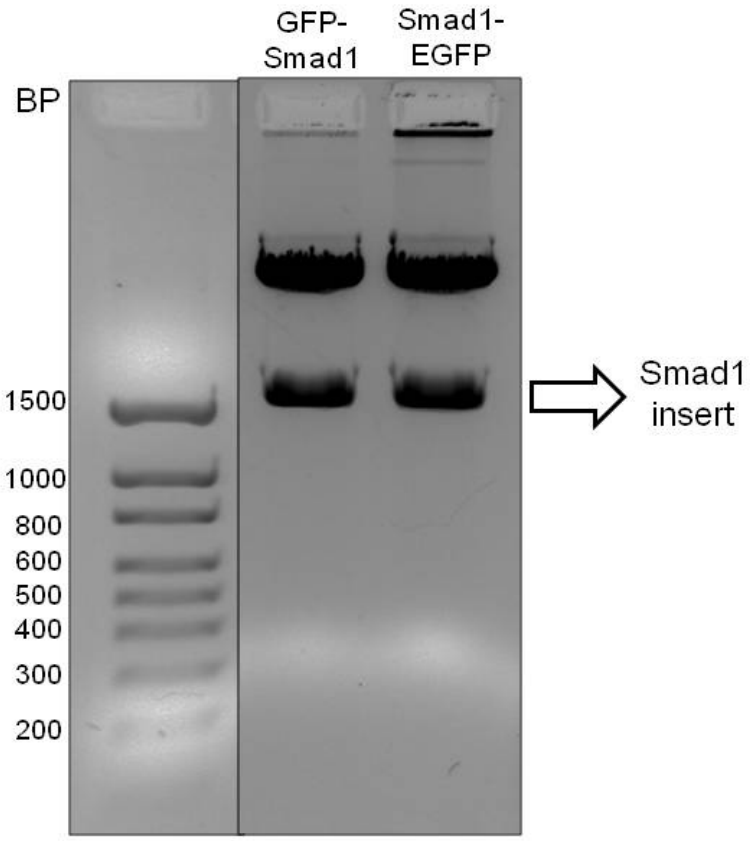

Figure 13: Agarose gel of a double restriction digest with Hind III and Apa I restriction enzymes to verify cloning of Smad1. Smad1 was cloned into a pcDNA3.1/NT-GFP-TOPO vector to produce a GFP-Smad1 construct, and into a pEGFP-N2 vector to generate the Smad1-EGFP fusion plasmid. Cloning was verified by a double restriction digest using *Hind III* and *Apa I* restriction enzymes to release the Smad1 insert (~1,400 bp) from the plasmid.

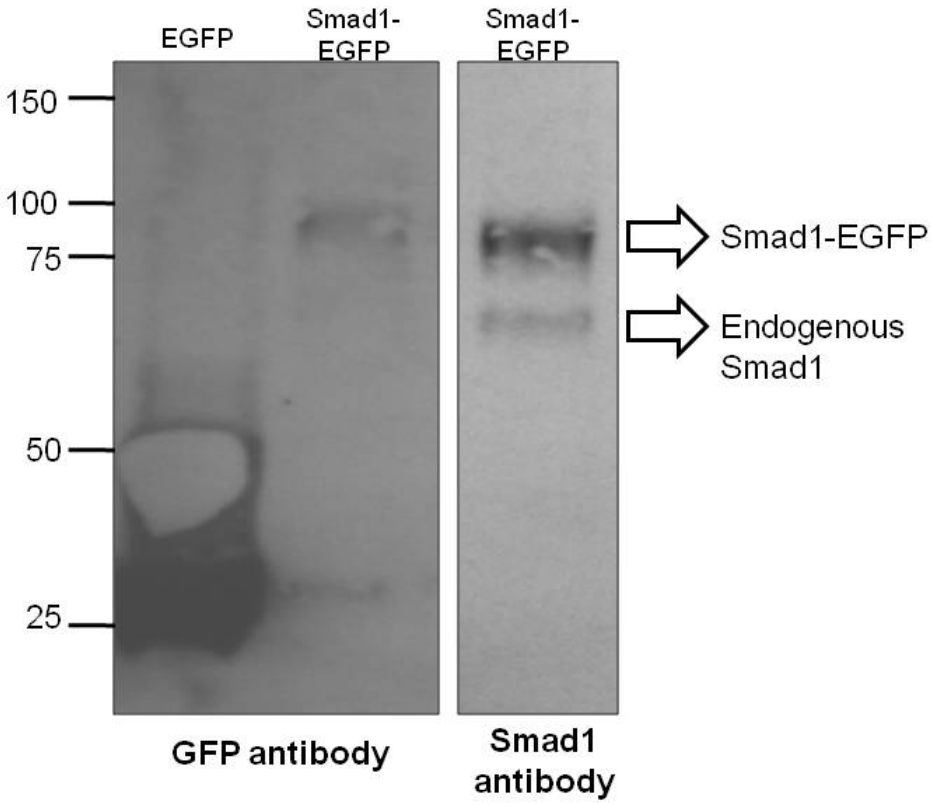

Figure 14: Western blot of COS-7 cells transiently transfected with EGFP or Smad1-EGFP. Protein expression of Smad1-EGFP fusion protein was detected at ~90 kD using an anti-GFP and an anti-Smad1 antibody. In addition, endogenous Smad1 expression was detected at ~60 kD using the anti-Smad1 antibody. Expression of free EGFP was detected using the anti-GFP antibody at ~30 kD.

1.1.4. Development of stable transfectants of CD44-ICD.

Using the Flp-In™ system from Invitrogen, two stable CD44-ICD transfectant cell lines were generated: HEK-293-CD44-ICD and RCS-CD44-ICD. Western blot analysis shows high CD44-ICD protein expression in both cell lines, when compared to the parental cells (Figure 15-16). In addition, it appears that endogenous CD44 expression is increased in the stable cell lines, possibly indicating that CD44-ICD does translocate to the nucleus and activates transcription of different genes, including CD44 itself, as reported by others (Nagano and Saya, 2004). The CD44-ICD stable chondrocyte cell line RCS was a useful tool to study CD44-ICD over-expression.

1.2. Cellular effects that occur following the introduction/over-expression of a rhCD44-ICD.

The effects of CD44-ICD over-expression on several cellular functions known or proposed to be dependent on CD44-FL were investigated. These included effects on CD44-FL proteolysis, effects on Smad1 nuclear translocation, and effects on matrix retention and binding to the actin cytoskeleton.

During the cleavage of CD44-FL by metalloproteinases and γ-secretase, accumulation of intracellular CD44-ICD is one expected result. As such, accumulation of CD44-ICD may exert a negative-feedback effect on further CD44-FL cleavage. To explore this possibility, over-expression of rhCD44-ICD was examined in a model cell system in which CD44-FL was naturally expressed (RCS, HEK-293), or co-transfected with pCD44-FL if the cell line lacked endogenous CD44-FL expression (COS-7).

In both stable CD44-ICD model systems (i.e. RCS and HEK-293), CD44-FL expression was compared in parental and stable CD44-ICD transfectant cells. HEK-293 parental cells expressed very little endogenous CD44-FL, and over-expression of CD44-ICD did not induce proteolytic cleavage of CD44-FL (Figure 15). RCS cells have higher expression of endogenous CD44-FL, and similar to HEK-293-CD44-ICD transfectants, RCS-CD44-ICD stable transfectants did not induce or inhibit fragmentation of the endogenous CD44-FL (Figure 16).

In a transient transfection system in COS-7 cells, pCDM8-CD44H was co-transfected either with empty GFP vector (control) or with GFP-CD44-ICD to examine effects of CD44-ICD on exogenous CD44-FL proteolysis. As shown in figure 17, under these conditions, CD44-FL was observed as a ~85 kD protein. In addition an 18-20 kD band indicative of CD44-EXT was again observed. Following pre-incubation with both GM6001 and DAPT inhibitors, generation of the 18-20 kD CD44-EXT band was reduced in both transfections. In addition, co-transfection with CD44-FL and GFP-CD44-ICD, showed a clearly defined band for GFP-CD44-ICD at 45 kD. However, over-expression of CD44-ICD did not appear to further induce or to inhibit CD44-FL proteolysis (Figure 17, lane 1 and 3).

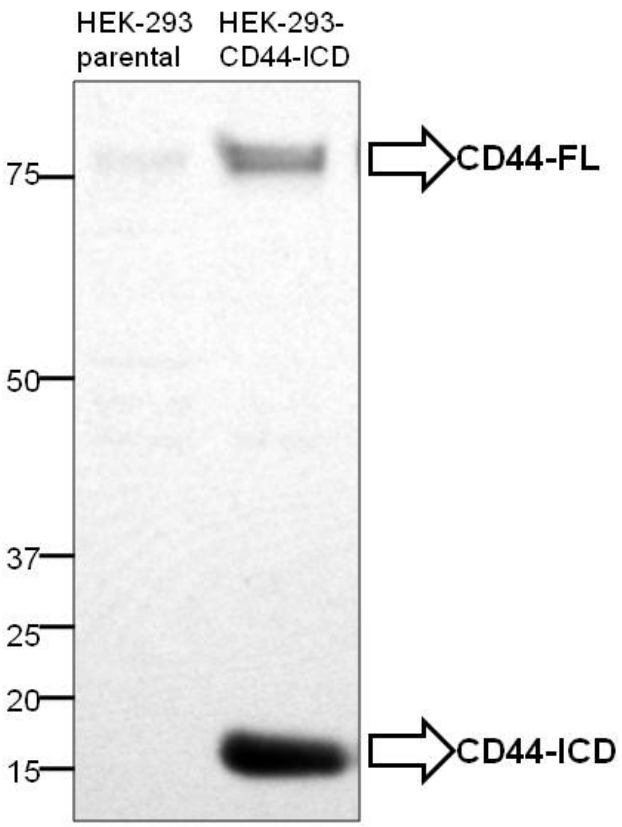

Figure 15: CD44 expression in parental HEK-293 and HEK-293-CD44-ICD stable transfectants. Protein expression of CD44-FL (~85 kD) and CD44-ICD (15 kD) was detected in lysates of HEK-293 parental cells and HEK-293-CD44-ICD stable transfectants by western blotting using CD44-cytotail antibody.

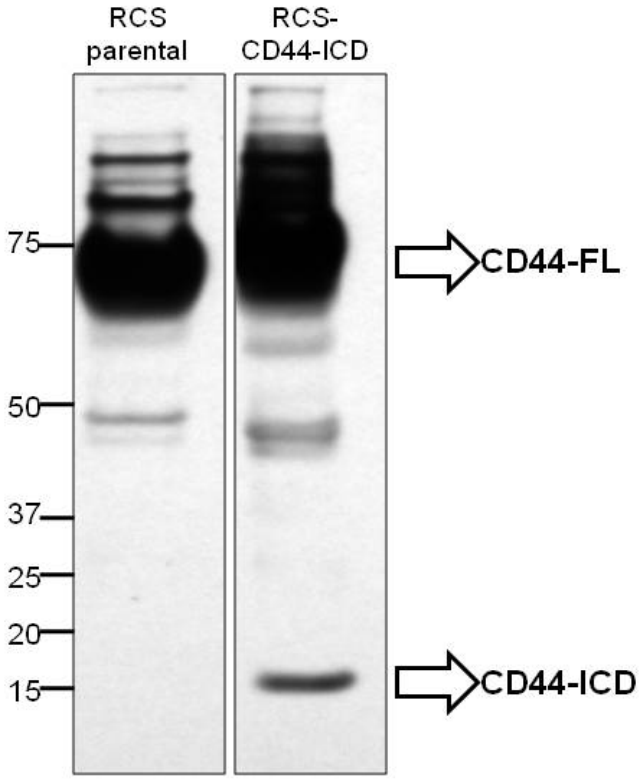

Figure 16: CD44 expression in parental RCS and RCS-CD44-ICD stable transfectants. Protein expression of CD44-FL (~70 kD) and CD44-ICD (15 kD) was detected in lysates of RCS parental cells and RCS-CD44-ICD stable transfectants by western blotting using CD44-cytotail antibody.

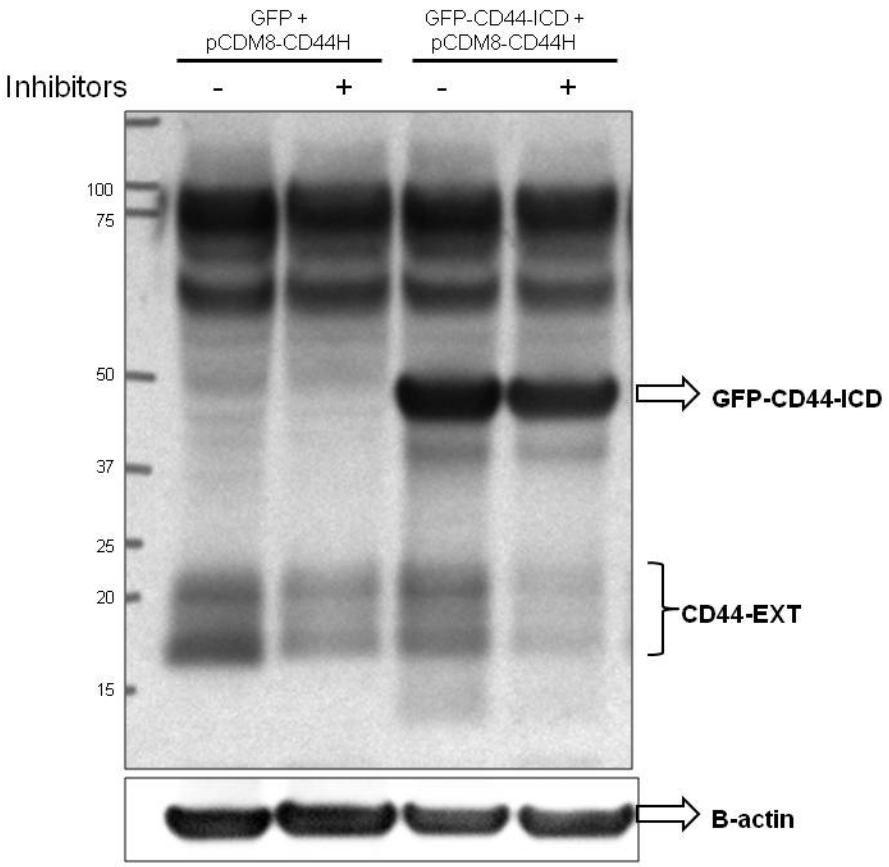

Figure 17: Effect of CD44-ICD over-expression on CD44-FL fragmentation in COS-7 cells. COS-7 cells were co-transfected with empty EGFP-N2 plasmid (as a transfection efficiency marker) and pCD44-FL or pGFP-CD44-ICD and pCD44-FL. Following transfection, the cells were treated with or without a combination of protease inhibitors, GM6001 and DAPT. Protein expression of CD44-FL (~85 kD), GFP-CD44-ICD (~45 kD) and, CD44-EXT (18-20 kD) were detected in lysates of transiently transfected COS-7 cells by western blotting using anti-CD44-cytotail antibody. In both co-transfections CD44-EXT fragments (indicative of CD44-FL fragmentation) were reduced in the presence of protease inhibitors. GFP-CD44-ICD over-expression had a only a minor effect on reducing CD44-FL fragmentation (lane 3 compared to lane 1; lane 4 compared to lane 2.

These results suggest that, at least in the model system, over-expression of CD44-ICD exerts little negative-feedback effects on subsequent CD44 cleavage activity.

CD44-FL as the receptor alone (pCDM8-CD44H) or as a fusion protein with EGFP (CD44-FL-EGFP) was transfected into a variety of cell types. As shown in Figure 18 transient transfection into COS-7 cells, C28/I2 cells and bovine articular chondrocytes was achieved. However, for subsequent western blot analyses, transfection into COS-7 cells was used as these cells had the highest transfection efficiency. It should be noted however, that under these non-activated control conditions, little EGFP appears in the nucleus of these cells.

On western blots, CD44-FL-EGFP expression in COS-7 cell lysates was observed using either anti-GFP antibody, an anti-CD44 cytotail antibody, as well as an anti-CD44 antibody (BU52) that recognized the N-terminal domain of CD44 (Figure 19). All three antibodies detected bands at the expected size of CD44-FL-EGFP (e.g., 85 kD + 30 kD = 115 kD). However, the anti-GFP and anti-cytotail antibodies, both of which recognize C-terminal domains, also detected additional lower molecular size bands of ~45 kD. This 45 kD band is indicative of CD44-ICD with the EGFP tag, the product of CD44 derived following the sequential metalloprotease and γ-secretase cleavage of CD44-FL. The CD44-cytotail antibody also detected a non-specific band at ~75 kD. COS-7 cells are CD44-negative and therefore should not express endogenous CD44-

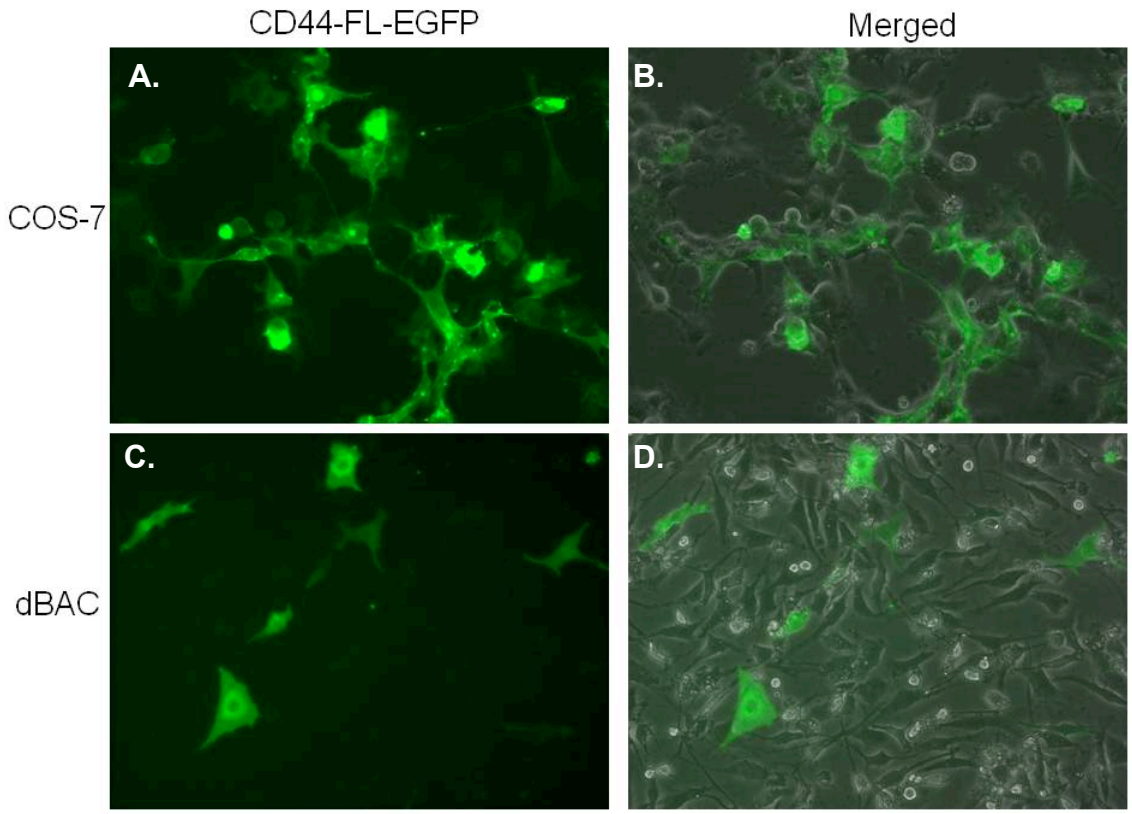

Figure 18: Transient transfections of CD44-FL-EGFP plasmid in COS-7 and dBACs. COS-7 cells (A and B) and dBACs (C and D) were nucleofected with CD44-FL-EGFP plasmid, and 24 hours after transfection, protein expression was analyzed by fluorescent microscopy. Merged images represent two-channel overlay images of green fluorescence and phase contrast images.

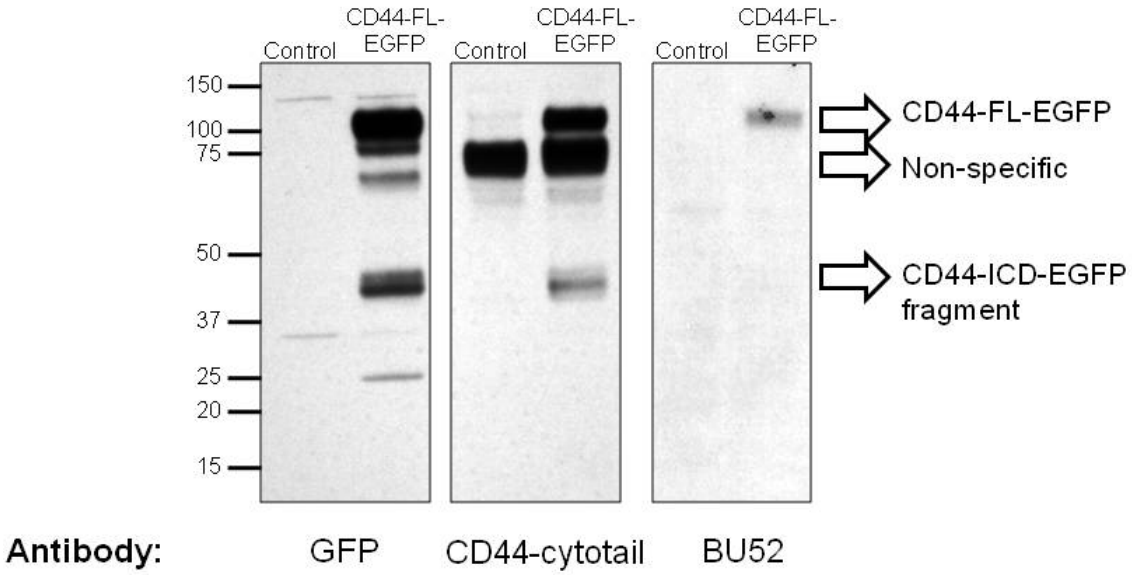

Figure 19: CD44-FL-EGFP fragmentation in COS-7 cells. The CD44-FL-EGFP fusion protein expressed in transiently transfected or control (non-transfected) COS-7 cells was detected using an anti-GFP, anti-CD44-cytotail and anti-CD44-ectodomain (BU52) antibodies. All three antibodies detected the CD44-FL-EGFP fusion protein at the expected size of ~115 kD. In addition, a ~45 kD fragment was also detected with the blots were probed using either the anti- GFP or the anti-CD44-cytotail antibodies. The presence of a 45 kD fragment is indicative of proteolytic fragmentation of CD44-FL-EGFP into CD44-EXT-EGFP or CD44-ICD-EGFP peptides. A non-specific band was also detected at~75 kD using the anti-CD44-cytotail antibody. This is not endogenous CD44-FL as COS-7 cells are CD44 negative, and BU52 antibody did not detect the same band.

FL. If this “non-specific” band was CD44-FL, it should also be recognized by the BU52 antibody, and as seen in Figure 19, BU52 only recognized CD44-FL-EGFP fusion proteins.

When the lysate from the transient transfection of COS-7 cells with CD44-FL-EGFP was loaded into lane adjacent to COS-7 transfected with GFP-CD44-ICD lysates, the fragmented band that resulted from the CD44-FL-EGFP transfection was of equivalent size to that of GFP-CD44-ICD transfection (Figure 20). This suggests that CD44-FL-EGFP undergoes proteolysis in COS-7 cells resulting in the generation of a CD44-ICD-EGFP.

1.2.2. Effect of CD44-ICD on activation of Smad1

BMP 7 is a member of the TGF-β superfamily, which binds to type I and type II receptors. Ligand binding induces phosphorylation of the receptors, which in turn activate R-Smads (Smad 1, 5 and 8) presented by transmembrane proteins such as CD44. The R-Smad dissociates from its receptor and binds to a Co-Smad (Smad 4) to form a Smad complex. The Smad complex translocates into the nucleus and regulates expression of target genes.

It is still unknown whether cleaved CD44-ICD can interact with Smad1 and translocate to the nucleus, or whether it blocks endogenous CD44-FL binding to Smad1

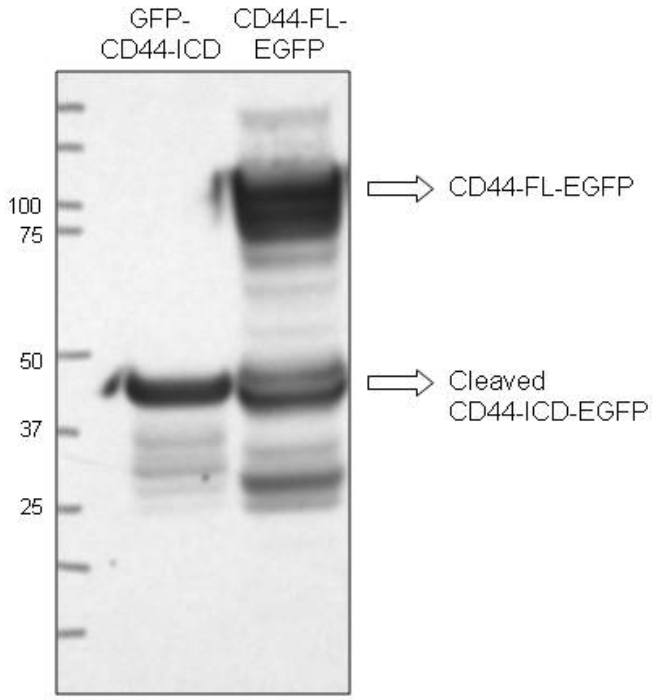

Figure 20: CD44-FL-EGFP fragments that accumulate in transfected COS-7 cells match the size of the GFP-CD44-ICD peptide. Western blot of lysates from COS-7 cells transiently transfected with either GFP-CD44-ICD plasmid (~45 kD) or CD44-FL-EGFP (~115 kD) were detected using an anti-GFP antibody. The CD44-FL-EGFP transfectants not only show expression of the full-length CD44-EGFP, but also a fragment at ~ 45 kD that is similar in size to GFP-CD44-ICD.

by sequestering Smad1 and thus interfering with the BMP 7/Smad1 signaling pathway. Therefore, our goal in this section was to determine if CD44-ICD over-expression affected the CD44/Smad1 signaling pathway.

1.2.2.1. Effects on Smad1 cellular localization

In the search for a good cell line model responsive to BMP 7 activation, several cell lines were transfected with Smad1-EGFP and treated with BMP 7. C28/I2 cells were the only cells that exhibited, albeit limited, translocation of the Smad1-EGFP fusion protein to the nucleus after BMP 7 activation.

For these studies, C28/I2 cells were transfected with Smad1-EGFP and plated in a chamber slide. After 48 hours of transfection, the cells were incubated first for 30 minutes in serum free DMEM and then treated with BMP 7 for 1 hour (control cells were left in serum free DMEM). In control C28/I2 cells without BMP 7 treatment, Smad1-EGFP displayed mainly a cytoplasmic localization (Figure 21 A-B). In response to 1 hour BMP 7 treatment in live cells, enhanced nuclear concentration of the Smad1-EGFP fusion protein was observed (Figure 21 C-D), indicative of Smad1-EGFP nuclear translocation.

De-differentiated bovine articular chondrocytes (dBACs) were cultured in monolayer for three passages. dBACs allow for a higher transfection efficiency than primary chondrocytes (BACs). The dBACs were transfected with empty EGFP vector

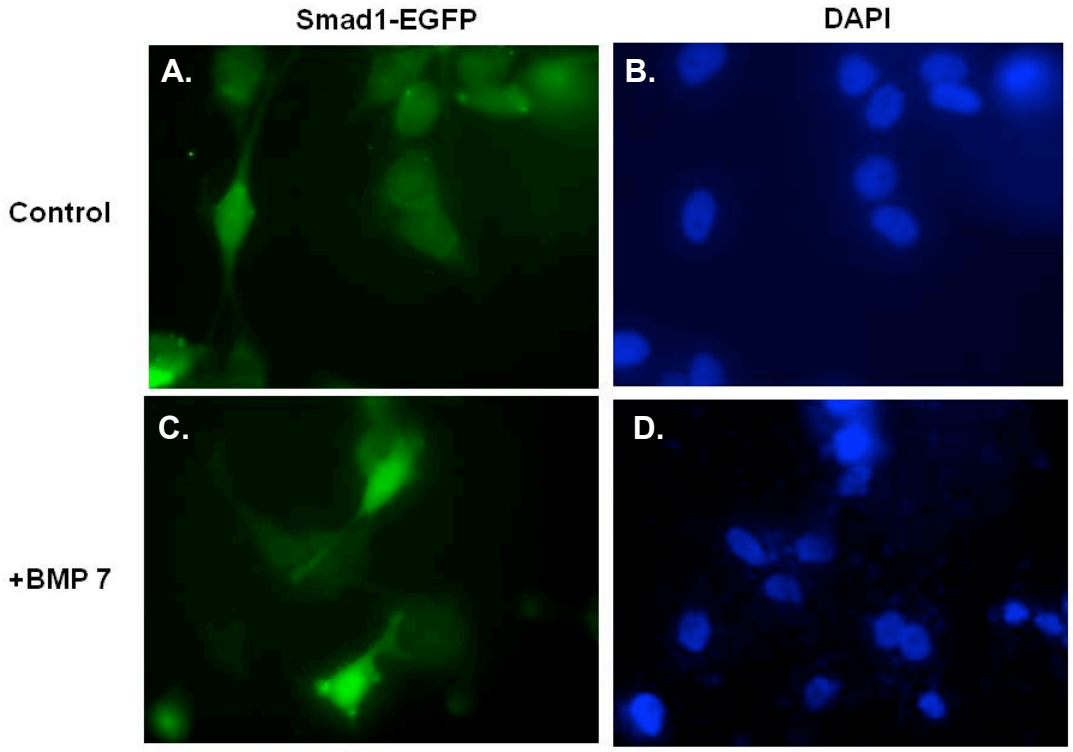

Figure 21: Smad1-EGFP translocation in response to BMP 7 treatment in the immortalized human chondrocyte cell line, C28/I2. Panels A and B, C28/I2 cells incubated in serum-free media; panels C and D, C28/I2 cells incubated in serum-free media containing 100 ng/ml BMP 7 for 1hr. Smad1-EGFP and DAPI nuclear staining (blue fluorescence) are shown separately. Control C28/I2 cells display a cytoplasmic localization of the Smad1-EGFP fusion protein. After cells were treated with BMP 7 for 1hr, nuclear translocation was observed in some of the successfully transfected cells.

or the Smad1-EGFP expression vector to determine cellular localization of each protein (Figure 22). Free EGFP showed both nuclear and cytoplasmic localization (Figure 22 A-B) while the Smad1-EGFP expression was predominantly cytoplasmic (Figure 22 C-D). These results suggest that EGFP domain does not influence the cytoplasmic localization of the Smad1-EGFP fusion protein.

When dBACs were transfected with Smad1-EGFP and then treated with BMP 7, no nuclear translocation was observed. The lack of a nuclear translocation response is likely complex and may have included a diminished responsiveness of the dBACs to BMP 7 as well as other morphological and biological changes that occur as these cells begin to de-differentiate. At this early stage of my studies, given that primary BACs were difficult to transfect with high efficiency and dBACs exhibited limited responsiveness to BMP 7, examining the potential effects of CD44-ICD over-expression on Smad1 localization in chondrocytes was not pursued further.

1.2.2.2. Effects on Smad1 phosphorylation

Smad1 binds to the intracellular domain of CD44-FL. Upon BMP 7 activation, Smad1 gets phosphorylated and dissociates from the receptor. Phosphorylated Smad1 then forms a complex with a Smad 4, and together as a complex, this Smad protein complex translocates to the nucleus and activates transcription of target genes. As such, measuring phosphorylation of Smad1 (pSmad1) levels in a model system, is one way to examine activation of the CD44/Smad1 signaling pathway.

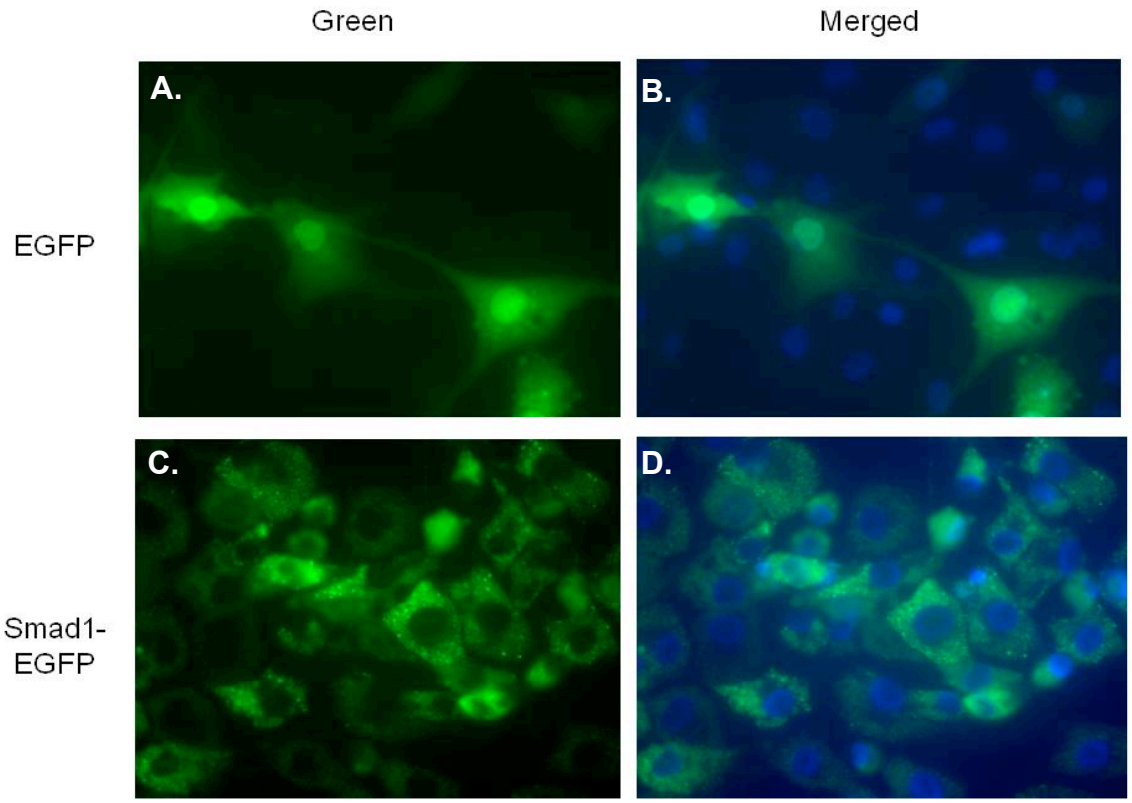

Figure 22: Smad1-EGFP translocation in dBACs. Localization of free EGFP derived from the empty EGFP-N2 vector is both cytoplasmic and nuclear in dBACs (panels A and B). Smad1-EGFP was primarily cytoplasmic (panels C and D) in resting dBACs. These results imply that the EGFP tag does not influence Smad1-EGFP localization. Right panels (B and D) depict two-color overlay images of green (EGFP) and blue fluorescence (DAPI).

To investigate the effects of CD44-ICD over-expression on CD44/Smad1 interactions, cell lysates of parental RCS and RCS-CD44-ICD stable transfectants were prepared and Smad1 phosphorylation levels examined using a phosphorylation specific antibody. As shown in figure 23, basal levels of pSmad1 were lower in lysates of stable CD44-ICD transfectants as compared to control, parental cells. In addition, when RCS-CD44-ICD transfectants were treated for 1 hour with BMP 7, the cells did not seem to exhibit a strong pSmad1 response to the ligand activation as compared to the RCS parental cell line (Figure 23B).

1.2.3. Changes in CD44-ICD generated from CD44-FL-EGFP degradation

Data shown in Figure 20 demonstrated that CD44-FL-EGFP expressed in transiently transfected COS-7 cells underwent proteolytic cleavage resulting in the generation of a CD44-ICD-EGFP. Fluorescence microscopy was then used to visualize whether any of this newly generated CD44-ICD-EGFP translocated into the nucleus. If nuclear accumulation was observed, we could then determine whether blocking the fragmentation by adding the general MMP inhibitor GM6001 and γ-secretase inhibitor DAPT inhibitors, blocked this accumulation.

Twenty-four hours after transfection, the COS-7 cells were treated overnight with a combination of GM6001 and DAPT inhibitors, or left untreated in DMEM media containing 10%FBS. In control non-treated cells, the EGFP fluorescent tag was localized not only along the plasma membrane but also within the nucleus (Figure 24A).

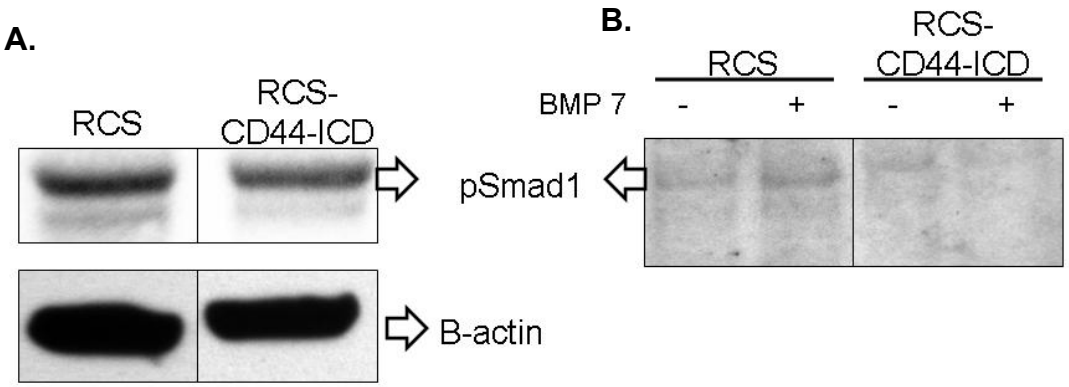

Figure 23: Effects of CD44-ICD on Smad1 phosphorylation. A. Shown are basal levels of pSmad1 present in direct lysates of RCS parental and RCS-CD44-ICD transfectants. The basal level of pSmad appears to be down-regulated in RCS-CD44-ICD transfectants as compared to RCS parental cell lines. β-actin was used to verify that equal protein was loaded. **B.** Lysates of RCS parental and RCS-CD44-ICD transfectants following activation with BMP 7. Parental RCS cells responded to BMP 7 activation by having up-regulation of pSmad. However, stable RCS-CD44-ICD transfectants did not appear to be responsive to BMP 7 activation signaling.

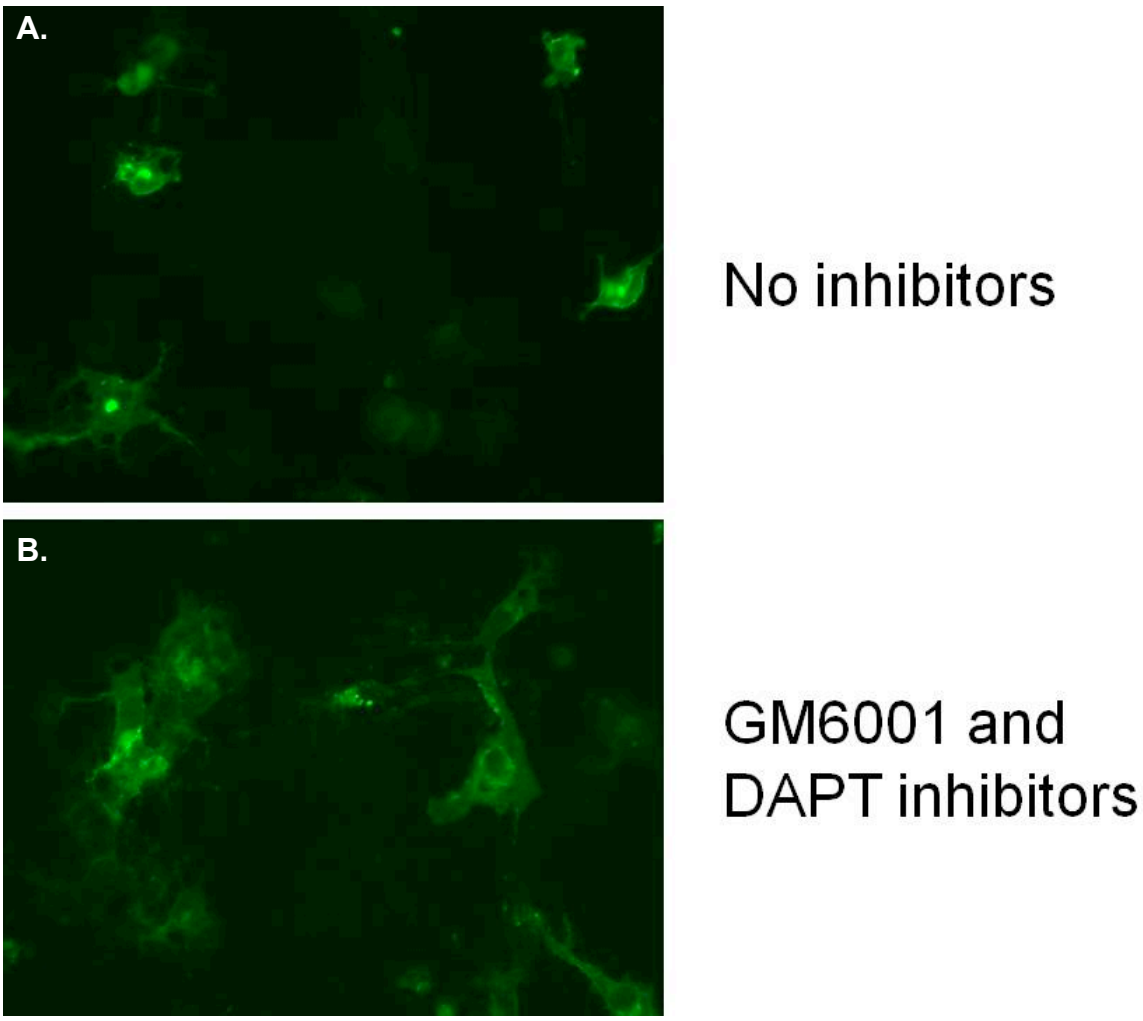

Figure 24: Transient transfection of COS-7 cells with pCD44-FL-EGFP treated with and without GM6001 and DAPT inhibitors. COS-7 cells were transfected with pCD44-FL-EGFP. Following transfection, the cells were treated without (A) or with (B) a combination of protease inhibitors, GM6001 and DAPT.

On the other hand, in cells treated with both metalloproteinase and γ-secretase inhibitors, the nuclear accumulation of EGFP was not observed (Figure 24B). These results are consistent with our hypothesis that the nuclear EGFP observed in control cells represented CD44-ICD-EGFP fragments that had translocated into the nucleus.

1.2.4. Effect of CD44-ICD on chondrocyte capacity to retain a pericellular matrix.

CD44 acts as a mediator between individual chondrocytes and the extracellular matrix to fine tune cellular responses to cytokines and growth factors. The extracellular domain of CD44 binds to the HA/proteoglycan rich extracellular matrix, which can be visualized by several assays such as particle exclusion assay or specific staining of HA using a biotinylated HA binding protein (HABP) probe.

Our goal was to use these two assays to determine if CD44-ICD over-expression had an effect on CD44-FL ability to retain a pericellular matrix (also called a pericellular "coat"). We hypothesized that CD44-ICD would have a dominant-negative effect on CD44-FL, competing with CD44-FL binding to the cytoskeleton. Similar to disruption of the cytoskeleton with cytochalasin or latrunculin, a loss of interaction with the cytoskeleton would result results in a loss of the pericellular coat (Nofal and Knudson, 2002). This implies that CD44-ICD would affect inside-out functions of CD44-FL, namely the critical function of maintaining chondrocyte/matrix interactions.

1.2.4.1. Observation of pericellular matrix loss by particle exclusion assay.

The first approach to study the effects of CD44-ICD over-expression on endogenous CD44-FL-mediated coat retention was to do a particle exclusion assay on transfected or control chondrocytes. CD44-ICD constructs including a GFP tag were often used to distinguish transfected cells (green fluorescence) from non-transfected cells (non-fluorescent) within the same culture. Matrix retention was also examined using chondrocytes transfected with an empty GFP vector to ensure that the GFP tag had no effect on coat retention. Forty eight hours after transfection, a suspension of exclusion particles (fixed red blood cells) was applied to the cultures and living cells were observed using inverted fluorescence as well as inverted phase contrast microscopy.

Transient co-transfections of BACs with a CD44-ICD-myc construct, together with an EGFP marker plasmid, resulted in a reduction of the pericellular coat when compared to the non-transfected chondrocytes. One example is shown in Figure 25. The control cell (GFP-negative) exhibited a prominent pericellular coat whereas the GFP-positive cells displayed little or no coat. No coat was defined as particles coming to settle directly adjacent to the cell plasma membrane, resulting in no exclusion zone. Another example of a particle exclusion assay of RCS cells transiently transfected with CD44-ICD-EGFP is shown in Figure 26. Again, most of the transfected cells were devoid of coats. However, occasionally some transfected cells would have a pericellular coat and, some non-transfectants would not exhibit a coat.

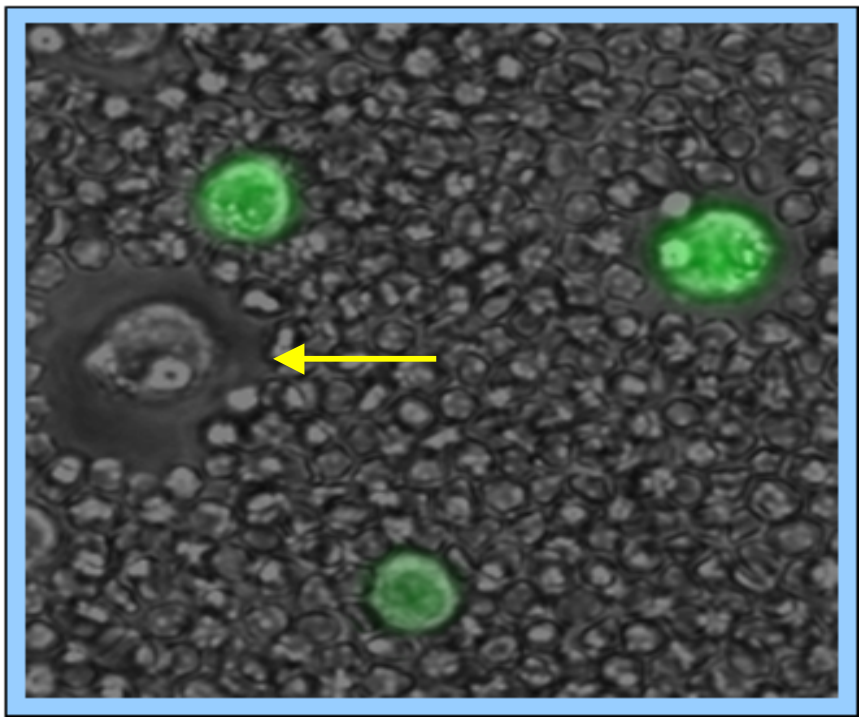

Figure 25. Effect of CD44-ICD over-expression in bovine articular chondrocytes on pericellular coats. BACs were co-transfected with empty GFP vector and CD44-ICD-myc. Successfully transfected BAC are GFP-positive and express the CD44-ICD; non-transfected cells within the same field are GFP-negative and serve as controls. GFP-negative cell (yellow arrow) displays a pericellular coat (particle exclusion zone due to the presence of cell-bound extracellular matrix). The GFP-positive cells exhibit a reduced pericellular coat.

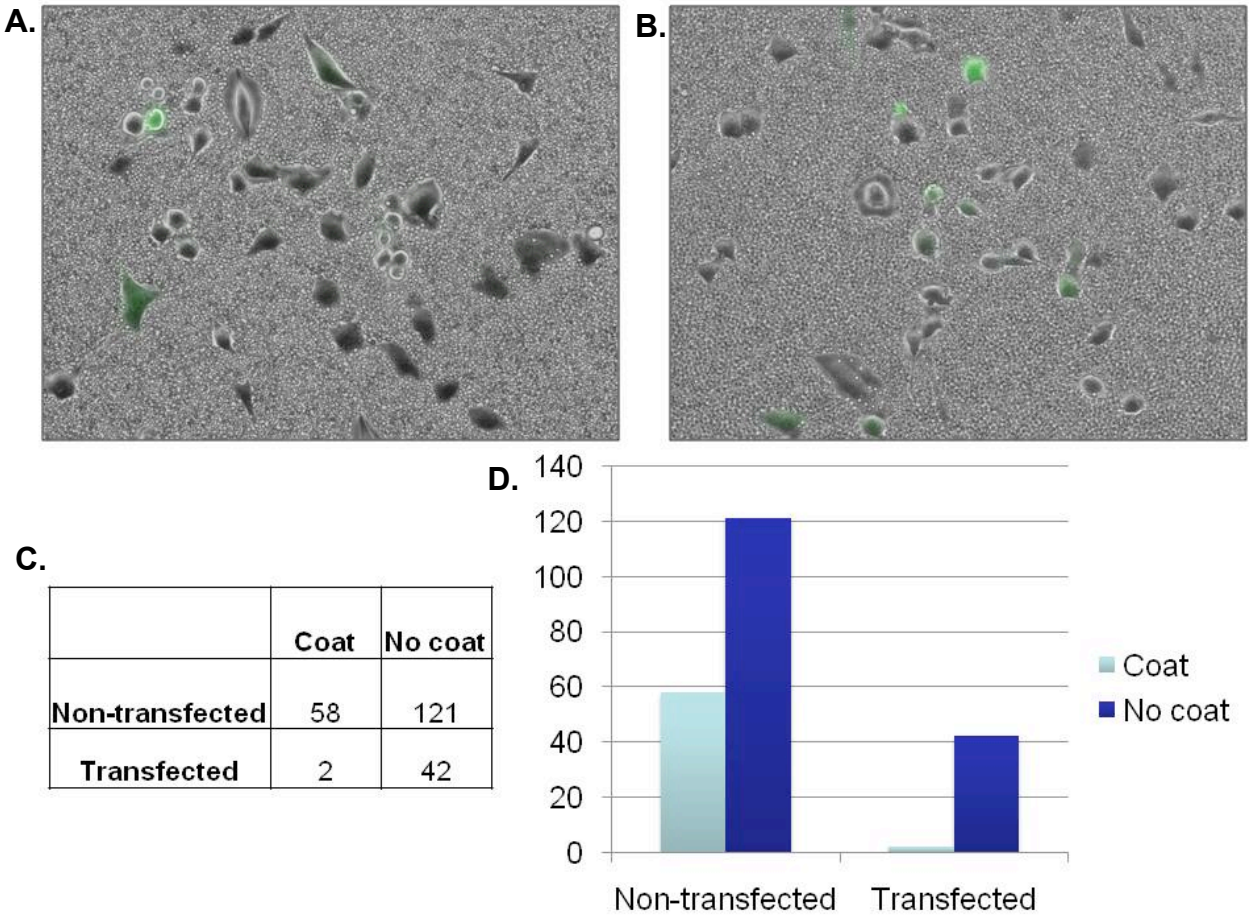

Figure 26: Effect of CD44-ICD over-expression on pericellular coats in transiently transfected RCS cells. Panels A and B depict overlay images of two representative fields of view of RCS cells transiently transfected with CD44-ICD-EGFP. Two days following transfection the cells were analyzed by the particle exclusion assay. Most of the CD44-ICD-EGFP positive cells (green fluorescence) had no pericellular matrix (coat). However, some non-transfected control cells also appeared to have no coat. Panel C is a numerical count of transfected versus non-transfected cells with or without a coat; panel D is a graphic depiction of the same data, with the total number of cells counted on the y-axis. Data represents a total of 223 cells counted, taken from one pilot experiment.

In order to account for this variability, images were prepared from several fields of view, taken from the same transfection. Each cell was placed in one of four categories: Non-transfected with coat, non-transfected without coat, transfected with coat and transfected without coat. Out of a total of 223 cells, 44 cells were transfected and 42 of the transfected cell did not retain a coat (98% of transfected cell had no coat). Out of the 179 non-transfected cells, 58 cells had a coat (33% of non-transfected cells had a coat) (Figure 26C and D). These results were duplicated with similar results. Although convincing, I continued to optimize conditions to improve on this approach. The particle exclusion assay was optimized for use on RCS cells. Together with careful control of RCS growth in culture, fewer control RCS cells displayed without coats. Secondly, stable CD44-ICD transfectants of RCS cells were developed.

As shown in Figure 27A, prominent coats are observed on cells of the parental RCS cell line. In these studies the cells were treated with calcein-AM (*Invitrogen)* prior to coat analysis to provide contrast and delineate the extent of the plasma membrane. Calcein-AM is a hydrophobic compound that permeates into live, intact cells, becomes cleaved intracellularly releasing a strong fluorescent signal (Figure 27). In contrast, all of the stable RCS-CD44-ICD transfectants exhibited a complete reduction in the ability to retain a pericellular coat.

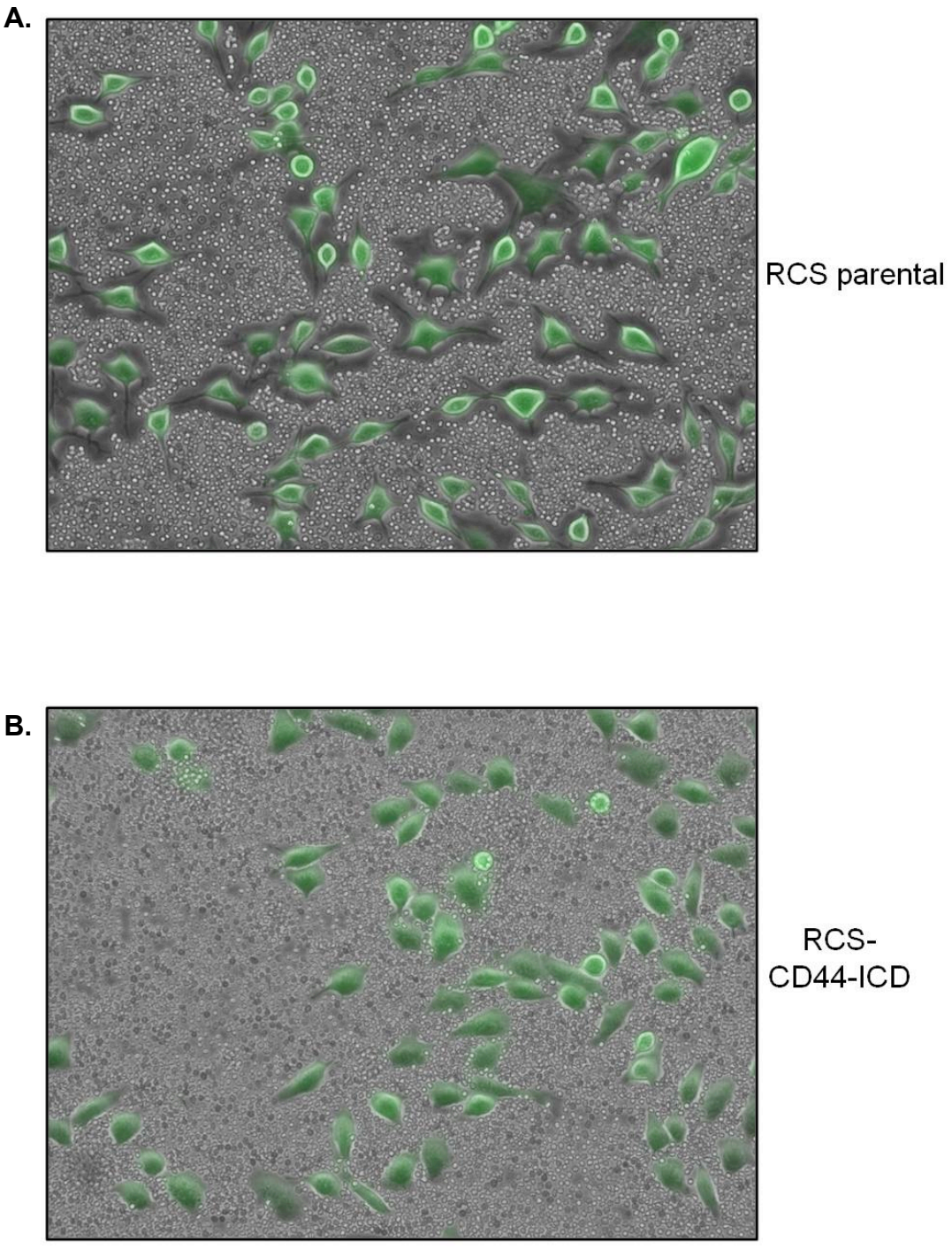

Figure 27: Effect of CD44-ICD over-expression on pericellular coats in stably transfected RCS cells. Parental RCS cells (panel A) display intact pericellular coats as detected using the particle exclusion assay. Stable hygromycin-resistant RCS-CD44-ICD transfectants (panel B) do not display pericellular coats. Both panels depict two-color overlay of phase contrast and green fluorescence images. Green fluorescence in both images is due to calcein-AM that stains live cells and was used to provide contrast.

Bovine articular chondrocytes (BACs) were treated with IL-1 or PMA to induce proteolytic cleavage of CD44-FL (Takahashi et al., 2010). Twenty-four hours after treatment, calcein-AM was added to the cells to fluorescently stain the live cells shortly before adding the red blood cells for the particle exclusion assay. Untreated chondrocytes display an intact pericellular coat, while cells treated with both IL-1 and PMA lost their pericellular coats (Figure 28).

These data suggest that CD44-ICD over-expression has a dominant-negative effect on one of the most important functions of endogenous CD44-FL, namely the role of this matrix receptor to retain the pericellular coat in chondrocytes.

1.2.4.2. Observation of pericellular matrix loss by immunostaining of hyaluronan.

Another assay that allows visualization of CD44 ability to retain a pericellular coat is to directly visualize HA retained on chondrocytes through use of a biotinylated HABP probe. No antibodies have been developed to recognize the polysaccharide HA. However, the HABP probe binds HA with high affinity and specificity similar to that of a conventional antibody. In this assay, a chondrocyte that retains an intact coat is expected to exhibit a cortical staining of green fluorescence at the plasma membrane when incubated with neutravidin-FITC as a secondary reagent.

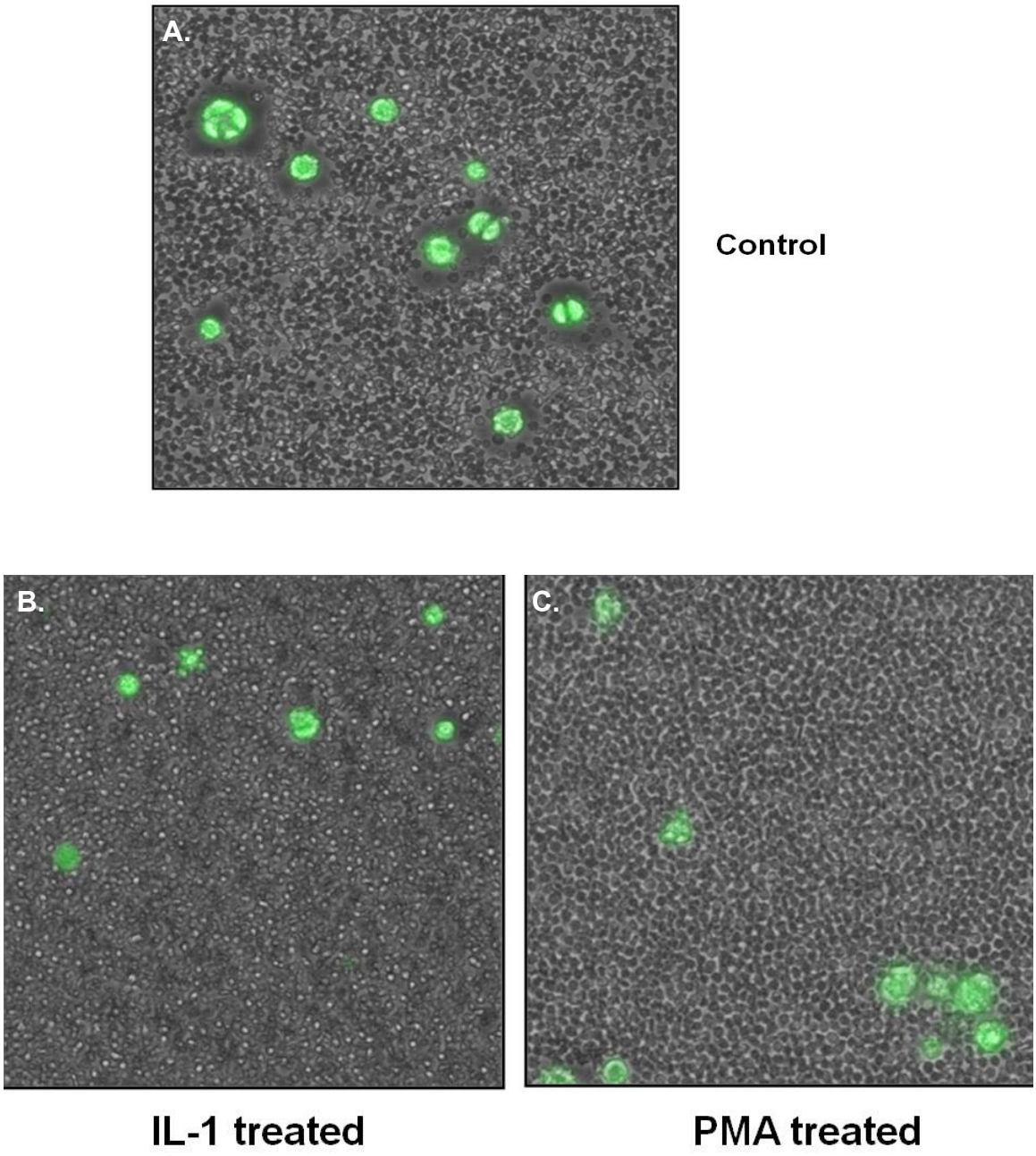

Figure 28: Particle exclusion assay of BACs treated with agents that induce proteolytic cleavage of endogenous CD44-FL. All panels depict two-color overlay of phase contrast and green fluorescence images. Green fluorescence in all images is due to calcein-AM that stains live cells and was used to provide contrast. All control, untreated BACs (panel A), display intact pericellular coats. BACs treated with IL-1α (panel B) or PMA (panel C) exhibited nearly complete coat loss in all cells.

Stable RCS-CD44-ICD transfectants were compared to the parental RCS using this assay. Parental RCS chondrocytes exhibited a near-continuous staining of green fluorescence surrounding the entire plasma membranes of all cells. This suggests that HA is retained along the perimeter of the cell, providing a stable pericellular coat around the cell (Figure 29A). On the other hand, RCS-CD44-ICD stable transfectants did not show a continuous green staining along the entire plasma membrane (Figure 29B). There were scattered green patches in most of the cells. These results indicate that one mechanism for retention of HA to the chondrocytes plasma membrane has been lost in the RCS-CD44-ICD stable transfectants. Our hypothesis would predict that the fraction of HA not retained was the fraction dependent on binding to CD44-FL What remains could represent HA that is being newly synthesized (HAS-bound HA) rather than CD44-bound HA. Nonetheless, there was a clear difference between the two cell lines when compared side-to-side.

2. Determine the mechanism for CD44-ICD effects on cells

2.1. Differential extractability of endogenous CD44-FL

Previous studies from our laboratory have demonstrated that membrane-associated CD44 exists in two pools (Nofal & Knudson, 1999). One pool can be readily extracted in a relatively low concentration of detergent (light condition) while another pool requires detergent conditions that disrupt not only membranes but protein-protein interactions as well (harsh condition). Applying these two extraction approaches sequentially provided a method that we have termed differential extraction. It was suggested that the CD44-FL pool released under harsh conditions represented

A.

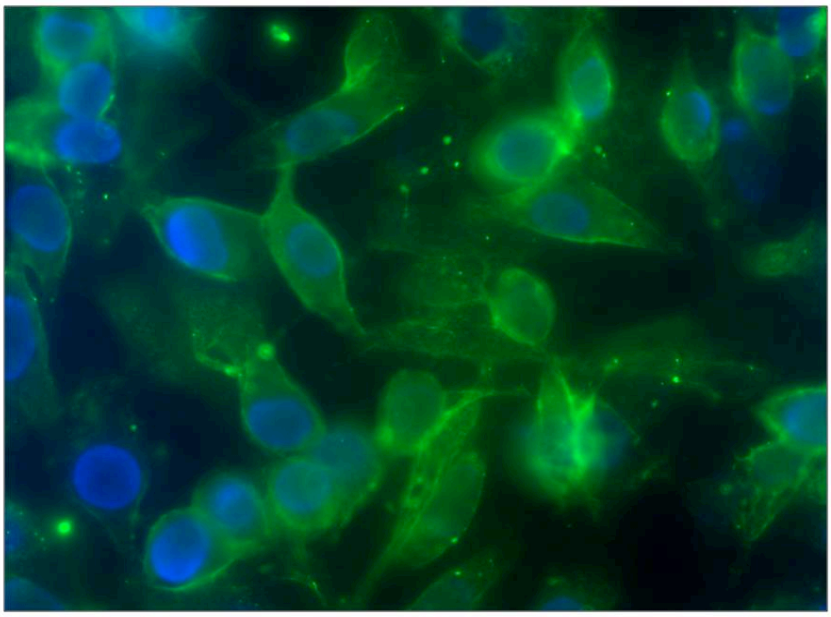

RCS parental

B.

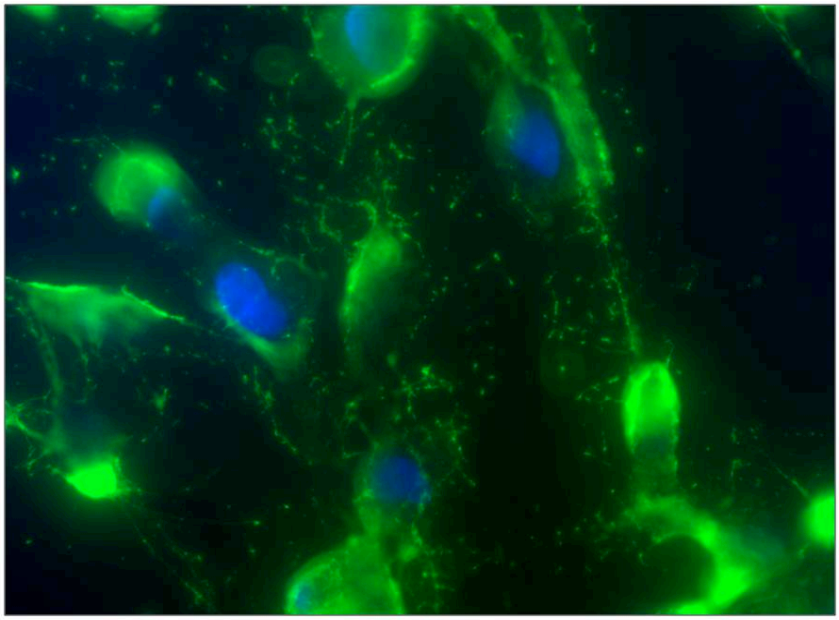

RCS-CD44-ICD

Figure 29: Changes in HA expression in parental RCS and RCS-CD44-ICD stable transfectants. Depicted are two-color overlay images of parental RCS cells (panel A) or RCS-CD44-ICD stable transfectants (panel B) stained for HA using the biotinylated HABP probe (green fluorescence from neutravidin-FITC) and DAPI stain for nuclei (blue fluorescence). Parental RCS cells display a continuous cortical ring of HA along their plasma membrane likely due to interactions between CD44 and HA. However, RCS-CD44-ICD stable transfectants (panel B) exhibit a disrupted pattern of cell surface HA. HA that is retained in the RCS-CD44-ICD cells may represent HA bound to HAS rather than HA bound to CD44.

receptors bound to the underlying actin cytoskeleton. The light condition-extractable CD44-FL, represents the non-bound pool of free receptors (Nofal & Knudson, 1999). Differential extraction was used to study whether CD44-ICD exhibited a dominant-negative effect on CD44-FL by competing with endogenous CD44 binding to the actin cytoskeleton.

First, to ensure that the effects of the light detergent has no effect on the actin cytoskeleton, C28/I2 chondrocytes in monolayer culture were pre-treated with no detergent (Figure 30A), light detergent [0.1% Igepal (aka NP-40)] (Figure 30B), or harsh detergent (0.5% Igepal containing 1% Empigen BB) (Figure 30C). The actin cytoskeleton was stained with rhodamine-phalloidin after fixation and permeabilization. Filamentous actin can be detected under all conditions but the harsh detergent treatment does result in some disruption of the actin cytoskeleton.

2.1.1. Changes in extractability due to conditions that promote CD44 fragmentation.

Treating BACs with IL-1β or HA oligos (Takahashi et al., 2010) or PMA (Nagano et al., 2004) are conditions known to induce proteolytic cleavage of endogenous CD44-FL. This cleavage also results in the release of an endogenous pool of CD44-ICD. Previous data on coat retention of treated and untreated chondrocytes revealed that BACs treated with IL-1 or PMA resulted in coat reduction when compared to untreated cells (Figure 28).

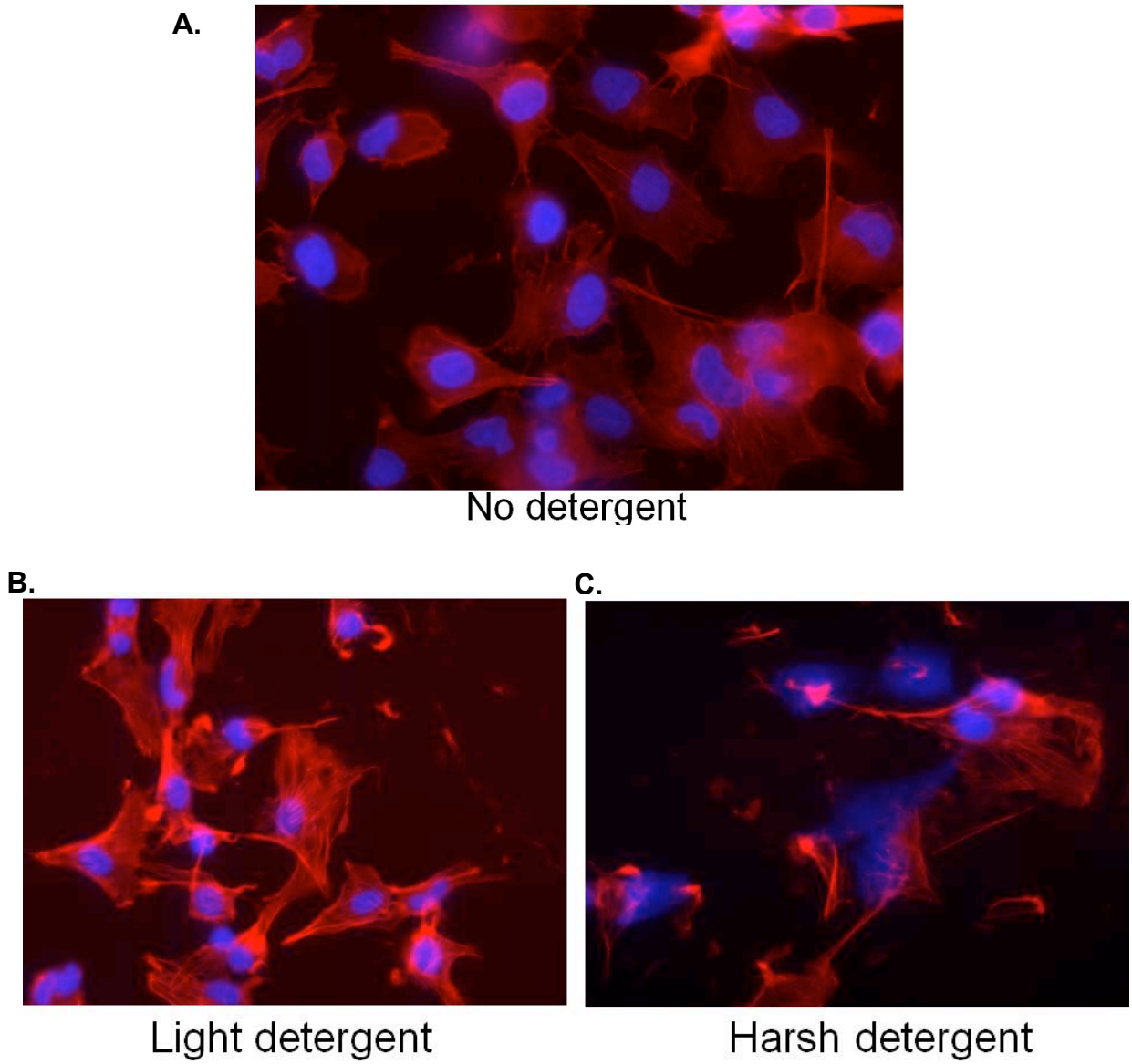

Figure 30: Changes in the organization of the actin cytoskeleton following differential extraction of C28/I2 cells with light or harsh detergents. C28/I2 cells were incubated without (panel A) or with light detergent (panel B) or, light detergent followed by harsh detergent (panel C). Following incubations the cells were fixed, permeabilized and stained with RITC-phalloidin (red fluorescence) and DAPI stain for nuclei (blue fluorescence). Two-color overlay of red and blue fluorescence images are shown. The light detergent did not affect a serious disruption of the actin cytoskeleton (panel B) and the cells appeared similar to untreated control cells (panel A). The harsh detergent not only disrupted the cytoskeleton but also was associated with an enlargement of the nuclei, suggestive of cells undergoing cell death.

When investigating CD44 extractability in chondrocytes, untreated BACs had a higher percentage of the CD44-FL extracted with the harsh detergent as compared to the light extraction. However, after treatment of BACs with IL-1β, HA oligos or PMA, a higher percentage of the CD44-FL was extracted using light conditions when compared to the pool of CD44 extracted under harsh conditions (Figure 31). Interpretation of these results are complicated by the pleiotropic effects of IL-1β, HA oligos or PMA on BACs in addition to generating endogenous CD44-ICD.

2.1.2. Changes in extractability due to over-expression of CD44-ICD.

To test directly the effects of CD44-ICD on CD44-FL, we next explored whether over-expression of CD44-ICD affects endogenous CD44-FL/cytoskeleton interactions by using the differential extraction method. BACs were transiently transfected with CD44-ICD-myc or GFP-CD44-ICD and compared to non-transfected chondrocytes. Both transfections resulted in a larger percentage of CD44-FL extracted with the light detergent when compared to the CD44-FL extracted with the harsh detergent (Figure 32). The non-transfected control chondrocytes again yielded a higher percentage of CD44 extracted with the harsh detergent.

In a second set of experiments, stable RCS-CD44-ICD transfectants were compared to RCS parental cells. A higher percentage of the CD44-FL was recovered under the light conditions in the RCS-CD44-ICD transfectants as compared to the harsh conditions (Figure 33). Like the control BACs, a higher percentage of the CD44-FL was extracted with harsh conditions in the control, parental RCS cells.

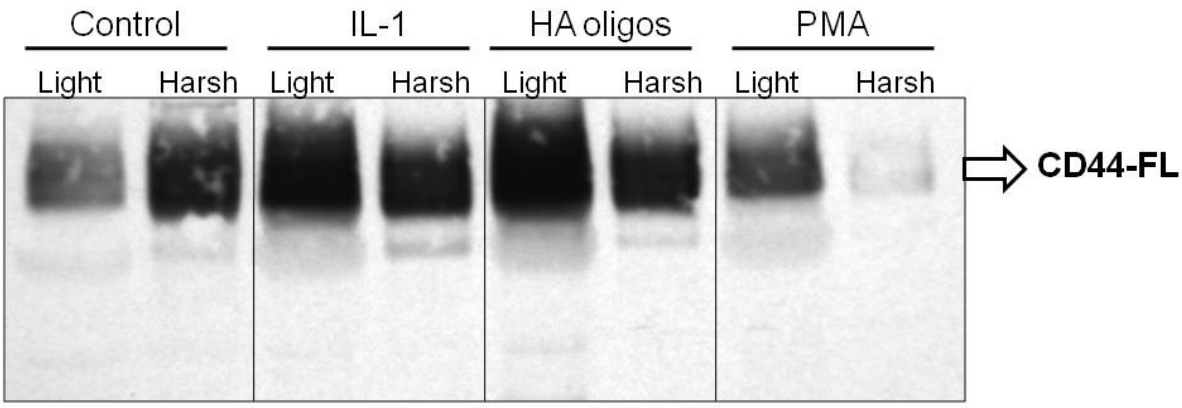

Figure 31: Differential extraction of BACs treated with IL-1, HA oligos or PMA. High density monolayers of BACs were treated under a variety of conditions known to induce CD44 fragmentation and then detergent extracted using the sequential differential extraction approach. Equal volume aliquots were analyzed by western blotting using the anti-CD44 cytotail antibody for detection. In untreated cells (control) BACs, the majority of CD44-FL was extracted under harsh conditions, suggesting a strong interaction with the cytoskeleton. However, in cells treated with IL-1, HA oligos or PMA, the majority of CD44-FL was extracted under light conditions, suggesting that the interaction between CD44-FL with the actin cytoskeleton was disrupted.

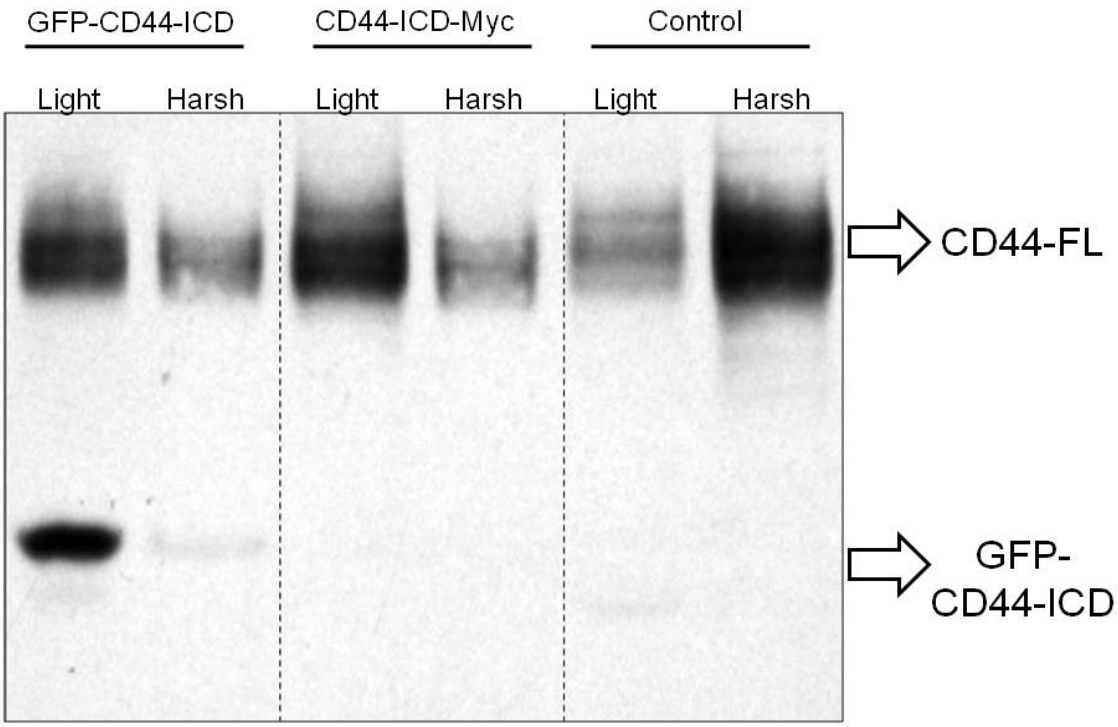

Figure 32: Differential extraction of BACs transiently transfected with CD44-ICD. Following nucleofection, BACs were allowed to recover as high density monolayer cultures for 2 days before preparation of cell lysates using the sequential differential extraction approach. Equal volume aliquots were analyzed by western blotting using the anti-CD44 cytotail antibody for detection. In non-transfected cells (control), the majority of CD44-FL was extracted under harsh conditions, suggesting a strong interaction with the cytoskeleton. However, in cells transfected either with GFP-CD44-ICD or with CD44-ICD-Myc, the majority of CD44-FL was extracted under light conditions, suggesting that a disruption of CD44-FL interaction with the actin cytoskeleton had occurred.

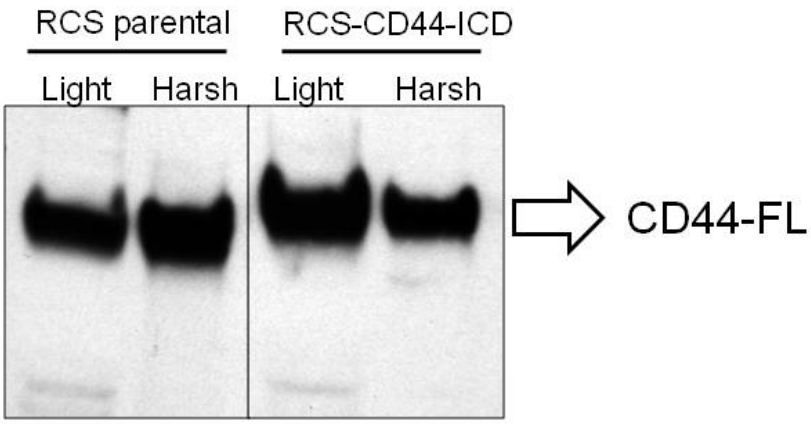

Figure 33: Differential extraction of RCS parental and RCS-CD44-ICD stable transfectants. High density monolayers of parental and CD44-ICD stable transfectants of RCS were extracted using the sequential differential extraction approach. Equal volume aliquots were analyzed by western blotting using the anti-CD44 cytotail antibody for detection. In parental RCS cells, more CD44-FL was recovered following extraction under the harsh conditions than recovered using the light conditions. In RCS-CD44-ICD stable transfectants, more of the CD44-FL was extracted under light conditions alone, suggesting a disruption in CD44-FL/cytoskeleton interactions.

Taken together, the data demonstrate that the extractability of the CD44-FL was altered in the presence of over-expressed CD44-ICD. It was suggested previously (Nofal and Knudson, 2000) that this extractability was dependent on CD44-FL interaction with the actin cytoskeleton, suggesting that CD44-ICD may be a negative competitor to CD44-FL binding to the cytoskeleton. Therefore, CD44-ICD effects on interactions between CD44-FL and cytoskeletal components were explored in more detail.

2.2. Co-immunoprecipitation to study the effects on CD44-FL binding to the cytoskeleton

Based on differential extraction data, it was hypothesized that CD44-ICD over-expression had an effect on endogenous CD44-FL binding to the cytoskeleton. To directly determine effects on these interactions, co-immunoprecipitation assays of CD44-FL with potential cytoskeletal binding proteins (e.g. ERM and Ankyrin) were developed.

There is conflicting evidence on how CD44 binds to the underlying actin cytoskeleton. One group of data suggests that the cytoplasmic tail of CD44-FL binds to members of the ezrin/radixin/moesin (ERM) family of adaptor proteins (Duterme et al., 2009; Hirao et al., 1996b; Tsukita et al., 1994). Other investigators have documented CD44 binding to the Ankyrin family of adaptor proteins (Lokeshwar et al., 1994; Singleton and Bourguignon, 2004). Either way, there is no direct evidence on how CD44

binds to the cytoskeleton in chondrocytes; therefore, both CD44/ERM and CD44/ankyrin interactions were evaluated in this study.

2.2.1. Immunoprecipitation assays for CD44-FL

After evaluating several approaches to immunoprecipitation assays, the *Invitrogen* dynabeads® approach proved the most successful. Initial experiments were performed on RCS cell lysates, in which ~100 µg were incubated with the anti-CD44 cytotail antibody. To avoid problems due to immunoblotting with the same rabbit polyclonal, horseradish peroxidase (HRP) was directly conjugated to the anti-CD44 antibody and used for detection. As shown in Figure 34, the eluted fraction (antigens that bound to the beads) successfully pulled both CD44-FL and CD44-ICD, and the not-bound fraction had some CD44-FL, likely due to saturation of protein to the amount of antibody beads.

2.2.2. CD44/ERM interactions

Co-immunoprecipitation experiments were used to study potential interactions between CD44-FL and ERM proteins. A recent study by Duterme and colleagues observed successful co-immunoprecipitation of CD44 with pERM in rat fibroblasts (Duterme et al., 2009). Therefore, our initial experiments examined CD44/pERM co-immunoprecipitations using their lysis buffer conditions.

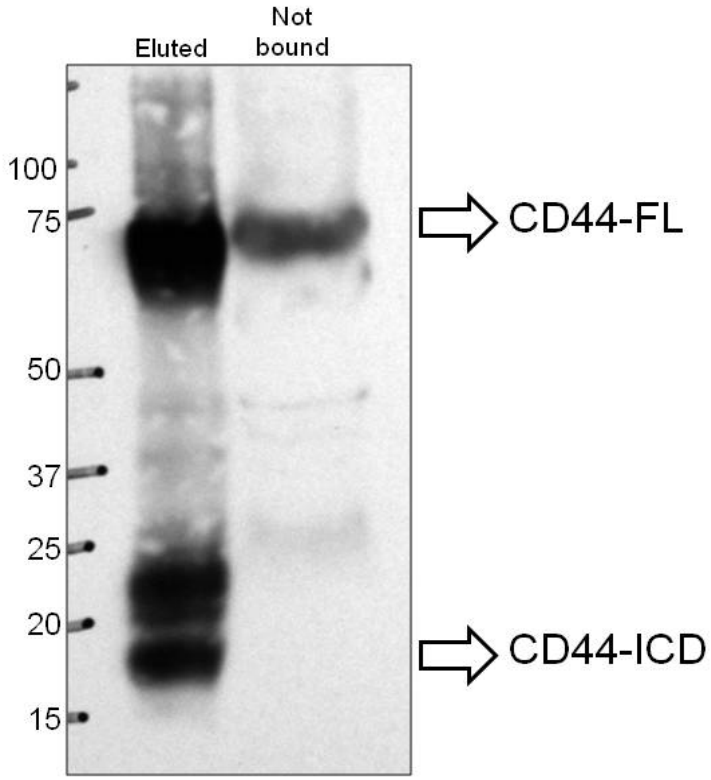

Figure 34: Immunoprecipitation of CD44 in RCS cells. RCS cell lysates were immunoprecipitated with the rabbit anti-CD44-cytotail antibody. Equal volume aliquots of eluted and not-bound fractions were analyzed by western blotting using an HRP-conjugated anti-CD44-cytotail antibody for immunodetection. The eluted fraction (antibody-bound fraction) displays both CD44-FL and CD44-ICD. Some CD44-FL was also detected in the not-bound fraction, possibly due to saturation of antibody-beads complex.

RCS were transiently transfected with CD44-ICD and treated with IL-1β. These cells were compared to RCS transfected with the non-relevant peptide or non-transfected cells as controls. First, the anti-CD44-cytotail antibody was used to pull down all CD44, and then probed with anti-pERM antibody (HRP-conjugated anti-pERM). However, under these conditions, all pERM was detected in the not-bound fraction (Figure 35A). The same blots were then re-probed with anti-CD44-cytotail-HRP antibody. CD44-FL and CD44-ICD were both successfully immunoprecipitated, and in fact, CD44-FL was in the antibody-retained fraction for all conditions (Figure 35B).

In a second series of experiments, possible co-immunoprecipitation of CD44 and pERM was compared between parental RCS and BAC to determine whether there was a difference between the two chondrocyte cell lines. Again using anti-CD44-cytotail for immunoprecipitation and anti-pERM for immunoblotting, all the pERM was found in the not-bound fraction and none in the eluted fraction (Figure 36A). Re-probing the same blot with anti-CD44-cytotail-HRP antibody confirmed that all CD44 was successfully immunoprecipitated in these samples (Figure 36B).

The Duterme et al., study also suggested that disruption or removal of HA leads to CD44 dissociation from the cytoskeleton through ERM (Duterme et al., 2009). Therefore we next compared parental RCS cells treated with testicular or *Streptomyces* hyaluronidase (to remove HA), to non-treated RCS cells. Once again, using anti-CD44-cytotail for immunoprecipitation and anti-pERM for immunoblotting, all the pERM was detected in the not-bound fraction (Figure 37A). Re-probing with anti-CD44-

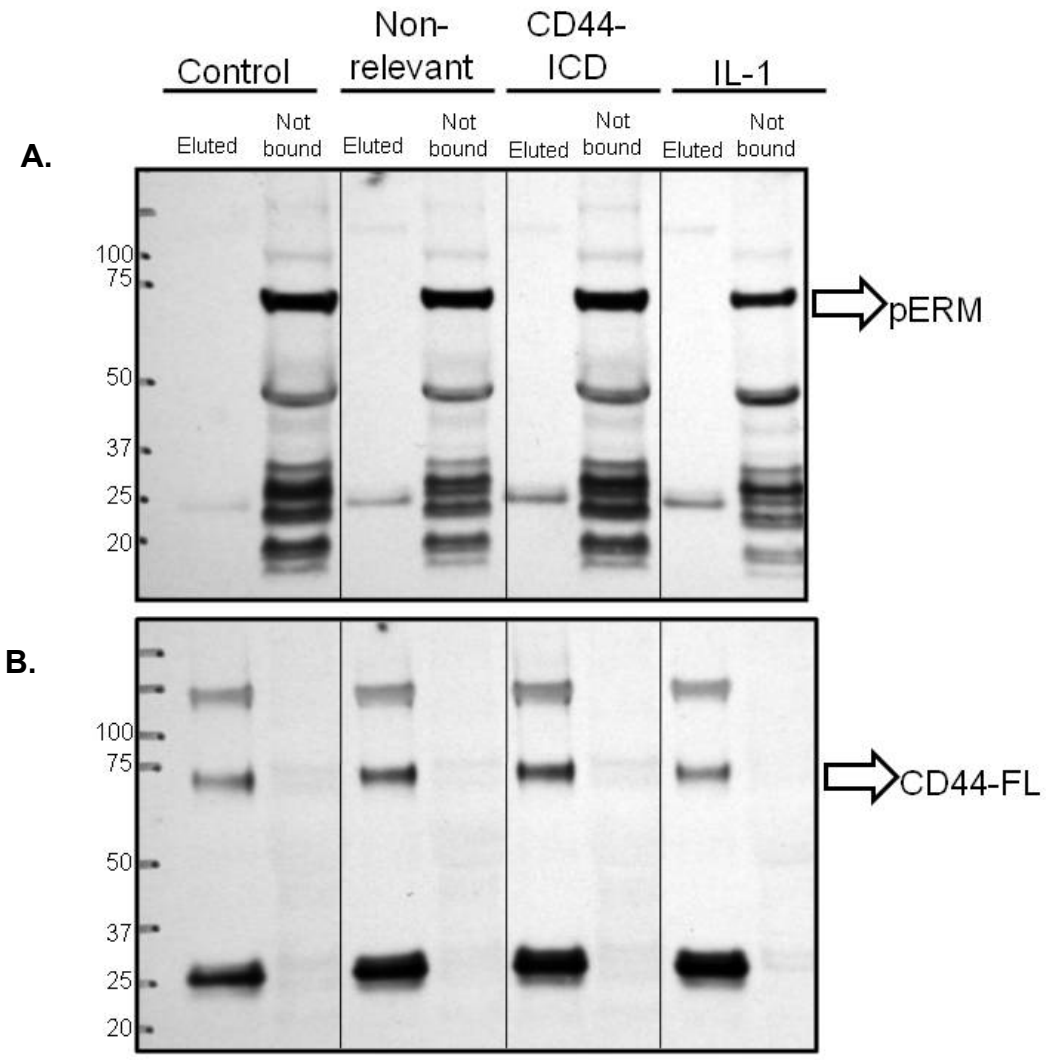

Figure 35: Co-immunoprecipitation of CD44 and pERM in RCS cells. RCS cells were either transiently transfected with the non-relevant peptide or with CD44-ICD, or treated with IL-1. **A.** Cell lysates were immunoprecipitated with CD44-cytotail antibody and western blots probed with HRP-conjugated pERM antibody. All pERM was detected in the not-bound fraction. **B.** Re-probing of the same blots using HRP-conjugated anti-CD44 cytotail antibody confirmed that the majority of the CD44-FL was recovered in the eluted fraction.

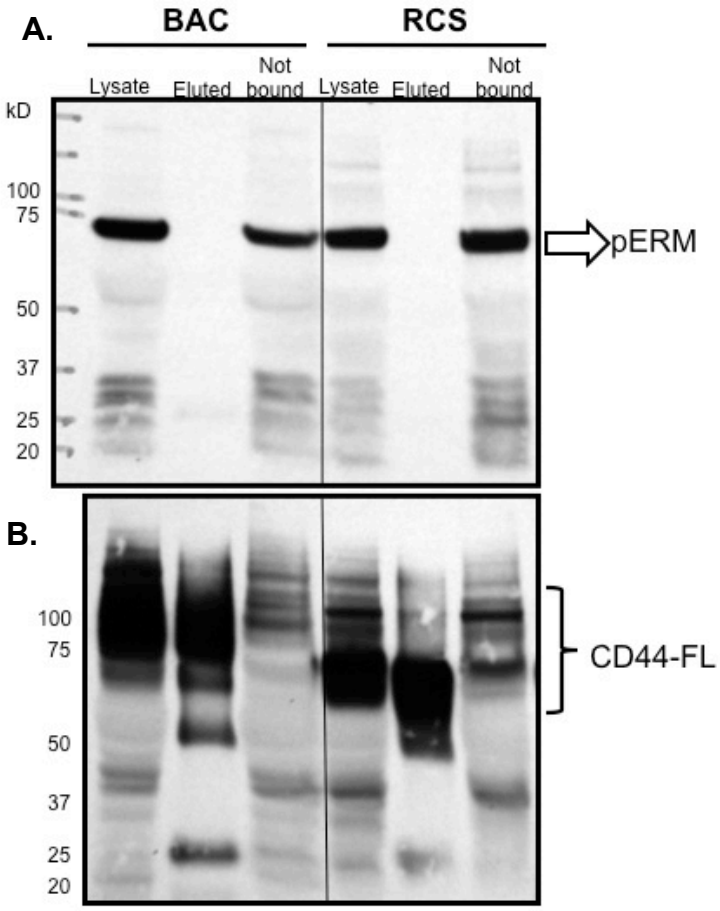

Figure 36: Co-immunoprecipitation of CD44 and pERM in BAC and RCS cells. A. Cell lysates of BAC and RCS cells were immunoprecipitated with CD44-cytotail antibody and western blots were probed with an HRP-conjugated pERM antibody (top panel). In addition, lysates derived from direct extraction of BAC or RCS cells were also examined. All pERM was detected in the not-bound fraction for both cell lines. **B.** Blot was re-probed with HRP-conjugated CD44-cytotail antibody, and most of the CD44-FL was detected in the eluted fraction (CD44-FL displays a different molecular mass in BAC compared to RCS possibly due to post-translational glycosylation).

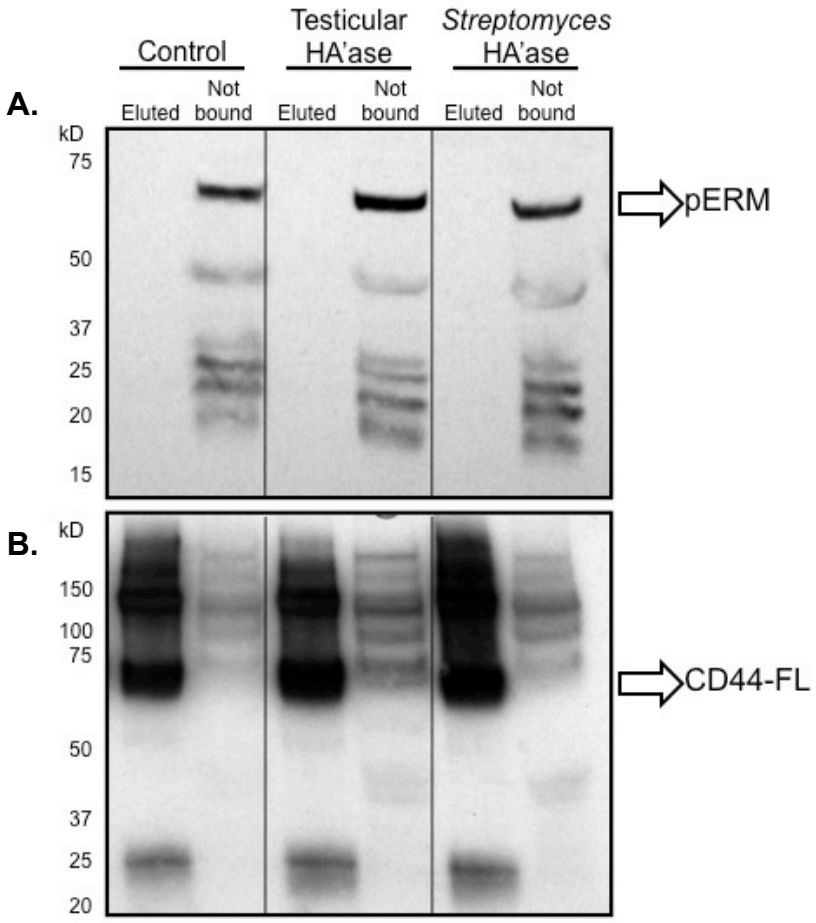

Figure 37: Co-immunoprecipitation of CD44 and pERM in RCS treated with HA'ase. Cell lysates of RCS cells were prepared from untreated (control) RCS cells or RCS cells treated with testicular or *Streptomyces* HA'ase. **A.** The lysates were immunoprecipitated with CD44-cytotail antibody and the western blot probed with a HRP-conjugated pERM antibody. All pERM was detected in the not-bound fraction for both cell lines and for all three conditions. **B.** The blot was re-probed with HRP-conjugated CD44-cytotail antibody, and most of the CD44-FL was detected in the eluted fraction (CD44-FL have different molecular mass in BAC and RCS likely due to post-translational glycosylation).

cytotail-HRP antibody confirmed that CD44 was successfully immunoprecipitated (eluted fraction) (Figure 37B).

Numerous reports have noted that the interaction between CD44 and ERM is weak, especially in, *in vitro* assays. Therefore, we examined the effects of detergent conditions on co-immunoprecipitations of CD44 and ERM in chondrocytes. In this study lysates were made from monolayers of BACs and RCS cells. Separate RCS cultures were extracted using a lysis buffer containing 50 mM Tris-HCl, 150 mM NaCl and, 5 mM EDTA and varying concentrations of NP-40 (0.1%, 0.25% and 0.5%). Again, anti-CD44-cytotail was used for immunoprecipitation and anti-pERM for immunoblotting. However, the results were similar to previous attempts to co-immunoprecipitate CD44 and pERM, that is, all of the pERM was recovered in the not-bound fraction (Figure 38A). In another series of experiments with BACs, Triton X-100 and CHAPS at different concentrations (Figure 38C) were tested in comparison with 1% NP-40. Under all these conditions, all pERM was detected in the non-bound fraction (Figure 38B).

These data would suggest that CD44 does not directly interact to pERM in chondrocytes. To determine whether indirect interactions occur, the effect of CD44-ICD over-expression on overall ERM phosphorylation was examined. In this series of experiments, parental RCS cells were compared to RCS-CD44-ICD stable as well as CD44-ICD transient transfectants. Western blots of total cell lysates demonstrated that ERM phosphorylation was lower in CD44-ICD over-expressing transfectants (Figure 39). These results suggest that CD44-ICD does affect ERM phosphorylation even

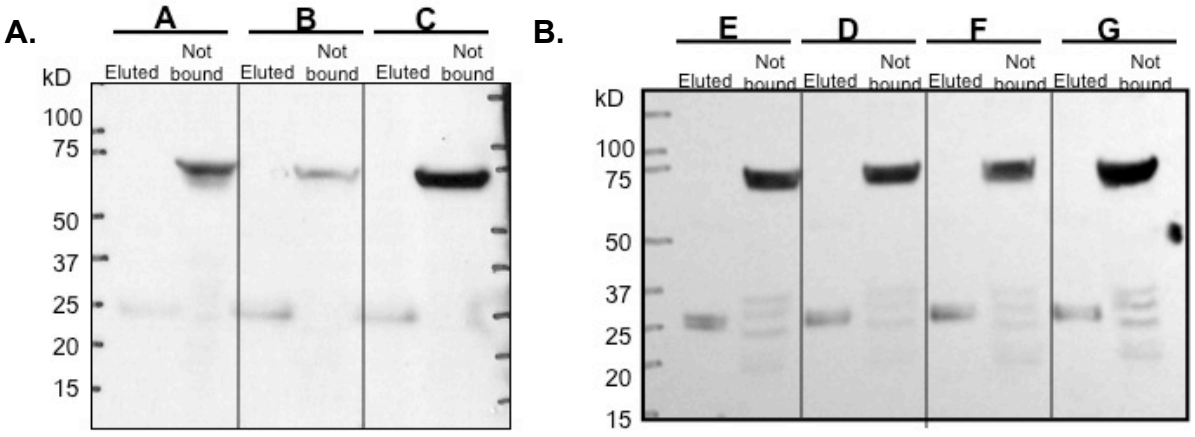

C.

	Concentration	Detergent
A	0.10%	NP-40
B	0.25%	NP-40
C	0.50%	NP-40
D	1%	NP-40
E	0.50%	Triton X-100
F	0.50%	CHAPS
G	1%	CHAPS

Figure 38: Co-immunoprecipitation of CD44 and pERM in BACs and RCS cells using different cell lysis detergents. Cell lysates were prepared from high density cultures of RCS cells (panel A) or BACs (panel B) using a select series of detergent conditions (panel C). Cell lysates were immunoprecipitated with CD44-cytotail antibody and western blots probed with an HRP-conjugated pERM antibody. Under all detergent conditions, all pERM was detected in the non-bound fraction only. No pERM was detected in the eluted fraction.

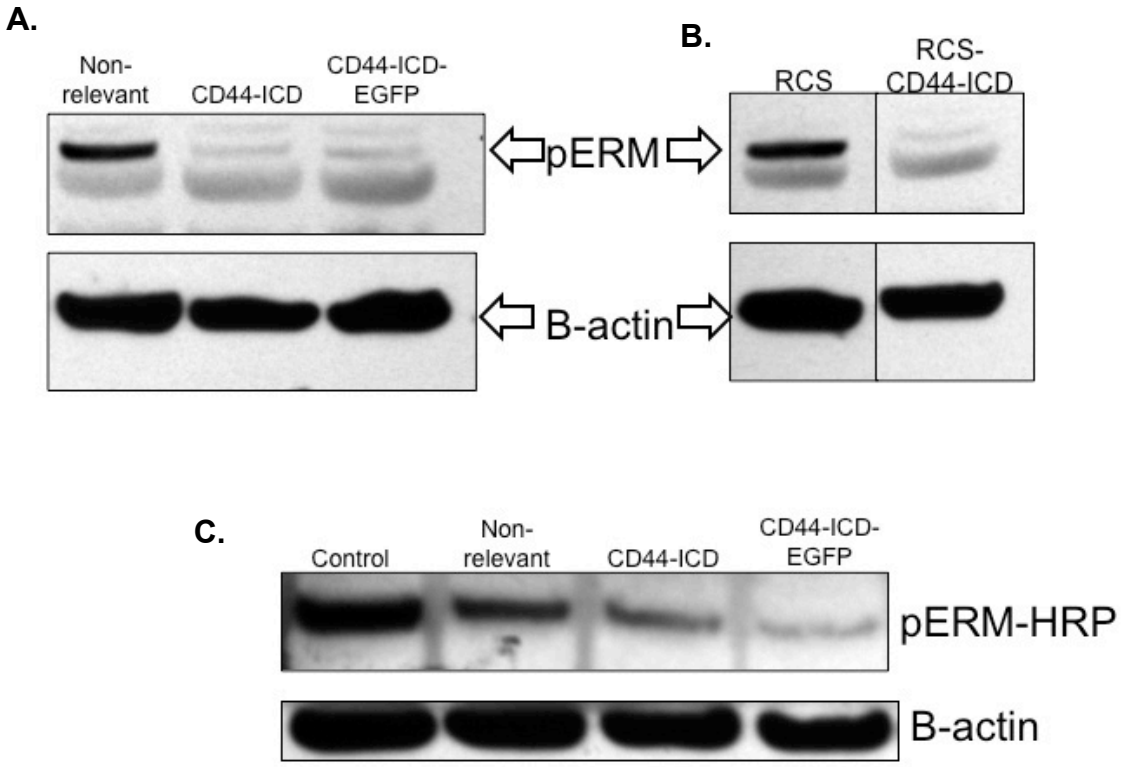

Figure 39: Effect of over-expression of CD44-ICD on phosphorylation of ERM proteins in RCS cells. RCS cells were transiently transfected with CD44-ICD, non-relevant peptide plasmid, or plasmids expressing CD44-ICD or CD44-ICD-EGFP. **A and C.** Lysates from these cells were directly extracted and analyzed by western blotting using an HRP-conjugated pERM antibody. RCS cells transfected with the control non-relevant peptide, exhibited higher ERM phosphorylation compared to the two CD44-ICD transfectants suggesting that CD44-ICD does affect ERM phosphorylation. **B.** Lysates were also obtained from control parental RCS cells and CD44-ICD stable transfectants. Western blot analysis of these lysates also demonstrated a reduction in ERM phosphorylation in CD44-ICD over-expressing RCS cells as compared to control RCS cells. All blots were re-probed using an anti-β-actin antibody.

though we cannot detect direct interaction between CD44 and pERM. There remained the possibility that, in cartilage and chondrocytes, instead of CD44-FL binding to pERM, CD44 binds to non- phosphorylated ERM.

To determine whether CD44-FL in chondrocytes binds to non-phosphorylated ERM, a series of co-immunoprecipitation experiments were performed using anti-CD44-cytotail for immunoprecipitation and anti-total ERM for immunoblotting. We first treated both parental RCS and RCS-CD44-ICD stable transfectants with or without *Streptomyces* hyaluronidase and then immunoprecipitated the cell lysates with anti-CD44-cytotail antibody and immunobloted with anti-ERM antibody (HRP-conjugated). Similar to previous results with pERM, all ERM came down in the not-bound fraction and none was in the eluted fraction (Figure 40A). Re-probing the blot with an HRP-conjugated CD44-cytotail antibody, detected all CD44-FL in the eluted fraction (Figure 40B). As a control, beads were incubated with CD44-CD44-cytotail antibody but no lysate was added to the CD44-cytotail-beads complex. If any bands were detected in the eluted fraction, then they were considered as non-specific.

In addition, RCS cells were lysed with four different detergents (D, E, F and G from figure 41B), immunoprecipitated with CD44-cytotail antibody and then immunoblotted with HRP-conjugated ERM antibody. Once again, no ERM was detected in the eluted portion (Figure 41A).

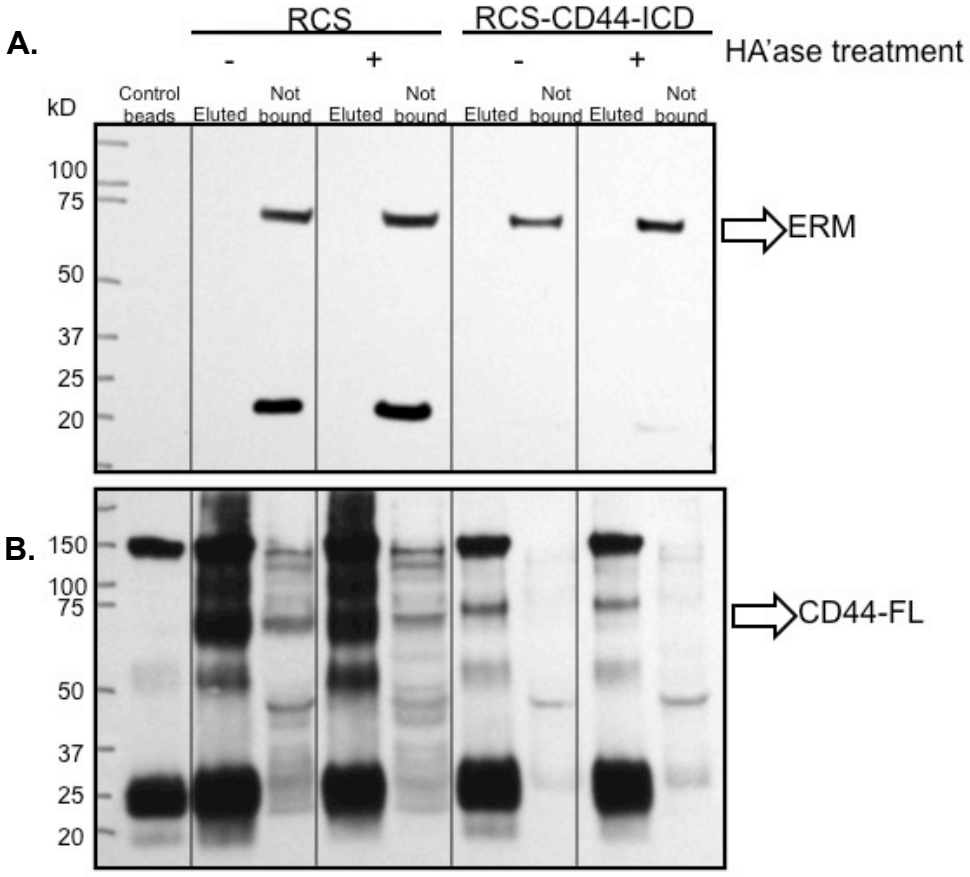

Figure 40: Co-immunoprecipitation of CD44 and total ERM in parental RCS and RCS-CD44-ICD stable transfectants treated with HA'ase. RCS parental and RCS-CD44-ICD stable transfectant cells were treated with or without testicular HA'ase. The control bead column represents non-specific bands. **A.** Cell lysates were immunoprecipitated with CD44-cytotail antibody and western blots probed with HRP-conjugated total ERM antibody. All ERM was detected in the not-bound fraction for both cell lines with or without HA'ase treatment. **B.** Blot was re-probed with HRP-conjugated CD44-cytotail antibody, and most of the CD44-FL was detected in the eluted fraction. As a control, Dynabeads were incubated with the anti-CD44-cytotail antibody but without addition of a cell lysate. Any bands present in the control beads fraction are considered non-specific possibly due to breakdown of the beads. No nonspecific bands were detected using then anti-ERM antibody but, 25, 55 and 150 kD nonspecific bands were detected using HRP-CD44 cytotail antibody.

A.

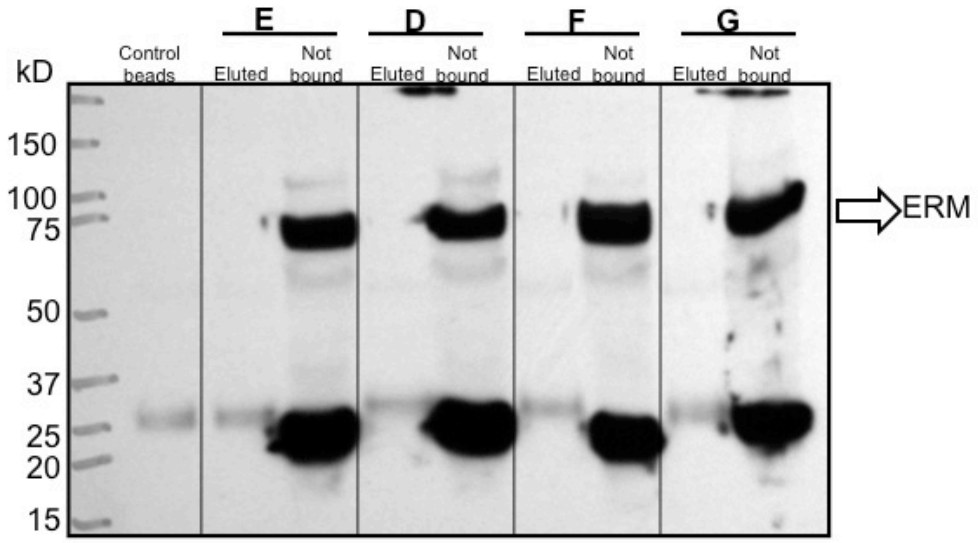

B.

	Concentration	Detergent
A	0.10%	NP-40
B	0.25%	NP-40
C	0.50%	NP-40
D	1%	NP-40
E	0.50%	Triton X-100
F	0.50%	CHAPS
G	1%	CHAPS

Figure 41: Co-immunoprecipitation of CD44 and ERM in RCS using different cell lysis detergents. A. RCS cells were lysed using four different select detergent conditions (D, E, F and G from panel B), immunoprecipitated with CD44-cytotail and western blots probed with an HRP-conjugated total ERM antibody. All total ERM was detected in the not-bound fraction for all four different cell lysis detergent conditions. No ERM proteins were detected in the eluted fraction. Re-probing of blots with HRP-conjugated CD44-cytotail antibody detected all CD44-FL in the eluted portion (not shown). Dynabeads incubated with the anti-CD44-cytotail antibody but without addition of a cell lysate exhibited a single nonspecific band detected using the anti-ERM antibody. Control beads column represents non-specific bands.

On our last attempt to detect CD44/ERM or pERM interactions, dBACs were lysed and immunoprecipitated with CD44-cytotail antibody. Lysates were immunobloted with either ERM or pERM-HRP conjugated antibodies, and in either case no ERM or pERM was detected in the eluted portion (Figure 42).

At this point, we were unable to detect direct binding between CD44 and ERM or pERM. Nonetheless over-expression of CD44-ICD resulted in a down-regulation of ERM phosphorylation. The interaction between CD44-FL and pERM may be too weak to detect under immunoprecipitation conditions or a different actin adaptor protein is utilized in chondrocytes. Our next attempt was to determine whether CD44 links to the cytoskeleton via members of the Ankyrin adapter family.

2.2.3. CD44/Ankyrin interactions

Previous studies of demonstrated that in some cells including ovarian cancer cell line SKOV3, CD44 links to the underlying actin cytoskeleton by interactions with ankyrin (Lokeshwar et al., 1994; Singleton and Bourguignon, 2004). Whether ankyrin interacts with CD44 in chondrocytes is unknown. Which member of the ankyrin family (ANK1, ANK2 and ANK3) interacts with CD44 in chondrocytes or, whether usage of a particular ankyrin with CD44 is tissue dependent, is also unknown.

In our first study, cell lysates were prepared from parental RCS and SKOV3 cells and were immunoprecipitated with anti-CD44-cytotail antibody to pull down all CD44, and the western blot was probed with an HRP-conjugated ankyrin-3 antibody. Several

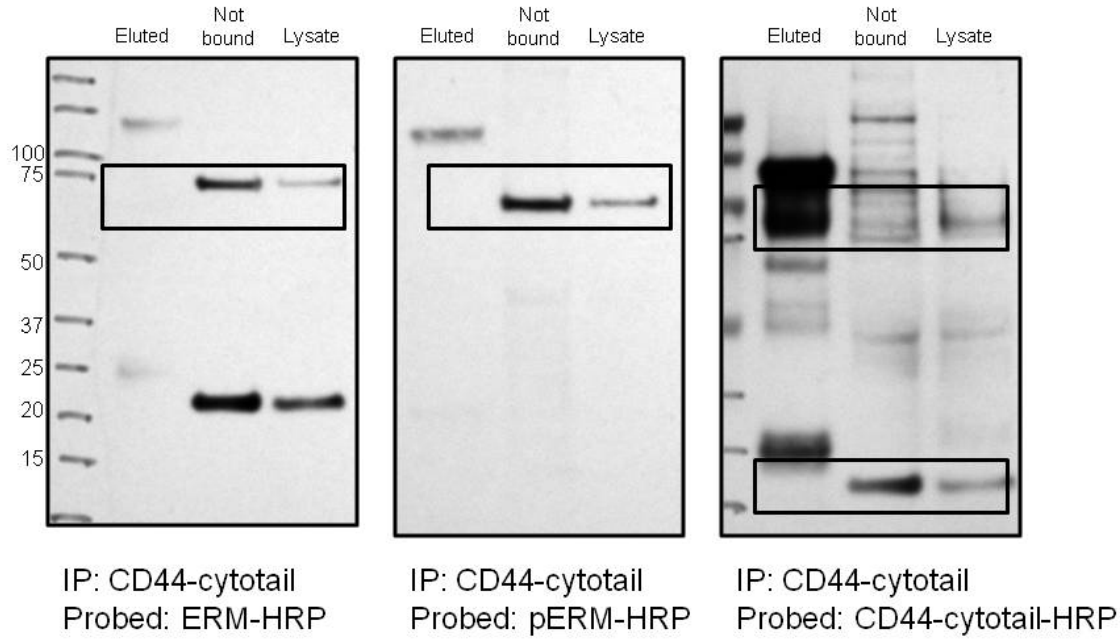

Figure 42: Co-immunoprecipitation of CD44 and total ERM and pERM in dBACs. Cell lysates were prepared from confluent cultures of dBAC, immuno-precipitated with CD44-cytotail antibody, and then probed with HRP-conjugated total ERM antibody (left panel) or HRP-conjugated pERM antibody (middle panel). The pERM blot was then re-probed with HRP-conjugated CD44-cytotail antibody (right panel). In addition, lysates derived from direct extraction of dBACs were also examined. All ERM and pERM proteins were detected in the not-bound fraction. CD44-FL (upper box in right panel) was detected in the eluted fraction. Interestingly, protein bands equivalent in size to a CD44-ICD (lower box in right panel) were detected in the not-bound fraction and in the total cell lysate.

bands were detected in the eluted fraction and others in the not-bound fraction, likely as a result of different isoforms of Ankyrin-3 present in both cells lines (Figure 43A top panel). In addition, SKOV3 lysates were probed for pERM and ERM, but neither was detected in the eluted fraction (Figure 43B). Re-probing with HRP-conjugated CD44-cytotail antibody detected most of CD44-FL in the eluted fraction (Figure 43A bottom panel).

In another set of experiments, cell lysates were prepared from parental RCS and stable RCS-CD44-ICD transfectants. The anti-CD44-cytotail antibody was used to pull down all CD44, and the western blots were probed with a HRP-conjugated anti-Ankyrin-3 antibody. Two bands of ~65 kD and ~130 kD were highly expressed in lysates from both the parental RCS cell line and RCS-CD44-ICD stable transfectants (Figure 44A). These two bands likely represent isoforms of Ankyrin-3 reported at 50-190 kD (Santa Cruz Biotechnology product sheet). More importantly, in parental RCS, the 65 and 130 kD bands were present in both the lysates before immunoprecipitation and the eluted fractions following immunoprecipitation of CD44. However, in the RCS-CD44-ICD stable transfectants, although both 65 and 130 kD bands were present in the lysates prior to immunoprecipitation, only the high molecular mass band (~130 kD) was detected in the eluted fraction following immunoprecipitation of CD44. All of the low molecular weight, 65 kD band was detected in the not-bound fraction (Figure 44A). These results were replicated three times.

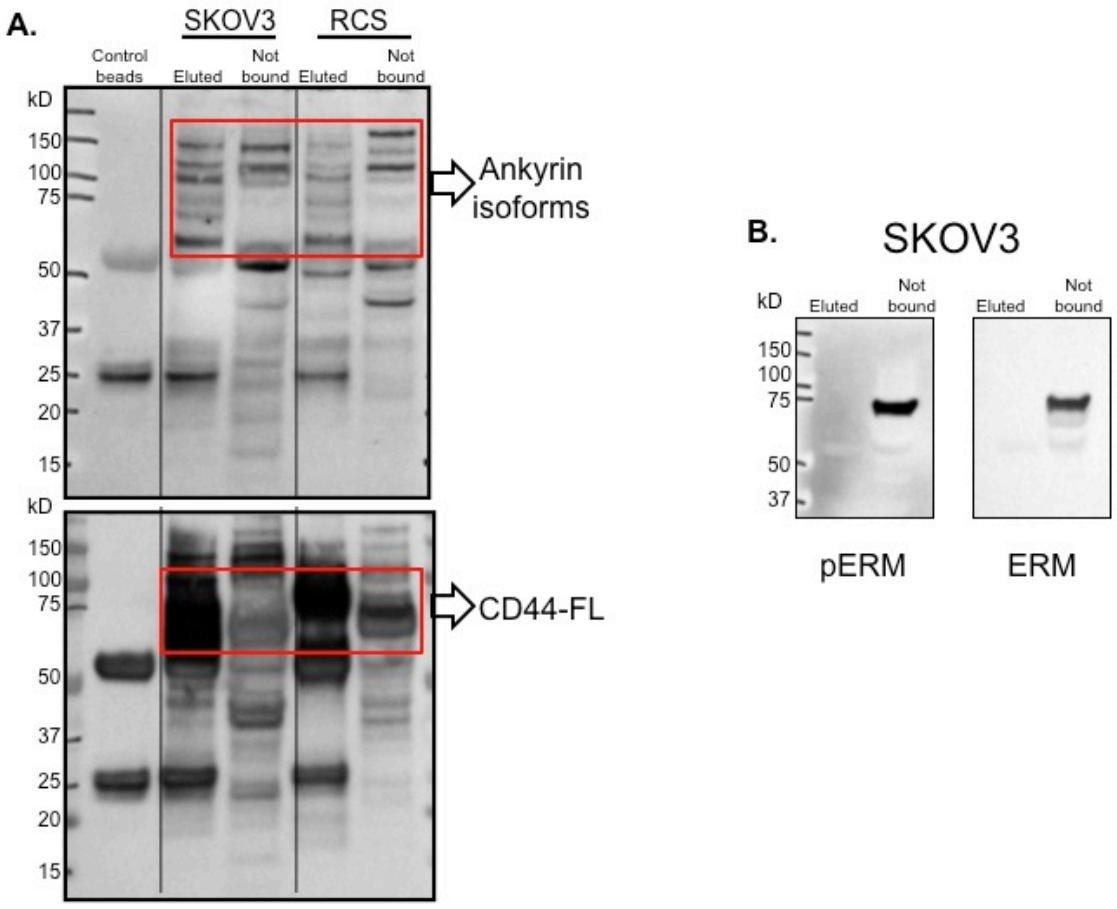

Figure 43: Co-immunoprecipitation of CD44 and cytoskeletal adaptor proteins in SKOV3 and RCS cells. A. Cell lysates were prepared from SKOV3 and parental, control RCS cells. The lysates were immunoprecipitated with CD44-cytotail antibody, and the western blots probed with HRP-conjugated ankyrin-3 antibody (top panel). As seen in the red box area, many isoforms of ankyrin-3 were detected in the eluted fraction, as well as the not-bound fraction in lysates from both cell types. Re-probing of blots with HRP-conjugated CD44-cytotail antibody (lower panel) detected CD44-FL predominately present in the eluted portion (red box area) in both cell types. Dynabeads incubated with the anti-CD44-cytotail antibody but without addition of a cell lysate exhibited a single 25 kD nonspecific band detected using the anti-ankyrin-3 antibody and two nonspecific bands, ~25 and 60 kD using the anti-CD44 cytotail antibody. **B.** Western blots of SKOV3 immunoprecipitates with CD44-cytotail antibody in panel A were re-probed with HRP-conjugated pERM and anti-total ERM antibodies, and in both cases ERM and pERM were detected in the not-bound fraction. Control eluted bands represent non-specific bands.

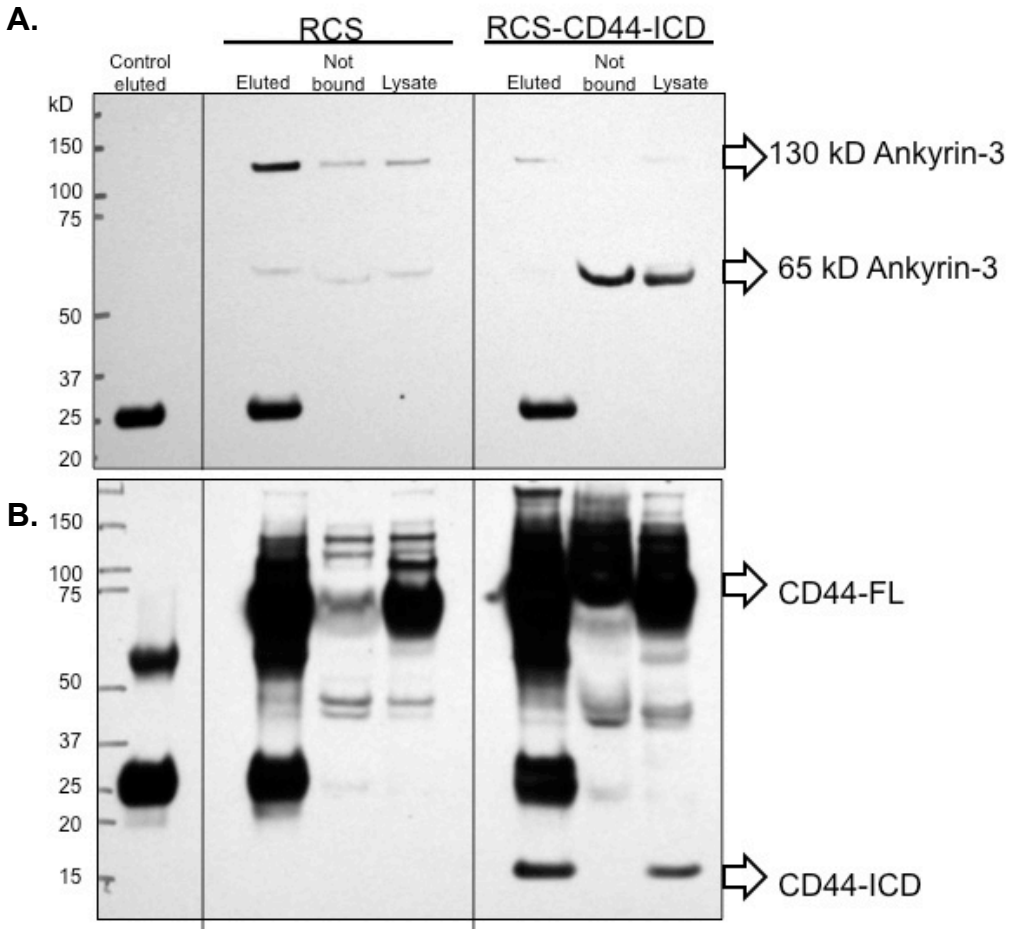

Figure 44: Co-immunoprecipitation of CD44 and Ankyrin-3 in RCS and RCS-CD44-ICD stable transfectant cell lines. A. Cell lysates of parental RCS and RCS-CD44-ICD stable transfectants were immunoprecipitated with CD44-cytotail antibody and probed with an HRP-conjugated ankyrin-3 antibody. Two ankyrin isoforms (65 kD and 130 kD) were detected in the cell lysate of both RCS lines however, the 130 kD was the predominate isoform in the parental cells and the 65 kD isoform in the CD44-ICD stable transfectants. Both isoforms were also detected in the eluted fraction of parental RCS cell lysates, however, the 130 kD isoform was predominate. In RCS-CD44-ICD transfectants, only the high molecular mass, 130 kD isoform was detected in the eluted portion, and all of the lower molecular mass (65 kD) isoform was detected in the not-bound fraction, suggesting that CD44-ICD over-expression directly affects CD44 interactions with this ankyrin isoform. **B.** Re-probing of blots with HRP-conjugated CD44-cytotail antibody detected CD44-FL predominately present in the eluted fraction of both RCS and RCS-CD44-ICD. Additionally, the CD44-ICD, expressed in the stable RCS-CD44-ICD transfectants, was also recovered in the eluted fraction. Dynabeads incubated with the anti-CD44-cytotail antibody but without addition of a cell lysate exhibited a single 25 kD non-specific band detected using the anti-ankyrin-3 antibody and two nonspecific bands, ~25 and 60 kD using the anti-CD44 cytotail antibody.

This same experiment was repeated with an ankyrin-1 antibody. Many bands were detected in both RCS and RCS-CD44-ICD cell lysates, but none of the isoforms were detected in the eluted fraction of either cell line after immunoprecipitation with CD44-cytotail antibody (Figure 45).

These data suggest that CD44 binds to the actin cytoskeleton via two isoforms of ankyrin-3 in chondrocytes, and over-expression of CD44-ICD affects direct binding of CD44-FL with the lower molecular weight isoform of ankyrin-3. These data might explain why endogenous CD44-FL can be extracted easily in RCS-CD44-ICD stable and transient transfectants when compared to parental cell line.

2.2.4. Effect of CD44-ICD on CD44-FL phosphorylation (immunoprecipitation study).

In resting cells, the majority of CD44 is phosphorylated at Ser^{325} (Peck and Isacke, 1998) and phosphorylation of Ser^{291} is required to dephosphorylate Ser^{325} to control and modulate receptor function (Legg et al., 2002). However, it is difficult to study specific CD44 phosphorylation due to lack of commercial antibodies specific to CD44 phosphorylation sites.

In order to determine whether CD44-ICD has an effect on endogenous CD44-FL phosphorylation, cell lysates were immunoprecipitated with CD44-cytotail antibody and then probed with a general phosphor-serine antibody. The phosphorylation of CD44 appears to decrease in stable RCS-CD44-ICD transfectants (Figure 46A), suggesting

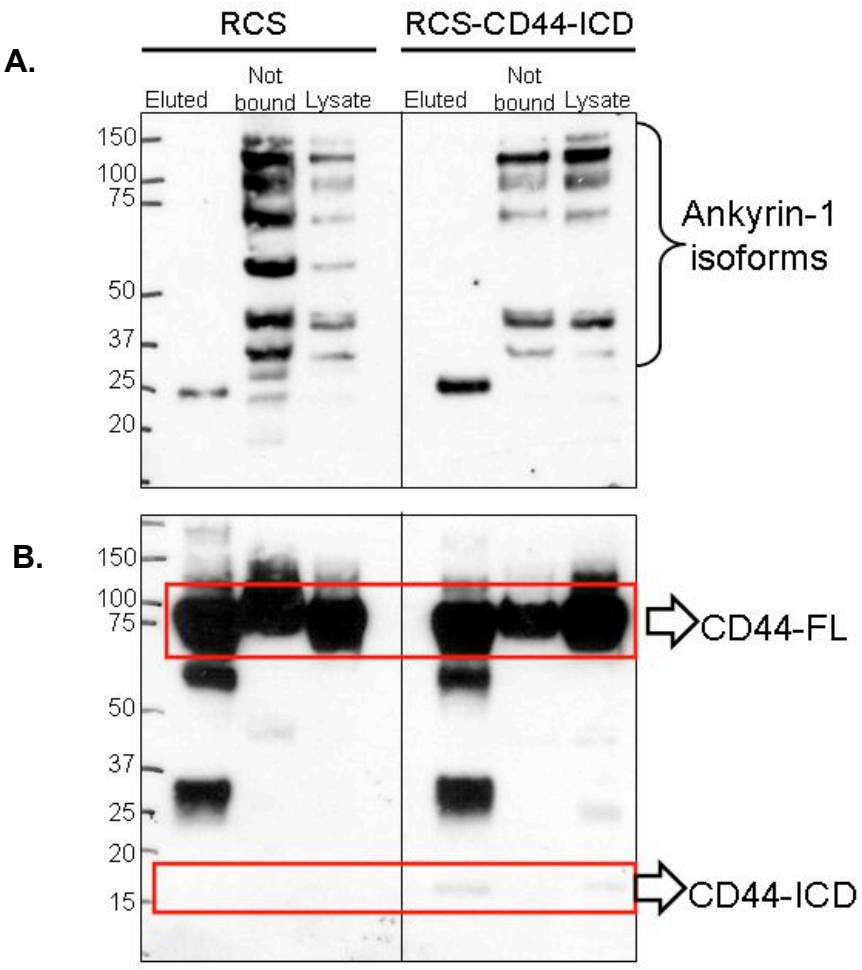

Figure 45: Co-immunoprecipitation of CD44 and Ankyrin-1 in RCS and RCS-CD44-ICD stable transfectant cell lines. A. Cell lysates of parental RCS and RCS-CD44-ICD stable transfectants were immunoprecipitated with CD44-cytotail antibody and probed with an HRP-conjugated ankyrin-1 antibody. Several ankyrin isoforms were detected in the direct cell lysates and not-bound fractions of both RCS lines, and no bands were detected in the eluted fraction. No ankyrin bands were detected in the eluted fraction. **B.** Re-probing of blot with HRP-conjugated CD44-cytotail antibody detected CD44-FL predominately present in the eluted fraction of both RCS and RCS-CD44-ICD. Additionally, the CD44-ICD, expressed in the stable RCS-CD44-ICD transfectants, was also recovered in the eluted fraction.

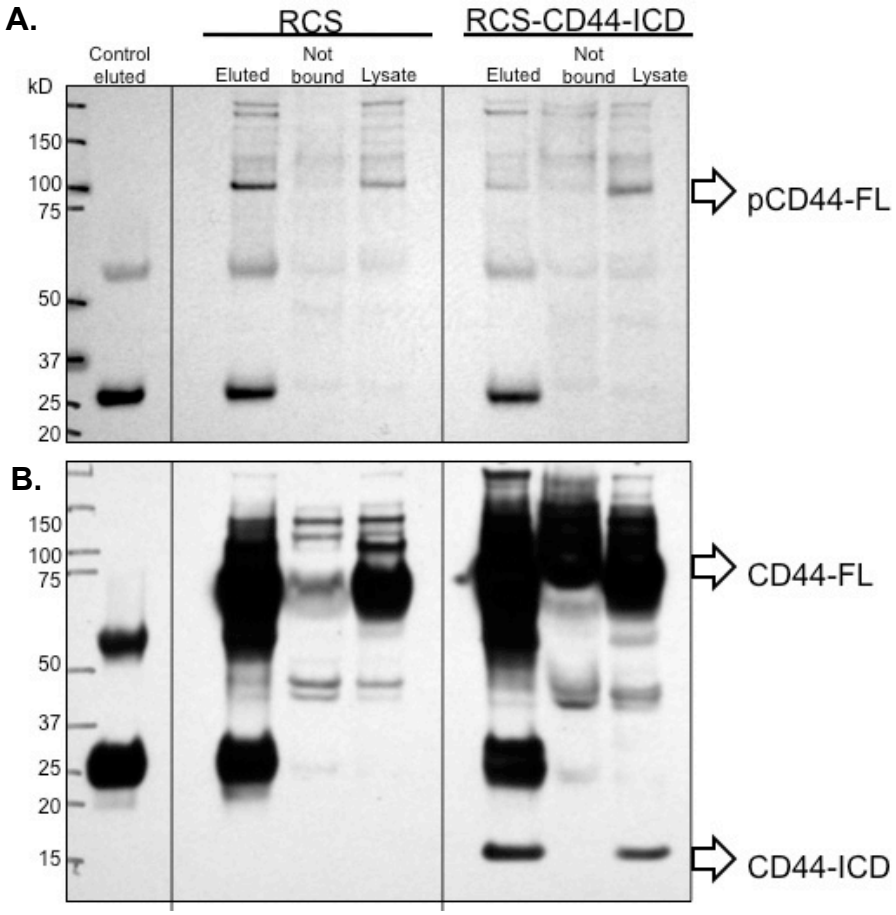

Figure 46: Changes in serine phosphorylation of CD44-FL in RCS and RCS-CD44-ICD stable transfectant cell lines. A. Cell lysates of parental RCS and RCS-CD44-ICD stable transfectants were immunoprecipitated with CD44-cytotail antibody and western blots probed with an anti-phospho-serine antibody. In addition, lysates derived from direct extraction of the two RCS lines were also examined. In parental RCS cells, a prominent band possibly indicative of phospho-CD44-FL was detected in the eluted fraction. The same band was also present in the total cell lysates of both RCS lines. However, in the eluted fraction of RCS-CD44-ICD stable transfectants, the expression of this band was down-regulated. **B.** Re-probing of blots with HRP-conjugated CD44-cytotail antibody detected CD44-FL predominately present in the eluted fraction of both RCS and RCS-CD44-ICD. Additionally, the CD44-ICD, expressed in the stable RCS-CD44-ICD transfectants, was also recovered in the eluted fraction. Dynabeads incubated with the anti-CD44-cytotail antibody but without addition of a cell lysate exhibited ~25 and 60 kD nonspecific bands using the anti-phosphoserine and anti-CD44 cytotail antibodies.

that CD44-ICD may downregulate endogenous CD44-FL phosphorylation. When the blot was re-probed with an HRP-conjugated CD44-cytotail, most of the CD44-FL and all of the CD44-ICD were detected in the eluted fraction (Figure 46B).

2.2.5. Generation of point mutations to block the effect of rhCD44-ICD on CD44-FL.

Two mutated CD44-ICD constructs were developed to try to block the effects of CD44-ICD on endogenous CD44-FL function using the GeneTailor™ Site Directed Mutagenesis System from *Invitrogen*. The first point mutation was targeted to three positively charged residues of the ERM binding domain, located just distal to the plasma membrane. According to Yonemura and colleagues, mutating $K^{298}K^{299}K^{300}$ to $Q^{298}I^{299}N^{300}$ resulted in no CD44-ERM binding (Yonemura et al., 1998). Therefore, our mutation strategy was to convert the positively charged KKK residues to QIN, as suggested by the previous study.

The next mutation was targeted to the ankyrin binding domain. It was more challenging to decide which amino acids were crucial for CD44 binding to ankyrin, since to our knowledge the only studies addressing CD44 binding to ankyrin include truncated versions of the CD44 sequence rather than point mutations. Our strategy was to target plausible residues within the putative ankyrin binding domain of CD44, similar to the approach we used with ERM mutation. Given that CD44 binding to ERM seemed to rely on a cluster of three positively charged amino acids, we identified two basic residues in the ankyrin binding domain sequence of CD44 as a reasonable first step:

Arg^{313}-Lys^{314}. Following a similar strategy used to introduce point mutations into the ERM binding domain, we mutated these two residues to Ile^{313}-Asn^{314}.

These two mutated peptides (CD44-ICDΔERM and CD44-ICDΔAnk) were used in co-immunoprecipitation studies in an attempt to reverse any CD44-ICD effects on CD44-FL endogenous function. Because we were unable to detect any direct interaction between CD44 and ERM, we did not expect to see any different result with CD44-ICDΔERM. However, we found that CD44-ICD affects CD44-FL binding to a ~65 kD isoform of ankyrin3, and therefore expected to reverse these effects by transfecting RCS cells with CD44-ICDΔAnk. Unfortunately, no changes were detected (results replicated twice) when compared to previous results.

Definitive conclusions cannot be made for the lack of rescue of CD44-ICDΔAnk as compared to the activity of wild-type CD44-ICD to block interactions of CD44-FL with ankyrin. One possibility is that the amino acids that were chosen to alter within the ankyrin binding domain of the CD44-ICD were not crucial for CD44 binding to ankyrin, and therefore the results between the mutated peptide and CD44-ICD were similar. A second possibility is that the point mutation protocol failed to change the desired amino acids within the ankyrin binding domain. Subsequent DNA sequencing results confirmed that the Arg^{313}-Lys^{314} to Ile^{313}-Asn^{314} mutation was not present in the several of the bacterial colonies picked for expansion and plasmid purification. It was later determined that the One Shot® MAX Efficiency® DH5á™-$T1^R$ competent cells,

used as part of the *Invitrogen* GeneTailor™ protocol were not effective in destroying the methylated-parental strands. Thus, the resulting colonies likely contained a mixture of both parental and daughter strand clones. To resolve this problem our laboratory subsequently included part of the protocol used in the QuikChange® Site-Directed Mutagenesis Kit from *Stratagene*. In this protocol the CD44-ICD plasmid was methylated and re-amplified using the same strategy mutagenesis primers described previously in this study. However, following the reaction, the *Stratagene* approach was carried out as the next step, using the restriction enzyme *Dpn I* to destroy all methylated parental DNA strands, instead of using the DH5á™-T1^{R} bacteria. Bacteria were grown in chemically competent TOP 10 cells, and colonies selected were purified and sequenced. Sequencing results confirmed successful mutations, and these plasmids are now available for future studies.

2.2.6. Co-immunoprecipitation studies to re-explore CD44-FL binding to Smad1.

It still remains unclear whether cleaved CD44-ICD can interact with Smad1 and affect the natural signaling function of CD44-FL. To address this question, several co-immunoprecipitation assays were developed to detect interactions between CD44-FL and CD44-ICD with Smad1.

First we treated parental and CD44-ICD stable transfectant RCS cells with or without BMP 7. Cell lysates were immunoprecipitated with CD44-cytotail antibody and

probed with an HRP-conjugated Smad1 antibody. A 60 kD band was detected in all eluted fractions and did not seem to change between treatments or cell lines (Figure 47). It is still impossible to determine whether CD44-ICD is interacting with Smad1 based on these results, due to the fact that the CD44-cytotail antibody pulls down both CD44-FL and CD44-ICD.

We then tried to immunoprecipitate the same lysates using a Smad1 antibody, and probed with an HRP-conjugated CD44-cytotail antibody to determine whether CD44-ICD could interact with Smad1. A very small pool of CD44 was detected in the eluted fraction of both cell lysates when compared to the CD44 that did not bind (Figure 48). It appears that parental RCS had more CD44 binding to Smad1, but this could be due to unequal protein concentration between the two lysates (equal volume was loaded, and cell lysate fraction from the parental RCS contained more protein when compared to that of RCS-CD44-ICD). Interestingly, a very faint band the size of CD44-ICD is detected in the “not-bound” fraction of RCS-CD44-ICD stable transfectants, suggesting that CD44-ICD does not interact with Smad1.

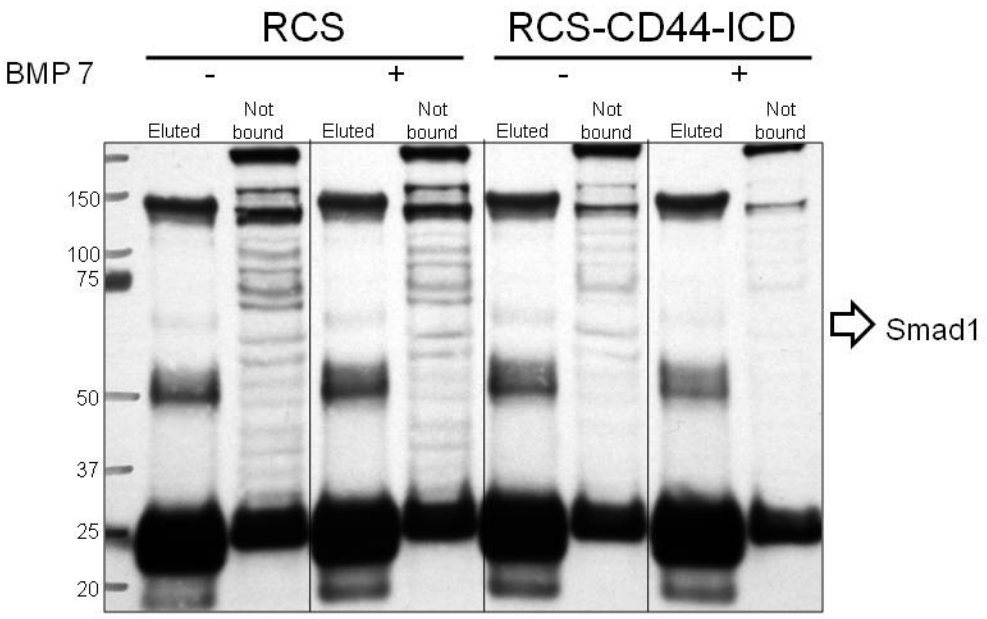

Figure 47: Co-immunoprecipitation of CD44 and Smad1 in RCS and RCS-CD44-ICD stable transfectant cell lines with or without BMP 7 treatment. RCS and RCS-CD44-ICD stable transfectants were either incubated with serum free media (control) or with BMP 7 for 1 hour. Cells were immediately lysed, and cell lysates were immunoprecipitated with CD44-cytotail antibody and probed with an HRP-conjugated Smad1 antibody. In all lysates, some Smad1 was detected in the eluted fraction (~60 kD), but Smad1 interaction with CD44 did not seem to be affected by BMP 7 treatment or CD44-ICD over-expression.

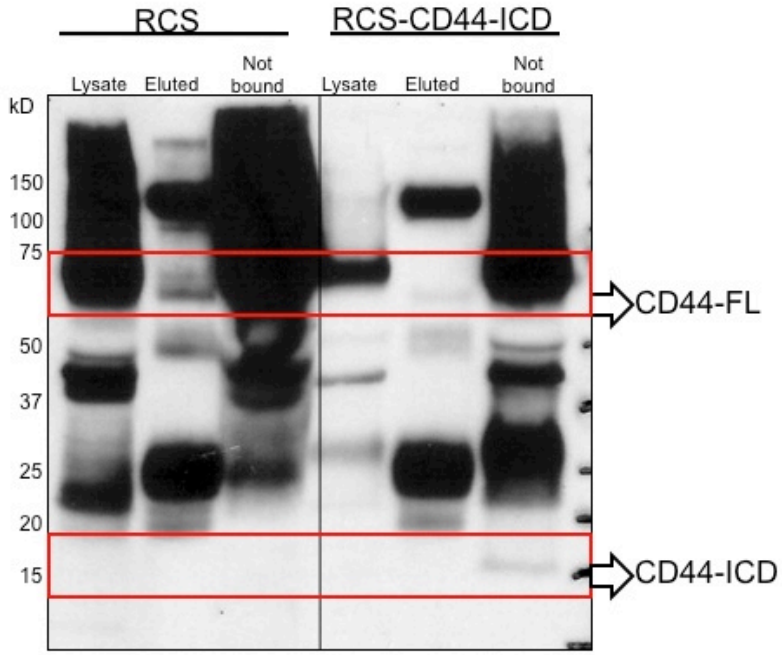

Figure 48: Co-immunoprecipitation of CD44-FL in RCS and RCS-CD44-ICD stable transfectant cell lines. RCS and RCS-CD44-ICD stable transfectants were lysed, immunoprecipitated with Smad1 antibody and probed with an HRP-conjugated CD44-cytotail antibody. Most of the CD44-FL was detected in the not-bound fraction; however a small pool was detected in the eluted fraction as well. In parental RCS cells, a larger pool of CD44-FL was detected in the eluted fraction when compared to CD44-RCS-ICD stable transfectants. In addition, all CD44-ICD from the RCS-CD44-ICD transfectants was detected in the not-bound fraction, suggesting that Smad1 does not bind to fragmented CD44-ICD. The other bands in the eluted fraction are non-specific.

CHAPTER 4: GENERAL DISCUSSION AND CONCLUSIONS

The main focus of this study was to investigate the effect of release of CD44-ICD fragments into the cytoplasm of cells, chondrocytes in particular. Our hypothesis was that the free CD44-ICD would exhibit a competitive or "dominant-negative" effect on CD44-FL functions. There are several reports in the literature that CD44 undergoes sequential proteolytic cleavage, releasing a soluble CD44 into the extracellular space as well as an intracellular fragment (CD44-ICD). Proteolytic cleavage of CD44 is associated with pathological conditions such as cancer invasion and metastasis (Cichy and Pure, 2003; Guo et al., 1994; Lammich et al., 2002; Masson et al., 1999; Murakami et al., 2003; Okamoto et al., 1999a; Okamoto et al., 2001; Pelletier et al., 2006; Yamane et al., 1999) and rheumatoid arthritis (Haynes et al., 1991b). Recently, our laboratory demonstrated that CD44 fragmentation was a prominent feature associated with osteoarthritic cartilage (Takahashi et al., 2010). Although CD44 fragmentation is known to occur, little is known about the effects of this event on cell physiology. While CD44-ICD may exert multiple of effects on cell behavior, this study focused on specific changes to cell functions dependent on CD44-FL.

The approach chosen to address more directly the effects of CD44-ICD release was to prepare a variety of eukaryotic expression plasmids containing the CD44-ICD domain. These expression plasmids, when introduced into cells would provide for the select over-expression of an individual domain, the CD44-ICD.

In the cloning of the CD44-ICD, several technical problems needed to be overcome to perform in-frame directional cloning, such as introducing the appropriate restriction sites in the primers, selecting the appropriate sequence to resemble the naturally-occurring cleaved CD44-ICD, introducing a start site in expression plasmids with a C-terminal epitope tag, selecting appropriate epitope tags and developing a control “untagged” plasmid.

After successfully generating and purifying a variety of CD44-ICD, CD44-FL and Smad1 plasmids (Figure 5), several cell lines, including chondrocytes, were transfected using the Amaxa nucleofection system. Transfection efficiency was typically determined by immunofluorescent imaging 2 days after transfection, and experiments were conducted shortly after to verify successful transfection.

Although, useful data was obtained in some transient transfection experiments of primary chondrocytes culture, variability in transfection efficiency continued to limit the interpretation of our results. In addition, after BAC transfection, cells had to be passaged at least once, which induced the chondrocytes to de-differentiate into more fibroblast-like cells (dBACs), therefore losing important characteristics of primary chondrocytes. For example, as shown in Figure 49, the circumferential cortical organization of the actin cytoskeleton of primary chondrocytes takes on the appearance

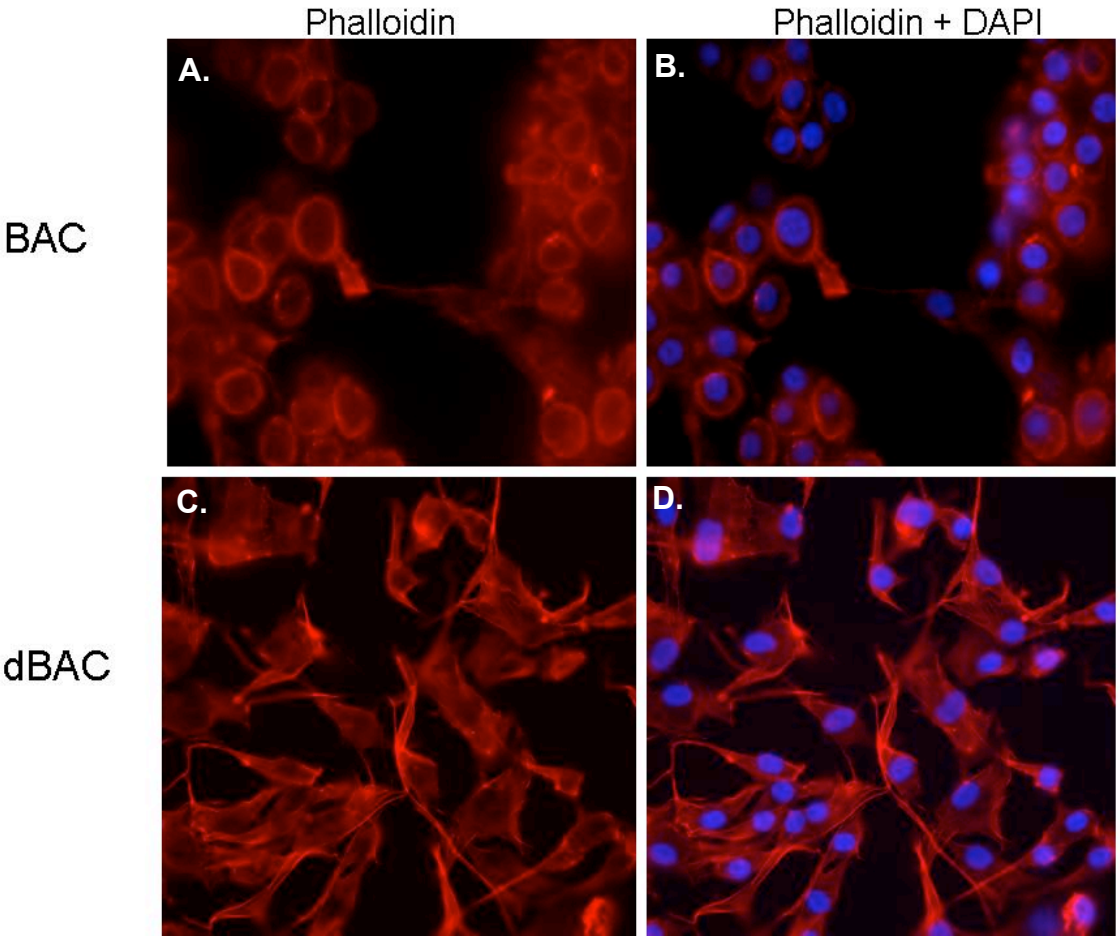

Figure 49: Rhodamine-phalloidin staining of primary BACs and dBACs. Primary cultures of BACs (A,B) and dBACs (C,D) were fixed, permeabilized and the actin cytoskeleton stained with rhodamine-phalloidin (red fluorescence). The slides were then mounted with DAPI –containing mounting media (blue fluorescence). As noted in A and B, the primary chondrocytes have a cortical actin cytoskeleton, characteristic of non-OA chondrocytes. On the other hand, as BACs are passaged several times, they begin to lose their cortical morphology, and change into more fibroblast-looking cells with elongated processes (C and D). This morphology has been reported in OA-chondrocytes (Holloway et al., 2004).

of fibroblast stress-fiber organization in dBACs. To address this problem, CD44-ICD-expressing stable cell lines were generated (HEK-293 and RCS) using the Flp-In system from *Invitrogen.* Once cells were successfully transfected, cells were kept in hygromycin-selective media to continue selection of CD44-ICD stable transfectants only. The stable transfectant chondrocyte cell line, RCS, became an important tool in this study.

Once a viable method to study effects of CD44-ICD on CD44-FL function was obtained, several CD44-FL functions were examined in this study, including the effects on CD44-FL/Smad1 signaling pathway and the ability of CD44 to bind to HA and retain a pericellular coat. If CD44-ICD does in fact have a dominant-negative effect on CD44-FL functions, our next goal was to investigate the mechanisms involved in these competitive interactions.

First, we examined the possible effects of CD44-ICD on the CD44-FL/Smad1 signaling pathway. The putative Smad1 binding site on CD44 is located at the distal C-terminal end of the CD44 intracellular domain (Peterson et al., 2004). Since this binding site is present and intact within the CD44-ICD, we hypothesize that the CD44-ICD could compete with CD44-FL for Smad1 binding. Through this binding, CD44-ICD might sequester Smad1. Because CD44-ICD is not anchored to the plasma membrane, it would not exhibit the same capacity to present Smad1 to the BMP receptor during the activation of the BMP 7 signaling pathway. As a result, any Smad1 bound to CD44-ICD will not be phosphorylated, and translocated to the nucleus. Thus, we predicted

that overall Smad1 phosphorylation would be down-regulated in CD44-ICD transfected cell lines as compared to control or parental cells. In addition, Smad1 would stay bound to CD44-ICD in a non-phosphorylated state and co-immunoprecipitate with CD44-ICD.

When Smad1 phosphorylation was investigated in RCS-CD44-ICD stable transfectants and parental cell lines, a down-regulation in Smad1 phosphorylation was observed in stable RCS-CD44-ICD cells. In addition, when parental and CD44-ICD stable RCS transfectants were treated with or without BMP 7 for 1 hour, the RCS-CD44-ICD cells did not respond to BMP 7 activation as strongly when compared to parental RCS. These results support part of our initial hypothesis that over-expression CD44-ICD would exert a negative effect on Smad1 phosphorylation.

Cell lysates of both parental RCS and RCS-CD44-ICD stable transfectants were immunoprecipitated using an anti-Smad1 antibody. The blots were then probed with an HRP-conjugated anti-CD44-cytotail antibody to determine if any CD44-ICD could be detected. Although CD44-FL was immunoprecipitated in parental RCS, a much smaller amount of CD44-FL was detected in anti-Smad1 immunoprecipitate of RCS-CD44-ICD stable transfectant lysates (Figure 48). This could a result of unequal protein concentration between the two lysates, because equal volume is loaded in co-immunoprecipitation assays as opposed to equal protein. However, our attempts to co-immunoprecipitate CD44-ICD with Smad1 were not successful (Figure 48). One the one hand, these results suggest that CD44-ICD may interfere with CD44-FL binding to Smad1.

Unfortunately, no CD44-ICD was detected in the eluted fraction of RCS-CD44-ICD stable transfectants. Nonetheless, the downregulation of Smad1 phosphorylation and reduced immunoprecipitation of CD44-FL in CD44-ICD transfectants supports our hypothesis that CD44-ICD affects CD44/Smad1 signaling pathway in response to activation. However, whether this is due to direct CD44-ICD / Smad1 sequestering or some other mechanism, remains to be determined.

Attempts were also made in this study to follow Smad1 translocation to the nucleus using immunofluorescence microscopy, as a measure of Smad1 activation in response to activation. Unfortunately, very limited translocation of the GFP/EGFP Smad1 fusion proteins was observed in parental C28/I2 cell line (Figure 21), and no translocation was observed in dBACs (Figure 22).

Our next goal was to investigate the effects of CD44-ICD on CD44-FL ability to retain a pericellular coat. In chondrocytes, CD44 binds to HA, and therefore, CD44 is a critical component for the retention of the proteoglycan rich ECM (Knudson, 2003). Particle exclusion assays have been used in the past to visualize the pericellular matrix of individual chondrocytes. We used this approach to investigate the effects of CD44-ICD over-expression on the ability of CD44-FL to retain a pericellular coat in transient and stable CD44-ICD transfectants.

In initial experiments, we examined the effects of CD44-ICD on coat retention by using culture conditions that our laboratory had recently determined could induce

cleavage of endogenous CD44-FL (Takahashi et al., 2010). Addition of agents such as IL-1β, PMA and HA oligosaccharides to normal BACs induced endogenous CD44-FL cleavage. PMA has been used in several studies to initiate the sequential proteolytic cleavage of CD44 (Nagano et al., 2004). Nagano and colleagues suggest that proteolytic cleavage is regulated by several signal pathways, including the extracellular influx of Ca^{2+}, and activation of PKC, Ras oncoprotein and Rho family GTPases (Kawano et al., 2000; Okamoto et al., 1999b).

The consequence of adding these reagents to chondrocytes was examined on one of the prime functions of CD44-FL, its role in retaining a HA/proteoglycan-rich pericellular matrix. Particle exclusion assay of BACs treated with IL-1β, PMA and HA oligosaccharides revealed a drastic reduction in the size of their pericellular coats. However, it is difficult to make unambiguous conclusions from these results because reagents like IL-1 and PMA are pleiotropic in their mechanism of action. For example, IL-1 exerts both a catabolic effect (upregulation of MMPs and ADAMs) as well as an anti-anabolic effect (downregulates aggrecan expression) (D'Souza et al., 2000; Flannery et al., 1999; Little et al., 1999; Nishida et al., 2000). A more direct approach was needed to determine the cellular consequences of released intracellular CD44-ICD.

Our next approach was to investigate the effects on coat retention in chondrocytes expressing either transient or stable CD44-ICD. Over-expression of CD44-ICD-EGFP in transiently transfected BAC (Figure 25) resulted in total loss of capacity to retain a pericellular coat as compared to non-transfected control cells.

Similar results were obtained with transient and stable CD44-ICD transfection of RCS cells (Figures 26-27). One interpretation of the loss of coats on CD44-ICD transfectants, is that the CD44-ICD alters the capacity of the CD44-FL to bind or retain a level of HA necessary to maintain a pericellular matrix. Other conclusions are also possible as the synthesis, retention and maintenance of pericellular matrices are dependent on multiple cellular events and pathways. These events might somehow be affected by over-expression of the CD44-ICD. Nonetheless, the overall effect on coats is consistent with our initial hypothesis that CD44-ICD has a negative effect on CD44-FL ability to retain a pericellular coat.

In addition, HABP staining of parental and stable CD44-ICD transfectants supported the results from the particle exclusion assay (Figure 29). Parental RCS cells, that were predicted to have an intact CD44/HA interaction, displayed a continuous cortical ring of fluorescent HABP along the plasma membrane, suggesting that HA is bound to cell surface receptors throughout the cell. However, stable RCS-CD44-ICD transfectants exhibited a disrupted pattern, rather than a total loss of HA. This disrupted pattern is again not definitive, but consistent with the hypothesis that CD44-ICD affects CD44/HA interactions. It is also possible that the green fluorescence represents HA bound to the membrane HA synthase (HAS) rather than bound to CD44. Nonetheless, data on pericellular coat retention and HABP staining in chondrocytes over-expressing CD44-ICD supports our hypothesis that CD44-ICD may act by competing with functions of CD44-FL.

Next we investigated whether CD44-FL binding to the cytoskeleton was affected by CD44-ICD over-expression. Previous studies reported that the interaction between CD44-FL and the actin cytoskeleton is crucial for cartilage matrix retention. Disruption of the actin network with reagents like cytochalasin D and latrunculin A resulted in easier extraction of CD44-FL, reduction in HA binding, pericellular matrix assembly and retention in chondrocytes (Nofal and Knudson, 2002). This is the only evidence to date showing that disrupting CD44-FL interactions with the cytoskeleton results in depletion of the pericellular matrix. Our study intends to determine whether CD44-ICD could have a similar effect on CD44-FL function by competing with CD44-FL binding to the cytoskeleton.

Our first approach was to study CD44-FL extractability in parental and CD44-ICD transient and stable transfectants, using a differential extraction method similar to the one used by Nofal and Knudson. In their study, they found that cytochalasin and latrunculin shifted CD44-FL from harsh to light extraction, suggesting that extraction with either harsh or with light detergents was dependent on CD44 attachment to the cytoskeleton (Nofal and Knudson, 2002). First, we used a variety of conditions known to affect CD44/cytoskeleton interactions to test the differential extraction method. For instance, it has been reported previously that disrupting CD44/HA interactions directly by adding competitors to the HA binding site such as HA oligos, results in disruption of CD44 with the cytoskeleton (Duterme et al., 2009). When we treated BACs with HA oligos, most of the CD44-FL was easily extracted with the light detergent whereas the untreated cells required a harsh detergent to extract the majority of CD44-FL,

supporting previous studies. Our goal in this study was to determine if the same effects can be replicated having an inside-out effect; that is, whether CD44-ICD over-expression can have the same effect on CD44-FL extractability as HA oligos.

Results from several transient and stable CD44-ICD transfections in BACs and RCS cells were consistent with our hypothesis that CD44-ICD acts as a negative competitor to CD44-FL binding to the cytoskeleton inside the cell. CD44-ICD transfectants had the majority of CD44-FL extracted under light conditions, compared to control cells, which required a harsh detergent to extract most of the CD44-FL. Although it could be argued that this method is not precise because it is dependent on the composition of the light detergent or lysis extractions conditions. Nevertheless, the method was very consistent throughout different experiments. It was important, however, to treat control and experimental lysates equally (i.e. lyse with the same detergent aliquots at the same time) for each experiment, and to load equal volume rather than equal protein for gel electrophoresis analysis.

At this point, particle exclusion assay, HABP staining and differential extraction data provided enough evidence to support our initial hypothesis that CD44-ICD was acting as a negative competitor to CD44-FL function. Our next goal was to explore the actual mechanism(s) involved in this competitive interaction. Our experimental approach was to perform several co-immunoprecipitation studies to investigate cytoskeletal binding partners of CD44-FL, and determine whether CD44-ICD was directly competing with CD44-FL binding to the actin cytoskeleton.

CD44, like other receptors, does not bind to the cytoskeleton directly but rather, via intermediary adaptor proteins. Those most commonly studied in relationship to CD44 are members of the ERM family and the ankyrin family (Bourguignon et al., 1998; Duterme et al., 2009; Hirao et al., 1996; Legg and Isacke, 1998a; Mori et al., 2008; Singleton and Bourguignon, 2004; Tsukita and Yonemura, 1997).

It remains unknown whether CD44 can interact with both ERM and ankyrin simultaneously forming a single complex, or if CD44/ERM and CD44/ankyrin represent two separate, mutually-exclusive complexes that are utilized in a tissue dependent manner. Alternatively, perhaps CD44 has the ability to switch between ERM and ankyrin within a single cell type so as to confer a particular function. There are several reports of CD44 binding to the cytoskeleton via ERM binding proteins (Duterme et al., 2009; Hirao et al., 1996; Legg and Isacke, 1998; Mori et al., 2008; Tsukita and Yonemura, 1997), as well as others that demonstrate CD44 binding via ankyrin (Bourguignon et al., 1998; Singleton and Bourguignon, 2004). However, to date, the cytoskeleton adaptor proteins that interact directly with CD44 in articular chondrocytes has not yet been identified.

In this project, CD44/ERM interactions in chondrocytes were first investigated since a recent, contemporary report described these interactions in rat fibroblasts BB16 cells (Duterme et al., 2009). Moreover, this study demonstrated that ERM phosphorylation levels were lower in BB16 fibroblasts over-expressing hyaluronidase-2 (Hyal2), as compared to parental cells. Hyal2 interacts with CD44 disrupting the

receptor's ability to bind to HA, which in turn, disrupts CD44/ERM binding and subsequent ERM phosphorylation. Such an event could be denoted as an outside-in effect. The effect of Hyal2 in this study is similar to changes in the differential extractability of CD44 that we observed in BACs treated with HA oligos. Treatment of chondrocytes with HA oligos generates outside-in effects similar to Hyal2. For example, HA oligos treatment results in loss of chondrocyte pericellular matrices, and shifts the percentage of CD44 recovered under light detergent conditions. A testable idea is that if Hyal2 alters CD44/ERM interactions in fibroblasts similar to the effects of HA oligos or purified hyaluronidase, either one of these treatments would similarly alter CD44/ERM interactions in chondrocytes.

However, as illustrated in Figures 35 – 42, all of our attempts to co-immuno-precipitate CD44 with ERM or pERM, under many different conditions, were unsuccessful. A lysis buffer similar to that used by Duterme and colleagues to successfully co-immunoprecipitate CD44 and pERM in fibroblasts was tested but, no pERM was recovered in the eluted fraction (Figure 35-37, 42). To more directly mimic their Hyal2 results, RCS cells were treated with our without testicular or *Streptomyces* HA'ase (Figure 37) yet we were still unable to co-immunoprecipitate pERM with CD44 under these conditions. The same negative results were obtained in experiments testing co-immunoprecipitation of either ERM or pERM with CD44 in both transient and stable CD44-ICD transfected chondrocyte cell lines using the same lysis buffer (Figure 35, 37, 40). Neither ERM nor pERM could be recovered in the immunoprecipitated CD44 fraction.

The study by Duterme and colleagues used a fibroblast cell line to demonstrate co-immunoprecipitation of CD44 with pERM (Duterme et al., 2009). We attempted to mimic their results using dBACs. As shown in Figure 49, dBACs exhibit several morphological features that are similar to fibroblasts including prominent actin stress fibers. However once again, we were unable to detect a direct interaction between CD44 and either ERM or pERM in lysates of dBACs (Figure 42). This suggests that that use of a specific cytoskeletal adaptor protein in association with CD44 is not dictated by the presence of a particular cytoskeletal architecture (cortical versus spread).

To discount the possibility that the detergent concentration of the standard lysis buffer disrupted CD44/ERM or pERM interactions (Duterme et al. buffer = 10 mM Tris, 2 mM EDTA, 1% Triton X-100, pH 7.5), a series of buffer conditions were tested to co-immunoprecipitate CD44 and ERM. All of the buffers were prepared in 150 mM NaCl, 50 mM Tris-HCl and pH 7.5, using different detergents at varying concentrations (including triton X-100, NP-40 and CHAPS). Under all extraction conditions, ERM or pERM did not co-immunoprecipitate with CD44 (Figure 38, 41). One conclusion from this study is that CD44 in chondrocytes or chondrocyte-derived cells, do not utilize or interact with ERM proteins as linkage adaptors to the actin cytoskeleton.

Although direct interactions between CD44 and ERM proteins could not be demonstrated in this study, it remains possible that CD44 may affect ERM via other unknown secondary pathways. In total cell extracts from CD44-ICD stable and

transient transfectants, ERM phosphorylation was consistently found to be downregulated as compared to non-transfected cells or cells transfected with the non-relevant control peptide (Figure 39). Thus, a possibility remains that CD44-ICD over-expression does affect the levels of pERM even though we were unable to detect direct interaction between CD44 and pERM.

Other studies have suggested that CD44 links to the actin cytoskeleton via interactions with members of the ankyrin family of adaptor proteins (Bourguignon et al., 1998; Lokeshwar et al., 1994; Singleton and Bourguignon, 2004; Zhu and Bourguignon, 2000). Moreover, some of these reports have demonstrated that the binding affinity between CD44 and ankyrin is much higher than that of CD44 and ERM (Lokeshwar et al., 1994; Tsukita and Yonemura, 1997). In addition, it has also been reported that CD44/ERM interactions cannot be detected *in vitro* or *in vivo* under normal physiological conditions. To detect any CD44/ERM interactions, it is necessary to activate the Rho or protein kinase C pathways, which appears to be a requirement to induce binding (Hirao et al., 1996; Matsui et al., 1998).

The ankyrin family consists of three different genes (ANK1, ANK2, ANK3) with each gene producing different isoforms through alternative splicing. It is not clear whether all three ankyrin gene products can interact with CD44, or whether the particular ANK utilized is tissue dependent. Several of the previous studies that document CD44/ankyrin interactions focused primarily on interactions of CD44 with the conserved Ankyrin Repeat Domain (ARD) present in all ankyrins. Once again, there

are no reports of which ankyrin family members are expressed in chondrocytes, no reports that CD44 binds to ankyrins and, no evidence concerning which ANK member or members participate in CD44 / actin interactions.

In this study, potential interactions between CD44 and ankyrin-1 (ANK1) in chondrocytes were used as a starting point. Zhu and Bourguignon had documented that CD44 and ANK1 co-immunoprecipitated with CD44 in SKOV3 human ovarian carcinoma cells (Zhu and Bourguignon, 2000). Cell lysates of parental RCS and stable RCS-CD44-ICD transfectants were immunoprecipitated with CD44-cytotail antibody and then probed with an HRP-conjugated Ankyrin-1 antibody. Although several bands were detected on the total cell lysates (possibly representing different Ankyrin isoforms), none of these isoforms were detected in the eluted fraction (Figure 45).

Our focus moved on to another ankyrin family member, Ankyrin-3 (ANK3). ANK3 had been previously found to be highly expressed in many tissues (Peters et al., 1995), but cartilage has not yet been specifically analyzed. Again, cell lysates of parental RCS and stable RCS-CD44-ICD transfectants as well as SKOV-3 cells, were immunoprecipitated with CD44-cytotail antibody and then analyzed with an HRP-conjugated anti-ANK3 antibody. In these experiments several ANK3-positive bands were detected in both the eluted and not-bound fractions, and these bands were similar in RCS and SKOV-3 cell lysates (Figure 43). However, two bands were highly expressed in the RCS cell line (Figure 44), likely representing two different isoforms of Ankyrin-3 (~130 kD and ~65 kD). In parental RCS cells, both bands were present in

total cell lysates and the eluted fractions, along with some in the not-bound fraction. This suggested that endogenous CD44-FL binds to both ANK3 isoforms. However, in the RCS-CD44-ICD stable transfectants, only the high molecular mass band (130 kD) was detected in the eluted fraction, while all of the low molecular weight ANK3 isoform (65 kD) was recovered in the not-bound fraction. These results were replicated three times. These data suggest that over-expression of CD44-ICD does affect the binding of CD44-FL with the lower molecular weight, 65 kD isoform of ankyrin-3.

Taken together, this study is the first to investigate the effects of having cytoplasmic CD44-ICD fragments on CD44-FL function in chondrocytes. We have proposed that release of the CD44-ICD into the cytoplasm of chondrocytes would exert a competitive or dominant-negative effect on the CD44-FL functions. This study has provided support for this hypothesis. The rationale for suggesting a dominant-negative effect of the CD44-ICD is that there remains sufficient CD44-FL to bind HA when CD44-ICD is over-expressed. There is little change in the overall content of CD44-FL. Nonetheless, the CD44-FL does not support proper pericellular coat or HA retention, the CD44-FL is not strongly-anchored to the cells and does not continue to bind 65 kD ANK3. This model is summarized in Figure 50.

Our study demonstrated that the expression of CD44-ICD prevents the formation and retention of a pericellular matrix. Loss of pericellular matrices such as the exposure of chondrocytes to HA oligosaccharides (Knudson et al., 2000; Ohno et al., 2006; Schmitz et al., 2010) hyaluronidase (Ohno-Nakahara et al., 2006) or CD44

antisense oligonucleotides (Chow et al., 1998) results in stimulation of catabolic activity in chondrocytes and chondrolysis in cartilage tissue. Loss of pericellular matrices due to exposure of chondrocytes to HA oligosaccharides also results in the proteolytic cleavage of CD44 and the generation of CD44-ICD (Takahashi et al., 2010). As such, these events could contribute to a continued, downward spiral that perpetuates degradation and limits repair of articular cartilage. An initial signal or trauma could result an initial disruption of pericellular matrix in cartilage, triggering enhanced production of proteases and, as a consequence, CD44-ICD formation. Our laboratory recently reported an increase of CD44-ICD fragments in OA chondrocytes when compared to non-OA chondrocytes (Takahashi et al., 2010). The release of CD44-ICD, in turn, would limit matrix repair and retention of the pericellular matrix. A delay in reforming a pericellular matrix would induce further protease synthesis, thus perpetuating matrix loss. Osteoarthritis is often considered a result of attempted-but-ultimately failed repair. As such, CD44-ICD formation could represent a contributing factor in the failed repair, perpetuating a downward spiral that results in progressive osteoarthritis. Thus, this study provides a better understanding on what may occur during early stages of cartilage degradation leading to osteoarthritis.

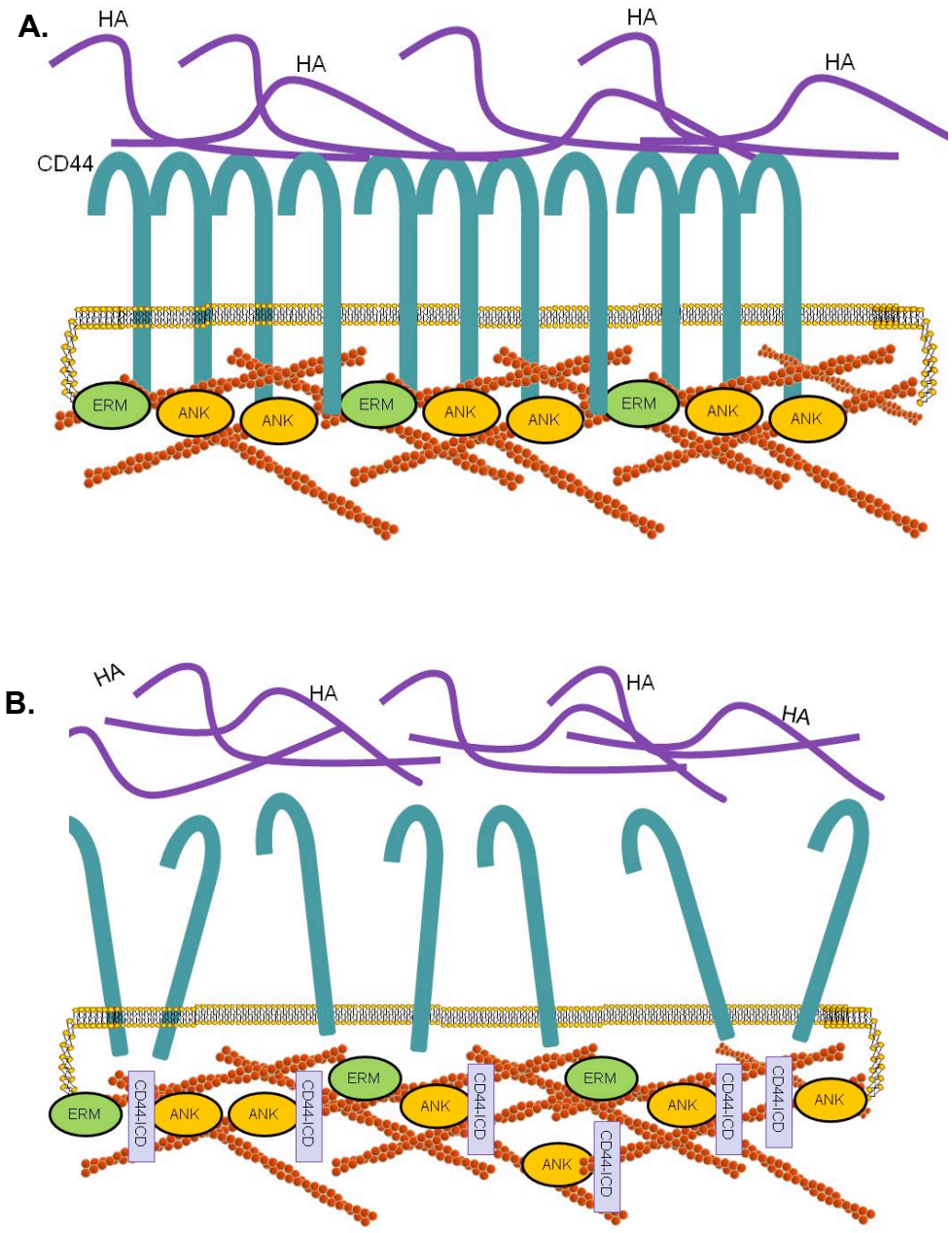

Figure 50: **CD44-ICD fragments compete with CD44-FL binding to the cytoskeleton via ankyrin-3 in chondrocytes. A.** Under normal conditions, CD44-FL binds to the actin cytoskeleton inside the cell via ankyrin-3, allowing proper binding to HA on the outside. **B.** When CD44-ICD fragments are produced and concentrate inside of the cell, they compete with CD44-FL by binding to low molecular weight ankyrin-3, allowing dissociation of CD44 from the actin cytoskeleton and thus affecting CD44/HA binding on the outside.

REFERENCES

Anderegg, U., Eichenberg, T., Parthaune, T., Haiduk, C., Saalbach, A., Milkova, L., Ludwig, A., Grosche, J., Averbeck, M., Gebhardt, C., Voelcker V, Sleeman JP, Simon JC. (2009). ADAM10 is the constitutive functional sheddase of CD44 in human melanoma cells. J Invest Dermatol *129*, 1471-1482.

Beel, A. J., and Sanders, C. R. (2008). Substrate specificity of gamma-secretase and other intramembrane proteases. Cell Mol Life Sci *65*, 1311-1334.

Benya, P. D., Brown, P. D., and Padilla, S. R. (1988). Microfilament modification by dihydrocytochalasin B causes retinoic acid-modulated chondrocytes to reexpress the differentiated collagen phenotype without change in shape. J Cell Biol *106*, 161-170.

Benya, P. D., and Shaffer, J. D. (1982). Dedifferentiated chondrocytes reexpress the differentiated collagen phenotype when cultured in agarose gels. Cell *30*, 215-224.

Blain, E. J. (2009). Involvement of the cytoskeletal elements in articular cartilage homeostasis and pathology. Int J Exp Pathol *90*, 1-15.

Bourguignon, L. Y. W., Zhu, D., and Zhu, H. (1998). CD44 isoform-cytoskeleton interaction in oncogenic signaling and tumor progression. Frontiers Biosci *3*, 637-649.

Bray, S. J. (2006). Notch signalling: a simple pathway becomes complex. Nat Rev Mol Cell Biol *7*, 678-689.

Brown, K. L., Birkenhead, D., Lai, J. C., Li, L., Li, R., and Johnson, P. (2005). Regulation of hyaluronan binding by F-actin and colocalization of CD44 and phosphorylated ezrin/radixin/moesin (ERM) proteins in myeloid cells. Exp Cell Res *303*, 400-414.

Cao, J., Sato, H., Takino, T., and Seiki, M. (1995). The C-terminal region of membrane type matrix metalloproteinase is a functional transmembrane domain required for pro-gelatinase A activation. J Biol Chem *270*, 801-805.

Choi, H. U., Meyer, K., and Swarm, R. (1971). Mucopolysaccharide and protein--polysaccharide of a transplantable rat chondrosarcoma. Proc Natl Acad Sci U S A *68*, 877-879.

Chow, G., Nietfeld, J., Knudson, C.B., Knudson, W. (1998). Antisense inhibition of chondrocyte CD44 expression results in cartilage chondrolysis. Arthritis Rheum 41,1411-1419.

Cichy, J., and Pure, E. (2003). The liberation of CD44. J Cell Biol *161*, 839-843.

D'Souza, A. L., Masuda, K., Otten, L., Nishida, Y., Knudson, W., and Thonar, E.-J. M. A. (2000). Differential effects of interleukin-1 on hyaluronan and proteoglycan metabolism in two compartments of the matrix formed by articular chondrocytes maintained in alginate. Arch Biochem Biophys *374*, 59-65.

Duterme, C., Mertens-Strijthagen, J., Tammi, M., and Flamion, B. (2009). Two novel functions of hyaluronidase-2 (Hyal2) are formation of the glycocalyx and control of CD44-ERM interactions. J Biol Chem *284*, 33495-33508.

Esler, W. P., and Wolfe, M. S. (2001). A portrait of Alzheimer secretases--new features and familiar faces. Science *293*, 1449-1454.

Felson, D. T. (1998). Preventing knee and hip osteoarthritis. Bull Rheum Dis *47*, 1-4.

Felson, D. T. (2009). Developments in the clinical understanding of osteoarthritis. Arthritis Res Ther *11*, 203.

Flannery, C. R., Little, C. B., Caterson, B., and Hughes, C. E. (1999). Effects of culture conditions and exposure to catabolic stimulators (IL-1 and retinoic acid) on the expression of matrix metalloproteinases (MMPs) and disintegrin metalloproteinases (ADAMs) by articular cartilage chondrocytes. Matrix Biol *18*, 225-237.

Goldring, M. B. (2000). Osteoarthritis and cartilage: the role of cytokines. Curr Rheumatol Rep *2*, 459-465.

Goldring, M. B., Birkhead, J. R., Suen, L. F., Yamin, R., Mizuno, S., Glowacki, J., Arbiser, J. L., and Apperley, J. F. (1994). Interleukin-1 beta-modulated gene expression in immortalized human chondrocytes. J Clin Invest *94*, 2307-2316.

Guo, Y. J., Liu, G., Wang, X., Jin, D., Wu, M., Ma, J., and Sy, M. S. (1994). Potential use of soluble CD44 in serum as indicator of tumor burden and metastasis in patients with gastric or colon cancer. Cancer Res *54*, 422-426.

Haynes, B. F., Hale, L. P., Patton, K. L., Martin, M. E., and McCallum, R. M. (1991). Measurement of an adhesion molecule as an indicator of inflammatory disease activity. Up-regulation of the receptor for hyaluronate (CD44) in rheumatoid arthritis. Arthritis Rheum *34*, 1434-1443.

Hirao, M., Sato, N., Kondo, T., Yonemura, S., Monden, M., Sasaki, T., Takai, Y., and Tsukita, S. (1996). Regulation mechanism of ERM (ezrin/radixin/moesin) protein/plasma membrane association: possible involvement of phosphatidylinositol turnover and Rho-dependent signaling pathway. J Cell Biol *135*, 37-51.

Holloway, I., Kayser, M., Lee, D. A., Bader, D. L., Bentley, G., and Knight, M. M. (2004). Increased presence of cells with multiple elongated processes in osteoarthritic femoral head cartilage. Osteoarthritis Cartilage *12*, 17-24.

Jiang, H., Peterson, R. S., Wang, W., Bartnik, E., Knudson, C. B., and Knudson, W. (2002). A requirement for the CD44 cytoplasmic domain for hyaluronan binding, pericellular matrix assembly and receptor mediated endocytosis in COS-7 cells. J Biol Chem *277*, 10531-10538.

Kainz, C., Tempfer, C., Winkler, S., Sliutz, G., Koelbl, H., and Reinthaller, A. (1995). Serum CD44 splice variants in cervical cancer patients. Cancer Lett *90*, 231-234.

Kajita, M., Itoh, Y., Chiba, T., Mori, H., Okada, A., Kinoh, H., and Seiki, M. (2001). Membrane-type 1 matrix metalloproteinase cleaves CD44 and promotes cell migration. J Cell Biol *153*, 893-904.

Kawano, Y., Okamoto, I., Murakami, D., Itoh, H., Yoshida, M., Ueda, S., and Saya, H. (2000). Ras oncoprotein induces CD44 cleavage through phosphoinositide 3-OH kinase and the rho family of small G proteins. J Biol Chem *275*, 29628-29635.

Knudson, C. B. (1993). Hyaluronan receptor-directed assembly of chondrocyte pericellular matrix. J Cell Biol *120*, 825-834.

Knudson, C. B. (2003). Hyaluronan and CD44: strategic players for cell-matrix interactions during chondrogenesis and matrix assembly. Birth Defects Res C Embryo Today *69*, 174-196.

Knudson, C. B., and Knudson, W. (1993). Hyaluronan-binding proteins in development, tissue homeostasis, and disease. FASEB J *7*, 1233-1241.

Knudson, C. B., and Knudson, W. (2005). The hyaluronan receptor, CD44 - an update. Glycoforum, Hyaluronan Today. http://www.glycoforum.gr.jp/science/hyaluronan/HA10a/HA10aE.html.

Knudson, C. B., and Toole, B. P. (1985). Changes in the pericellular matrix during differentiation of limb bud mesoderm. Dev Biol *112*, 308-318.

Knudson, C. B., and Toole, B. P. (1987). Hyaluronate - cell interactions during differentiation of chick embryo limb mesoderm. Dev Biol *124*, 82-90.

Knudson, W. (1996). Tumor-associated hyaluronan. Providing an extracellular matrix that facilitates invasion. Am J Pathol *148*, 1721-1725.

Knudson, W., and Peterson, R. S. (2004). The hyaluronan receptor: CD44. In Chemistry and Biology of Hyaluronan, H.G. Garg, and C.A. Hales, eds. (Boston: Elsevier), pp. 83-123.

Knudson, W., Casey, B., Nishida, Y., Eger, W., Kuettner, K.E., Knudson, C.B. (2000). Hyaluronan oligosaccharides perturb cartilage matrix homeostasis and induce chondrogenic chondrolysis, Arthritis Rheum 43,1165-1174.

Kojima, S., Itoh, Y., Matsumoto, S., Masuho, Y., and Seiki, M. (2000). Membrane-type 6 matrix metalloproteinase (MT6-MMP, MMP-25) is the second glycosyl-phosphatidyl inositol (GPI)-anchored MMP. FEBS Lett *480*, 142-146.

Kopp, R., Classen, S., Wolf, H., Gholam, P., Possinger, K., and Wilmanns, W. (2001). Predictive relevance of soluble CD44v6 serum levels for the responsiveness to second line hormone- or chemotherapy in patients with metastatic breast cancer. Anticancer Res *21*, 2995-3000.

Kucharska, A. M., Kuettner, K. E., and Kimura, J. H. (1990). Biochemical characterization of long-term culture of the Swarm rat chondrosarcoma chondrocytes in agarose. J Orthop Res *8*, 781-792.

Kuettner, K. E. (1994). Osteoarthritis: Cartilage integrity and homeostasis. In Rheumatology, J.H. Klippel, and P.A. Dieppe, eds. (St. Louis, MO: Mosby-Year Book Europe Limited), pp. 6.1-6.16.

Kuettner, K. E., Cole, A. (1998). Articular cartilage and osteoarthritis research. Zeitschrift fur Rheumatologie *57:3,* 176.

Lackner, C., Moser, R., Bauernhofer, T., Wilders-Truschnig, M., Samonigg, H., Berghold, A., and Zatloukal, K. (1998). Soluble CD44 v5 and v6 in serum of patients with breast cancer. Correlation with expression of CD44 v5 and v6 variants in primary tumors and location of distant metastasis. Breast Cancer Res Treat *47*, 29-40.

Lammich, S., Okochi, M., Takeda, M., Kaether, C., Capell, A., Zimmer, A. K., Edbauer, D., Walter, J., Steiner, H., and Haass, C. (2002). Presenilin-dependent intramembrane proteolysis of CD44 leads to the liberation of its intracellular domain and the secretion of an Ab-like peptide. J Biol Chem *277*, 44754-44759.

Legg, J. W., and Isacke, C. M. (1998). Identification and functional analysis of ezrin-binding site in the hyaluronan receptor, CD44. Current Biol *8*, 705-708.

Legg, J. W., Lewis, C. A., Parsons, M., Ng, T., and Isacke, C. M. (2002). A novel PKC-regulated mechanism controls CD44 ezrin association and directional cell motility. Nat Cell Biol *4*, 399-407.

Lesley, J., He, Q., Miyake, K., Hamann, A., Hyman, R., and Kincade, P. W. (1992). Requirements for hyaluronic acid binding by CD44: A role for the cytoplasmic domain and activation by antibody. J Exp Med *175*, 257-266.

Little, C. B., Flannery, C. R., Hughes, C. E., Mort, J. S., Roughley, P. J., Dent, C., and Caterson, B. (1999). Aggrecanase versus matrix metalloproteinases in the catabolism of the interglobular domain of aggrecan in vitro. Biochem J *344*, 61-68.

Liu, D., Zhang, D., Mori, H., and Sy, M.-S. (1996). Binding of CD44 to hyaluronic acid can be induced by multiple signals and requires the CD44 cytoplasmic domain. Cell Immunol *174*, 73-83.

Lockhart, M. S., Waldner, C., Mongini, C., Gravisaco, M. J., Casanova, S., Alvarez, E., and Hajos, S. (1999). Evaluation of soluble CD44 in patients with breast and colorectal carcinomas and non-Hodgkin's lymphoma. Oncol Rep *6*, 1129-1133.

Lokeshwar, V. B., Fregien, N., and Bourguignon, L. Y. W. (1994). Ankyrin-binding domain of CD44(GP85) is required for the expression of hyaluronic acid-mediated adhesion function. J Cell Biol *126*, 1099-1109.

Louvet-Vallee, S. (2000). ERM proteins: from cellular architecture to cell signaling. Biol Cell *92*, 305-316.

Maleski, M. P., and Knudson, C. B. (1996). Matrix accumulation and retention in embryonic cartilage and in vitro chondrogenesis. Connect Tis Res *34*, 75-86.

Marhaba, R., and Zoller, M. (2004). CD44 in cancer progression: adhesion, migration and growth regulation. J Mol Histol *35*, 211-231.

Marrero-Diaz, R., Bravo-Cordero, J. J., Megias, D., Garcia, M. A., Bartolome, R. A., Teixido, J., and Montoya, M. C. (2009). Polarized MT1-MMP-CD44 interaction and CD44 cleavage during cell retraction reveal an essential role for MT1-MMP in CD44-mediated invasion. Cell Motil Cytoskeleton *66*, 48-61.

Martin, T. A., Harrison, G., Mansel, R. E., and Jiang, W. G. (2003). The role of the CD44/ezrin complex in cancer metastasis. Crit Rev Oncol Hematol *46*, 165-186.

Masson, D., Denis, M. G., Denis, M., Blanchard, D., Loirat, M. J., Cassagnau, E., and Lustenberger, P. (1999). Soluble CD44: quantification and molecular repartition in plasma of patients with colorectal cancer. Br J Cancer *80*, 1995-2000.

Matsui, T., Maeda, M., Doi, Y., Yonemura, S., Amano, M., Kaibuchi, K., and Tsukita, S. (1998). Rho-kinase phosphorylates COOH-terminal threonines of ezrin/radixin/moesin (ERM) proteins and regulates their head-to-tail association. J Cell Biol *140*, 647-657.

Matsui, T., Yonemura, S., and Tsukita, S. (1999). Activation of ERM proteins in vivo by Rho involves phosphatidyl-inositol 4-phosphate 5-kinase and not ROCK kinases. Curr Biol *9*, 1259-1262.

Mori, T., Kitano, K., Terawaki, S., Maesaki, R., Fukami, Y., and Hakoshima, T. (2008). Structural basis for CD44 recognition by ERM proteins. J Biol Chem *283*, 29602-29612.

Murai, T., Miyauchi, T., Yanagida, T., and Sako, Y. (2006). Epidermal growth factor-regulated activation of Rac GTPase enhances CD44 cleavage by metalloproteinase disintegrin ADAM10. Biochem J *395*, 65-71.

Murakami, D., Okamoto, I., Nagano, O., Kawano, Y., Tomita, T., Iwatsubo, T., De Strooper, B., Yumoto, E., and Saya, H. (2003). Presenilin-dependent g-secretase activity mediates the intramembranous cleavage of CD44. Oncogene *22*, 1511-1516.

Nagano, O., Murakami, D., Hartmann, D., De Strooper, B., Saftig, P., Iwatsubo, T., Nakajima, M., Shinohara, M., and Saya, H. (2004). Cell-matrix interaction via CD44 is independently regulated by different metalloproteinases activated in response to extracellular Ca(2+) influx and PKC activation. J Cell Biol *165*, 893-902.

Nagano, O., and Saya, H. (2004). Mechanism and biological significance of CD44 cleavage. Cancer Sci *95*, 930-935.

Nakamura, H., Suenaga, N., Taniwaki, K., Matsuki, H., Yonezawa, K., Fujii, M., Okada, Y., and Seiki, M. (2004). Constitutive and induced CD44 shedding by ADAM-like proteases and membrane-type 1 matrix metalloproteinase. Cancer Res *64*, 876-882.

Nakamura, H., Ueno, H., Yamashita, K., Shimada, T., Yamamoto, E., Noguchi, M., Fujimoto, N., Sato, H., Seiki, M., and Okada, Y. (1999). Enhanced production and activation of progelatinase A mediated by membrane-type 1 matrix metalloproteinase in human papillary thyroid carcinomas. Cancer Res *59*, 467-473.

National Collaborating Centre for Chronic Conditions (2008). Osteoarthritis: national clinical guideline for care and management in adults. London Royal College of Physicians.

Naor, D., Sionov, R. V., and Ish-Shalom, D. (1997). CD44: Structure, function, and association with the malignant process. Adv Cancer Res *71*, 241-319.

Nishida, Y., D'Souza, A. L., Thonar, E. J., and Knudson, W. (2000). Stimulation of hyaluronan metabolism by interleukin-1alpha in human articular cartilage. Arthritis Rheum *43*, 1315-1326.

Nishida, Y., Knudson, C. B., Nietfeld, J. J., Margulis, A., and Knudson, W. (1999). Antisense inhibition of hyaluronan synthase-2 in human articular chondrocytes inhibits proteoglycan retention and matrix assembly. J Biol Chem *274*, 21893-21899.

Nofal, G. A., and Knudson, C. B. (2000). Cytoskeletal disruption by latrunculin A decreases chondrocyte matrix retention. Trans Ortho Res Soc *25*, 1005.

Nofal, G. A., and Knudson, C. B. (2002). Latrunculin and cytochalasin decrease chondrocyte matrix retention. J Histochem Cytochem *50*, 1313-1324.

Ohno, S., Im, H.J., Knudson, C.B., Knudson, W. (2006). Hyaluronan oligosaccharides induce matrix metalloproteinase 13 via transcriptional activation of NFkappaB and p38 MAP kinase in articular chondrocytes. J Biol Chem *281*,17952-17960.

Ohno-Nakahara, M., Honda, K., Tanimoto, K., Tanaka, N., Doi, T., Suzuki, A., Yoneno, K., Nakatani, Y., Ueki, M., Ohno, S., Knudson, W., Knudson, C.B., Tanne, K. (2004). Induction of CD44 and MMP expression by hyaluronidase treatment of articular chondrocytes. J Biochem *135*,567-575.

Okamoto, I., Kawano, Y., Matsumoto, M., Suga, M., Kaibuchi, K., Ando, M., and Saya, H. (1999a). Regulated CD44 cleavage under the control of protein kinase C, calcium influx, and the Rho family of small G proteins. J Biol Chem *274*, 25525-25534.

Okamoto, I., Kawano, Y., Murakami, D., Sasayama, T., Araki, N., Miki, T., Wong, A. J., and Saya, H. (2001). Proteolytic release of CD44 intracellular domain and its role in the CD44 signaling pathway. J Cell Biol *155*, 755-762.

Okamoto, I., Kawano, Y., Tsuiki, H., Sasaki, J., Nakao, M., Matsumoto, M., Suga, M., Ando, M., Nakajima, M., and Saya, H. (1999b). CD44 cleavage induced by a membrane-associated metalloprotease plays a critical role in tumor cell migration. Oncogene *18*, 1435-1446.

Peck, D., and Isacke, C. M. (1998). Hyaluronan-dependent cell migration can be blocked by a CD44 cytoplasmic domain peptide containing a phosphoserine at position 325. J Cell Sci *111*, 1595-1601.

Pelletier, L., Guillaumot, P., Freche, B., Luquain, C., Christiansen, D., Brugiere, S., Garin, J., and Manie, S. N. (2006). Gamma-secretase-dependent proteolysis of CD44 promotes neoplastic transformation of rat fibroblastic cells. Cancer Res *66*, 3681-3687.

Peters, L. L., John, K. M., Lu, F. M., Eicher, E. M., Higgins, A., Yialamas, M., Turtzo, L. C., Otsuka, A. J., and Lux, S. E. (1995). Ank3 (epithelial ankyrin), a widely distributed new member of the ankyrin gene family and the major ankyrin in kidney, is expressed in alternatively spliced forms, including forms that lack the repeat domain. J Cell Biol *130*, 313-330.

Peterson, R. S., Andhare, R. A., Rousche, K. T., Knudson, W., Wang, W., Grossfield, J. B., Thomas, R. O., Hollingsworth, R. E., and Knudson, C. B. (2004). CD44 modulates Smad1 activation in the BMP 7 signaling pathway. J Cell Biol *166*, 1081-1091.

Sato, H., Takino, T., Okada, Y., Cao, J., Shinagawa, A., Yamamoto, E., and Seiki, M. (1994). A matrix metalloproteinase expressed on the surface of invasive tumour cells. Nature *370*, 61-65.

Schmitz, I., Ariyoshi, W., Takahashi, N., Knudson, C.B., Knudson, W. (2010). Hyaluronan oligosaccharide treatment of chondrocytes stimulates expression of both HAS-2 and MMP-3, but by different signaling pathways. Osteoarthritis Cartilage *18*,447-454.

Singleton, P. A., and Bourguignon, L. Y. (2004). CD44 interaction with ankyrin and IP3 receptor in lipid rafts promotes hyaluronan-mediated Ca2+ signaling leading to nitric oxide production and endothelial cell adhesion and proliferation. Exp Cell Res *295*, 102-118.

Stamenkovic, I., and Yu, Q. (2009). Shedding light on proteolytic cleavage of CD44: the responsible sheddase and functional significance of shedding. J Invest Dermatol *129*, 1321-1324.

Strooper, B. D., and Annaert, W. (2001). Presenilins and the intramembrane proteolysis of proteins: facts and fiction. Nat Cell Biol *3*, E221-225.

Takahashi, N., Knudson, C. B., Thankamony, S., Ariyoshi, W., Mellor, L., Im, H. J., and Knudson, W. (2010). Induction of CD44 cleavage in articular chondrocytes. Arthritis Rheum *62*, 1338-1348.

Takeda, H., Inoue, H., Kutsuna, T., Matsushita, N., Takahashi, T., Watanabe, S., Higashiyama, S., and Yamamoto, H. (2010). Activation of epidermal growth factor receptor gene is involved in transforming growth factor-beta-mediated fibronectin expression in a chondrocyte progenitor cell line. Int J Mol Med *25*, 593-600.

Thankamony, S. P., and Knudson, W. (2006). Acylation of CD44 and its association with lipid rafts are required for receptor and hyaluronan endocytosis. J Biol Chem *281*, 34601-34609.

Tsukita, S., Oishi, K., Sato, N., Sagara, J., and Kawai, A. (1994). ERM family members as molecular linkers between the cell surface glycoprotein CD44 and actin-based cytoskeletons. J Cell Biol *126*, 391-401.

Tsukita, S., and Yonemura, S. (1997). ERM (ezrin/radixin/moesin) family: from cytoskeleton to signal transduction. Curr Opin Cell Biol *9*, 70-75.

Ueno, H., Nakamura, H., Inoue, M., Imai, K., Noguchi, M., Sato, H., Seiki, M., and Okada, Y. (1997). Expression and tissue localization of membrane-types 1, 2, and 3 matrix metalloproteinases in human invasive breast carcinomas. Cancer Res *57*, 2055-2060.

White, J., L. Bridges, D. DeSimone, M. Tomczuk and T. Wolfsberg (2005). Introduction to the ADAM family. In The ADAM family of proteases, N.M.H.a.U. Lendeckel, ed. (Netherlands: Springer), pp. 1-28.

Yamane, N., Tsujitani, S., Makino, M., Maeta, M., and Kaibara, N. (1999). Soluble CD44 variant 6 as a prognostic indicator in patients with colorectal cancer. Oncology *56*, 232-238.

Yonemura, S., Hirao, M., Doi, Y., Takahashi, N., Kondo, T., and Tsukita, S. (1998). Ezrin/radixin/moesin (ERM) proteins bind to a positively charged amino acid cluster in the juxta-membrane cytoplasmic domain of CD44, CD43, and ICAM-2. J Cell Biol *140*, 885-895.

Zhu, D., and Bourguignon, L. Y. (2000). Interaction between CD44 and the repeat domain of ankyrin promotes hyaluronic acid-mediated ovarian tumor cell migration. J Cell Physiol *183*, 182-195.